

Candidate Massive Galaxies at $z \sim 4$ in the Dark Energy Survey

Pierandrea Guarnieri,^{1*} Claudia Maraston,¹ Daniel Thomas,¹ Janine Pforr,² Violeta Gonzalez-Perez,¹ James Etherington,¹ Joakim Carlsen, Xan Morice-Atkinson,¹ Christopher J. Conselice,³ Julia Gschwend,^{4,5} Matias Carrasco Kind,^{6,7} Tim Abbott,⁸ Sahar Allam,⁹ David Brooks,¹⁰ David Burke,^{11,12} Aurelio Carnero Rosell,^{4,5} Jorge Carretero,¹³ Carlos Cunha,⁹ Chris D'Andrea,¹⁴ Luiz da Costa,^{4,5} Juan De Vincente,¹⁵ Darren DePoy,¹⁶ H. Thomas Diehl,⁹ Peter Doel,¹⁰ Josh Frieman,^{9,11} Juan Garcia-Bellido,¹⁷ Daniel Gruen,^{11,12} Gaston Gutierrez,⁹ Dominic Hanley,¹ Devon Hollowood,¹⁸ Klaus Honscheid,^{19,20} David James,²¹ Tesla Jeltema,¹⁸ Kyler Kuehn,²² Marcos Lima,^{4,23} Marcio A. G. Maia,^{4,5} Jennifer Marshall,¹⁶ Paul Martini,^{19,20} Peter Melchior,²⁴ Felipe Menanteau,^{25,26} Ramon Miquel,^{13,27} Andres Plazas Malagon,²⁸ Samuel Richardson,¹ Kathy Romer,²⁹ Eusebio Sanchez,¹⁵ Vic Scarpine,⁹ Rafe Schindler,¹² Ignacio Sevilla,¹⁵ Mathew Smith,³⁰ Marcelle Soares-Santos,³¹ Flavia Sobreira,^{4,32} Eric Suchyta,³³ Gregory Tarle,³⁴ Alistair Walker,⁶ William Wester⁷

¹*Institute of Cosmology and Gravitation, University of Portsmouth, Dennis Sciamia Building, Burnaby Road, Portsmouth PO1 3FX, UK*

²*ESTEC: European Space Research and Technology Centre, Keplerlaan 1, 2201 AZ Noordwijk, Netherlands*

³*University of Nottingham, School of Physics & Astronomy, Nottingham, NG7 2RD, UK*

⁴*Laboratorio Interinstitucional de e-Astronomia - LIneA, Rua Gal. Jose Cristino 77, Rio de Janeiro, RJ - 20921-400, Brazil*

⁵*Observatorio Nacional, Rua Gal. Jose Cristino 77, Rio de Janeiro, RJ - 20921-400, Brazil*

⁶*Department of Astronomy, University of Illinois at Urbana-Champaign, 1002 W. Green Street, Urbana, IL 61801, USA*

⁷*National Center for Supercomputing Applications, 1205 West Clark St., Urbana, IL 61801, USA*

⁸*Cerro Tololo Inter-American Observatory, National Optical Astronomy Observatory, Casilla 603, La Serena, Chile*

⁹*Fermi National Accelerator Laboratory, P. O. Box 500, Batavia, IL 60510, USA*

¹⁰*Department of Physics & Astronomy, University College London, Gower Street, London, WC1E 6BT, UK*

¹¹*Kavli Institute for Particle Astrophysics & Cosmology, P. O. Box 2450, Stanford University, Stanford, CA 94305, USA*

¹²*SLAC National Accelerator Laboratory, Menlo Park, CA 94025, USA*

¹³*Institut de Fisica d'Altes Energies (IFAE), The Barcelona Institute of Science and Technology, Campus UAB, 08193 Bellaterra (Barcelona) Spain*

¹⁴*Department of Physics and Astronomy, University of Pennsylvania, Philadelphia, PA 19104, USA*

¹⁵*Centro de Investigaciones Energeticas, Medioambientales y Tecnologicas (CIEMAT), Madrid, Spain*

¹⁶*George P. and Cynthia Woods Mitchell Institute for Fundamental Physics and Astronomy, and Department of Physics and Astronomy, Texas A&M University, College Station, TX 77843, USA*

¹⁷*Instituto de Fisica Teorica UAM/CSIC, Universidad Autonoma de Madrid, 28049 Madrid, Spain*

¹⁸*Santa Cruz Institute for Particle Physics, Santa Cruz, CA 95064, USA*

¹⁹*Center for Cosmology and Astro-Particle Physics, The Ohio State University, Columbus, OH 43210, USA*

²⁰*Department of Physics, The Ohio State University, Columbus, OH 43210, USA*

²¹*Harvard-Smithsonian Center for Astrophysics, Cambridge, MA 02138, USA*

²²*Australian Astronomical Observatory, North Ryde, NSW 2113, Australia*

²³*Departamento de Fisica Matematica, Instituto de Fisica, Universidade de Sao Paulo, CP 66318, Sao Paulo, SP, 05314-970, Brazil*

²⁴*Department of Astrophysical Sciences, Princeton University, Peyton Hall, Princeton, NJ 08544, USA*

²⁵*Department of Astronomy, University of Illinois at Urbana-Champaign, 1002 W. Green Street, Urbana, IL 61801, USA*

²⁶*National Center for Supercomputing Applications, 1205 West Clark St., Urbana, IL 61801, USA*

²⁷*Institucio Catalana de Recerca i Estudis Avancats, E-08010 Barcelona, Spain* ²⁸*Jet Propulsion Laboratory, California Institute of Technology, 4800 Oak Grove Dr., Pasadena, CA 91109, USA*

²⁹*Department of Physics and Astronomy, Pevensey Building, University of Sussex, Brighton, BN1 9QH, UK*

³⁰*School of Physics and Astronomy, University of Southampton, Southampton, SO17 1BJ, UK*

³¹*Brandeis University, Physics Department, 415 South Street, Waltham MA 02453*

³²*Instituto de Fisica Gleb Wataghin, Universidade Estadual de Campinas, 13083-859, Campinas, SP, Brazil*

³³*Computer Science and Mathematics Division, Oak Ridge National Laboratory, Oak Ridge, TN 37831*

³⁴*Department of Physics, University of Michigan, Ann Arbor, MI 48109, USA*

ABSTRACT

Using stellar population models, we predicted that the Dark Energy Survey (DES) - due to its special combination of area (5000 deg.sq.) and depth ($i = 24.3$) - would be in the position to detect massive ($\gtrsim 10^{11} M_{\odot}$) galaxies at $z \sim 4$. We confront those theoretical calculations with the first ~ 150 deg. sq. of DES data reaching nominal depth. From a catalogue containing ~ 5 million sources, ~ 26000 were found to have observed-frame $g-r$ vs $r-i$ colours within the locus predicted for $z \sim 4$ massive galaxies. We further removed contamination by stars and artefacts, obtaining 606 galaxies lining up by the model selection box. We obtained their photometric redshifts and physical properties by fitting model templates spanning a wide range of star formation histories, reddening and redshift. Key to constrain the models is the addition, to the optical DES bands g , r , i , z , and Y , of near-IR J , H , K_s data from the Vista Hemisphere Survey. We further applied several quality cuts to the fitting results, including goodness of fit and a unimodal redshift probability distribution. We finally select 233 candidates whose photometric redshift probability distribution function peaks around $z \sim 4$, have high stellar masses ($\log(M^*/M_{\odot}) \sim 11.7$ for a Salpeter IMF) and ages around 0.1 Gyr, i.e. formation redshift around 5. These properties match those of the progenitors of the most massive galaxies in the local universe. This is an ideal sample for spectroscopic follow-up to select the fraction of galaxies which is truly at high redshift. These initial results and those at the survey completion, which we shall push to higher redshifts, will set unprecedented constraints on galaxy formation, evolution, and the re-ionisation epoch.

Key words: galaxies: evolution – galaxies: high-redshift

1 INTRODUCTION

The formation and evolution of the most massive galaxies in the universe remains an open problem in cosmology and astrophysics.

The fossil stellar population in the local universe shows that the most massive galaxies host the oldest stellar populations and that they should have formed around $z \sim 5$ (Cowie, Songaila & Barger 1999; Thomas et al. 2005, 2010; Cowie & Barger 2008). Radial gradients in stellar populations which are flat in age and element abundance ratios (Mehlert et al. 2003; Pipino et al. 2007; Goddard et al. 2017; Sánchez et al. 2012) suggest that the early formation is a global property of the galaxy rather than of just its inner core.

Within the hierarchical galaxy formation paradigm (White & Rees 1978), the most massive objects assemble last, at relatively low redshift ($z \sim 0.5$) even if their building blocks may contain ancient stellar populations that later merge (De Lucia et al. 2006; Ricciardelli & Franceschini 2010). This model implies a scarcity of massive galaxies at high redshift and their gradual build-up towards our epoch (Gonzalez-Perez et al. 2009). Hence, one key approach for constraining galaxy formation on a cosmological scale is to search for the progenitors of the most massive galaxies at an increasingly larger look-back time.

Massive galaxies are indeed being found spectroscopically at increasingly higher redshifts, in the range $z \sim 1.5 - 3.0$ (Lonoce et al. 2015; Yan et al. 2004; Onodera et al. 2012; Cimatti et al. 2004; Kriek et al. 2016; Straatman et al. 2014; Conselice et al. 2007; Whitaker et al. 2013) and even $z \sim 3 - 4$ (Mancini et al. 2009; Santini et al. 2009; Caputi et al. 2012, 2015; Guo 2013; Ilbert et al. 2013; Muzzin et al.

2013; Stefanon et al. 2013; Marsan et al. 2017). At such high redshifts, usually the word ‘massive’ refers to stellar masses up to $\sim 10^{11} M_{\odot}$. The highest value reported so far is a $1.7 \times 10^{11} M_{\odot}$ galaxy at a spectroscopic redshift of 3.717 (Glazebrook et al. 2017). The detection of such an impressively massive galaxy at such a high redshift is a challenge to galaxy formation models. We shall return to these works in relation to our project.

In order to bridge the fossil record with the formation event and trace galaxy evolution over cosmic time, many works have attacked the problem in a statistical sense, by probing number density evolution as a function of galaxy mass. Studies of the galaxy mass function over the past decade reached the uniform conclusion that the abundance of the most massive galaxies ($M/M_{\odot} > 10^{11.5}$) hardly evolves since $z \sim 1$ (Cimatti, Daddi & Renzini 2006; Wake et al. 2006; Pozzetti et al. 2010; Marchesini et al. 2010; Muzzin et al. 2013; Gonzalez-Perez et al. 2009; Mortlock et al. 2015). One caveat to these studies has been that the observational database was drawn from small area, deep surveys, which carry the problem of cosmic variance. This is particularly severe at the highest mass where the galaxy mass function is steep and errors on photometric data are large. However, this has been recently solved by using the cosmological SDSS-III/BOSS survey (10,000 deg. sq.). This survey has allowed the calculation of the galaxy mass function around $M^* \sim 10^{12} M_{\odot}$ with unprecedented statistics (Maraston et al. 2013) thanks to the large area and the target selection centred on massive galaxies. The conclusion of this work is that the abundance of the most massive galaxies is constant in the redshift range 0.4-0.6, and larger than what is predicted by galaxy formation models. Bundy et al. (2017) using deeper photometry from the so-called Stripe82 region reached the same conclusion and showed that it is robust against the

* E-mail: pierandrea.guarnieri@port.ac.uk

way stellar masses are calculated. Furthermore, [Etherington et al. \(2017\)](#), using data from the Dark Energy Survey (DES) survey (see below), showed that the evolution of the high-mass end of the galaxy mass function does not seem to depend on the environment. [Thomas et al. \(2010\)](#) reached the same conclusion performing a different analysis, namely using the chemical information in the fossil stellar population properties of the most massive galaxies. They showed that ages, metallicities and chemical abundance ratios of the most massive galaxies do not depend on the environment, leading to the inference that their formation and evolution are mainly driven by internal processes, reinforcing down-sizing as the evolution paradigm for these galaxies ([Peng et al. 2010](#)).

As just mentioned, probing the massive end of the galaxy population requires a wide survey area. The Dark Energy Survey (DES) is a galaxy survey aimed at probing cosmic acceleration. The survey is collecting galaxy photometric data in the southern sky at magnitude depths of $\sim 25.5, 25.0, 24.4, 23.9$ and 22.0 in the g, r, i, z and Y bands respectively, for a very large portion of sky (5000 deg. sq.) ([Rossetto et al. 2011](#); [The Dark Energy Survey Collaboration 2005](#)). At completion (~ 2019), DES will have observed on the order of 300 million galaxies.

[Davies et al. \(2013\)](#) (hereafter D13) forecasted that - by virtue of its suitable combination of area and depth - DES is currently the best survey to detect the rare, massive ($\sim 10^{12} M_{\odot}$) galaxies at high redshift ($z \gtrsim 4$), should these exist (see Figure 2 in D13). D13 used stellar population models spanning a wide range of properties (e.g. age, metallicity, star formation history, stellar mass and dust reddening) to model galaxies as a function of DES magnitude, colours and redshift, identifying colour-colour selection maps for redshifts $z \sim 4, 5$, and 6 (see Figures 7,8,9 in D13).

The scope of the present paper is to apply the D13 theoretical selection maps to a sample of real DES data for the first time, specifically the latest available set of Year 3 (Y3) data, in order to find candidate massive high- z galaxies. The data we use consist of observations completed on a limited sky region (~ 150 sq. deg.) probed since the Science Verification (SV) programme (thus at the DES nominal depth) in order to test the observational process and general workflow.

We first proceed by plotting the new DES data on the D13 colour-colour plots, and then calculate the photometric redshifts and physical properties of those sources falling into the predicted boxes for $z \sim 4$ galaxies, after carefully removing artefacts of various kinds. We focus on $z \sim 4$, rather than on $z \sim 5$ or $z \sim 6$, as if these rare massive galaxies exist they are more likely to be observed at lower redshifts. We need to maximise our chances given the smaller area covered by the SV footprint compared to the one that will be available at DES completion.

Calculations of template-based photometric redshift are the common procedure at high redshift, but we shall also discuss the effect of using alternative redshifts from the DES neural network pipeline ([Sánchez et al. 2014](#)). Instrumental to the robustness of our fitting is the availability of near-IR bands from the Vista Hemisphere Survey (VHS) ([McMahon 2012](#); [Banerji et al. 2015a](#)), which could extend the baseline photometry to a total of 8 filters. It is interesting to test whether the final results are consistent with the D13

predictions, which were based on the sole g, r, i, z, Y DES magnitudes.

We then analyse in detail the fitting results for all candidates and conservatively retain only those obeying several quality criteria, including a unimodal probability distribution function in redshift, a good χ_r^2 and other model parameters.

At the end of the procedure we select 233 individual galaxies, of which some are selected with both reddening options. We find 109 using the SMC reddening law and 203 using the Calzetti law. For these, we examine their properties (including mass, age, SFR, SFH) and draw initial conclusions on galaxy evolution, using also galaxy formation simulations as a comparison.

The paper is structured as follows. Section 2 describes our method to find high- z candidates, which includes an initial colour selection (Section 2.2) and photometric template fittings to calculate photometric redshifts and physical properties (Section 2.3). In Section 3 we describe in detail our best candidate selection, including their physical properties. In the same section we detail further tests we completed to check the reliability of our sample. In Section 4 we perform a comparison with the literature. Lastly, in Section 6 we summarise our work and discuss our key findings as well as their relevance for future work and in the context of current research.

2 METHOD

2.1 Overview

Our aim is to identify the most likely high redshift ($z \sim 4$) massive galaxy candidates within a dataset of ~ 4.9 million objects. Starting from the simulations performed by D13 we proceed using real DES data in this context for the first time. In this paper we focused on the $z \sim 4$ case in order to maximise the chance to find objects in the small area covered by the SV data.¹ The process we followed in order to identify the best candidates is comprised of different steps. We summarise them here and discuss each of them in separate sections below.

At first all Y3 data were placed on the D13 colour-colour plots (Figure 1, top left-hand panel). Then, the catalogue was scanned to remove sources that could potentially be stars and/or those affected by the largest errors. The sources passing these two criteria (non-stars and small errors) are plotted in Figure 1, top right-hand panel. From this point, we focus on the objects lying within the D13 selection box for massive, $z \sim 4$ galaxies (solid black line in Figure 1). These candidates were further pruned of those potentially affected by blending (using the DES pipeline flags). The result of this further selection is shown in Figure 1, lower left-hand panel. Last, VHS archive data were matched to the selected sources in order to extend their DES photometry with J, H , and K_s bands. Some sources lacked one or more VHS bands

¹ An initial look at the $z \sim 5$ and 6 selection maps (from D13) did not result in any high- z candidates, but this does not exclude the possibility that they exist and it may be due simply to the fact that the SV data cover only ~ 150 deg. sq. We shall pursue the higher redshift bins when we look at the entire database.

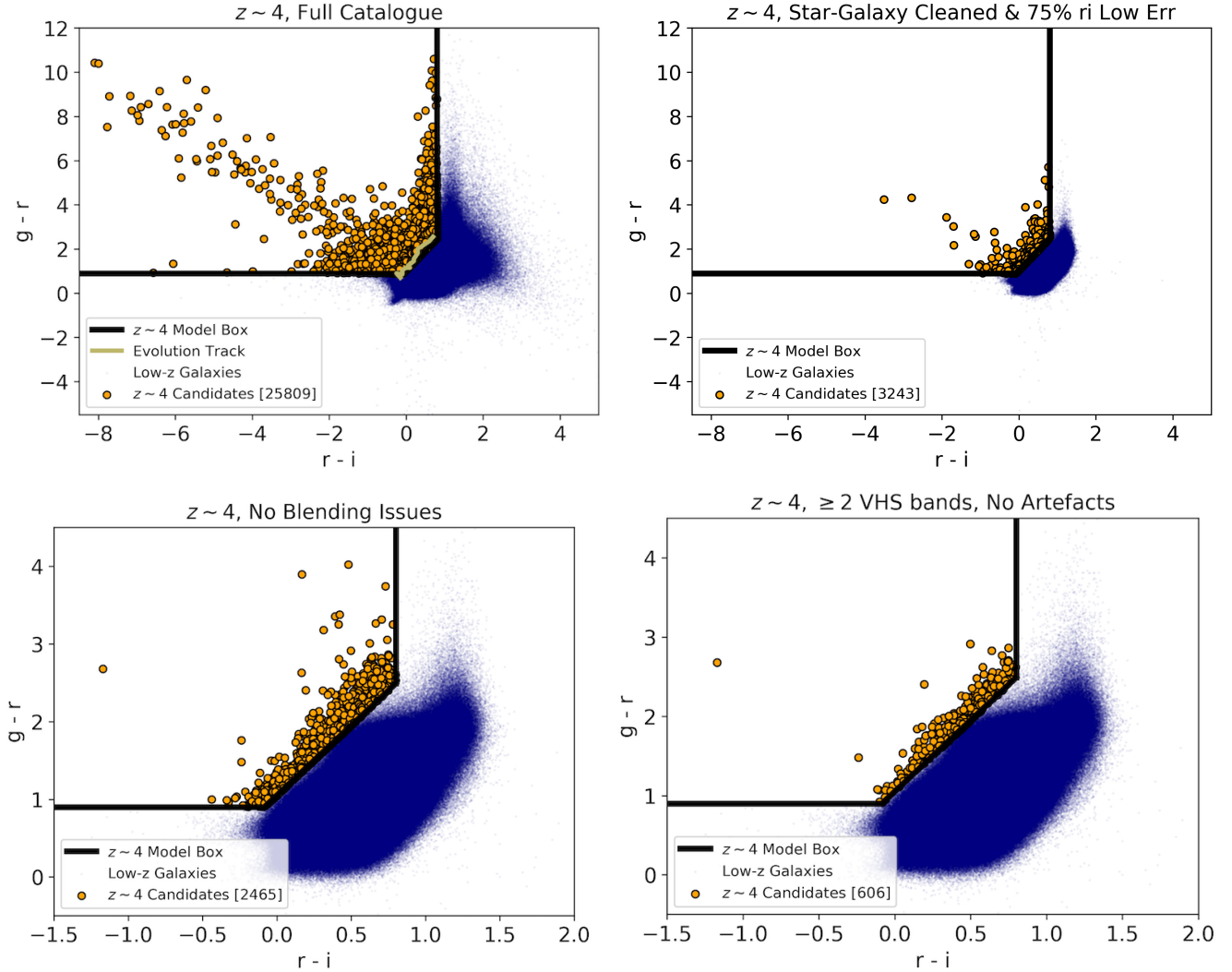


Figure 1. Colour-colour selection maps for selecting massive $z \sim 4$ candidates using DES photometry, as from D13. Black solid lines define the predicted selection boxes for $z \sim 4$ (red $g-r$, blue $r-i$ relative to the black line), with the khaki line in the top left panel showing the redshift evolution track for a model galaxy as illustration. Orange dots correspond to sources identified as high- z candidate galaxies lying in the model selection area. Objects that fall outside the selection area are plotted as a density map in blue (darker is denser). The top-left panel shows the full Commodore-selected Y3 catalogue without any cut applied. The top-right panel shows the map after the cuts for star-galaxy separation and against large errors in r and i . The bottom-left panel shows the final selection map after removal of objects potentially affected by blending and the bottom-right one contains only those sources with at least 2 VHS bands and no visual artefacts near the galaxies in the image cutouts. We use MAG_DETMODEL AB photometry.

and, as explained later, this has been taken into account when estimating the reliability of our fits. The matching was done automatically by inserting the RA and Dec coordinates of each DES object in the VHS data access pages² to find the closest VHS source. The maximum matching radius was kept to the web utility default value of 5 arcsec. However, we have visually checked every single image for each source to confirm that the DES and VHS photometry was matched correctly.

Those sources passing the condition of having data in at least two VHS bands populate the selection box in the lower right-hand panel of Figure 1. For these we calculated the photometric redshift and stellar population properties using

a template fitting procedure. Photometric redshifts and their probability distribution functions were compared to those calculated by the DES pipeline working groups (more details in Section 2.2.1).

Lastly, a full-fledged analysis of the results for each candidate was performed in order to identify only those that are convincing $z \sim 4$ galaxies.

2.2 Initial Selection

2.2.1 Catalogue of DES Data & Colour Selection Cuts

We used photometric data in the g , r , i , z , and Y bands from the DES Y3 Gold 2.0 release, which contains the latest, highest quality photometry for DES. Among the magnitude options, we use MAG_DETMODEL photometry (in the AB

² <http://horus.roe.ac.uk/vsa/index.html>

system), as it refers to the same physical aperture hence it is optimal for template fitting. As described in Melchior et al. (2015), magnitudes are measured by SExtractor in each filter using a model fit to the surface brightness of the source in each image. The detection image for each object was created by the DES pipeline by linearly combining the r , i , and z images (Abbott et al. 2018).

From the Y3 catalogue we wanted to choose those objects that had been observed since the SV stage, meaning that their photometry matches the full nominal depth of the survey. In order to select them, we used the *COMMODORE* catalogue (for details see Etherington et al. 2017, and Capozzi et al., *sub.*) which refers to the SV data and provides, among other entries³ the sky position (RA and Dec), the neural network redshift and a flag for performing star-galaxy separation.

The crossmatch between Y3 and the *COMMODORE* SV data resulted in ~ 4.9 million sources. The rest of the sources in Y3 (the vast majority, amounting to the impressive figure of 394 million objects) will need further observations for reaching the same depth levels.

First, we considered the star-galaxy separation parameter included in the catalogue and validated by the *COMMODORE* team (and detailed in Kim et al. 2015). This method uses a supervised machine learning technique to provide the probability of a given source of being either a galaxy or a star. Note that this procedure may lead to the exclusion of compact galaxies, and many high- z massive galaxies are compact (Straatman et al. 2014), but it makes it much more likely that we avoid star or pure AGN contamination (this last point is discussed in more detail in Section 3.1.1). Quantitatively, we kept those sources with $\geq 99.977\%$ probability of being a galaxy⁴. This first cleaning left us 73% of the original sample (i.e. ~ 3.7 million sources). We further performed a cut in photometric errors. We examined the error distributions in r and i separately and we conservatively decided to remove the tail of largest errors (i.e. $r_{err} < 0.060$ mag and $i_{err} < 0.063$ mag), which means removing $\sim 25\%$ of objects in each band. These cuts effectively identify the magnitude limits of our work in the r and i bands, which are ~ 23.7 and ~ 23.5 , respectively. This can be appreciated by looking at Figure 2, where we plot error against magnitude for the r and i bands (left-hand and right-hand panel, respectively) of our full catalogue after star-galaxy separation. The horizontal lines indicate our error cuts.

We then matched objects satisfying the error cuts in both bands. Note that we considered these bands as they were the ones used for the theoretical colour selection, see Section 2.2.2. We left the g band free of constraints as it is the drop-out band at high redshifts (see Figure 7 and visit this link⁵ for several examples).

After the star-galaxy separation and the lowest error

cut, we were left with ~ 2.7 million candidate galaxies. Furthermore, we removed all galaxies whose photometry was marked by the DES pipeline as being potentially affected by blending. Lastly, we extended the photometric baseline of the DES data with near-IR VHS data, and we decided to consider only those sources for which we could add at least two additional photometric data to the DES data (see Section 2.2.3 for more details).

It should be noted that the Y3 Gold 2.0 catalogue also contains a photometric redshift estimate for each source as calculated by the DES pipeline. This redshift is calculated using the so-called Bayesian Photometric Redshift (BPZ) code (Hoyle et al. 2017). The prior used in BPZ strongly disfavours high- z solutions for bright galaxies. This does not mean, however, that higher redshift objects do not exist and this is exactly what we aimed to find out. Later in the paper we shall also perform a comparison of the physical properties we would have obtained for galaxies had we used the z_{BPZ} .

2.2.2 Theoretical Colour - Colour Selection Maps

As recalled in the Introduction, D13 investigated colour combinations of DES bands for stellar population models (Maraston 2005; Maraston et al. 2006) with various parameters such as age, star formation history, dust, and stellar mass, as placed at various redshifts, in order to select those corresponding to the mass-redshift combinations of interest. The resulting selection boxes display regions within the colour-colour diagrams where high- z objects should be found.

Hence, our first step was to plot the DES galaxy candidates on the D13 $g-r$ vs $r-i$ plots in order to single out those entering the $z \gtrsim 4$ box. Note that by using this mapping first it is possible to substantially reduce the number of candidates for fitting, which is helpful because running a template fitting code for photometric redshift and physical properties for millions of sources is very time consuming. Even more importantly, using such a colour selection box is crucial to maximise the likelihood of the candidates to truly be at high redshift.

The colour-colour $g-r$ vs $r-i$ diagram using Y3 photometry for the sources in the *COMMODORE* catalogue is shown in the top-left panel of Figure 1, where the selection box for $z \sim 4$ objects is highlighted with a black solid line. In the same panel, the khaki line depicts the redshift evolution track for a model galaxy as taken from D13. The vast majority of the sources are consistent with being low-redshift objects (plotted as small, blue points; the darker, the denser). The high- z candidates falling in the selection area are plotted in orange. They total 25809 sources (top-left panel). After application of the cuts described in Section 2.2.1 - namely star-galaxy separation and removal of sources with highest error in bands r and i (for a total of 25% in each of the two bands) - we are left with 3243 objects as potential high- z candidates (top-right panel). We then removed candidates with blending issues, which left us with 2465 galaxies (bottom-left panel). Further visual inspection of the cutout images allowed us to remove any source that showed artefact traits, such as satellite trails and black-out areas, near the selected source. This does not mean that their photometry is necessarily compromised (as these were not flagged by the pipeline), but we decided to exclude them

³ The *COMMODORE* catalogue also contains the DES SV photometry (which was not used for this work as the Y3 one is of higher quality) and galaxy physical properties obtained with the same models and procedure as here, but using the neural network redshift as fixed redshift for the given source.

⁴ For DES users: the entry we used is called `TPZSG_CLASS` and we excluded sources with `TPZSG_CLASS > 0.00023`

⁵ Un-hidden hyperlink: <http://icg.port.ac.uk/~guarniep/>

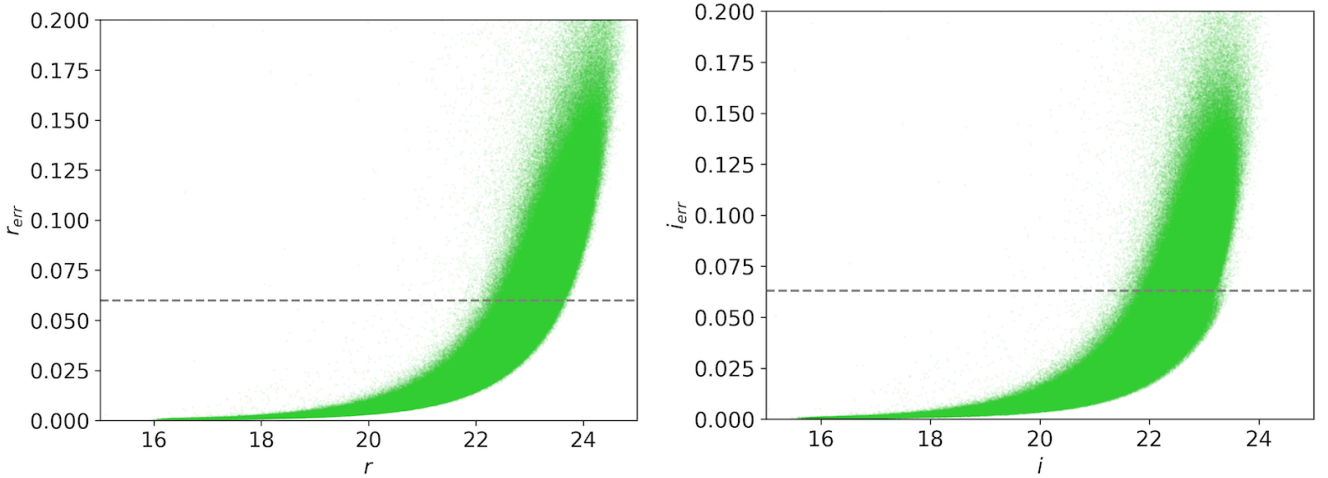


Figure 2. Error against magnitude for r and i bands. The horizontal lines mark the error cuts we applied (i.e. $r_{err} < 0.060$ and $i_{err} < 0.063$). These identify the effective magnitude limits of our analysis as ~ 23.7 and ~ 23.5 for the r and i bands, respectively.

as we could not verify their photometric quality. This is done along with further considerations on the number of near-IR bands we could match to our galaxies, as described in the next section.

2.2.3 Extending the Photometry to the Near-IR

As is well known, the accuracy of spectro-photometric model fitting depends on the number of available data points and especially on the baseline in wavelength they cover (e.g. Pforr et al. 2012, 2013; Banerji et al. 2008, 2015a). In order to strengthen the reliability of our photometric fitting procedure, as mentioned in the previous sections, we looked for additional bands for the sources within the colour-colour map. We were able to cross-match the DES optical data with the VHS survey (McMahon 2012), thereby extending our photometric catalogue to the near-infrared bands J , H , and K_s ⁶. We used the *Petrosian magnitudes* from the VHS Data Release 5, which rely on the Petrosian radii of galaxies to determine the photometric aperture. This allows to recover the flux also for extended sources, making them ideal to work in combination with the DES DET_MODEL magnitudes discussed earlier. We do not expect the atmospheric seeing to have an effect on our template fitting results since we use extended magnitude types (DES DET_MODEL and VHS *Petrosian*; Cross et al. 2012) and the median seeing among the eight DES+VHS bands was shown to be similar (Banerji et al. 2015a). Additionally, the point spread function (PSF) full width at half maximum (FWHM) of the DES and VHS camera and telescope configurations are 0.49

arcsec⁷ and 0.51 arcsec⁸, respectively. Therefore we consider DES and VHS photometry to be compatible without further manipulation.

We noted that the majority of DES sources does not have all three VHS bands available. There could be several reasons for this. First of all, VHS has not imaged in the H band all regions overlapping with DES (Reed et al. 2017). Additionally, VHS is shallower than DES and the optimal depth depends on the nature of the candidates. For example, young star forming objects could be faint in the rest-frame optical (sampled by the VHS at high- z) simply because they are dominated by massive hot stars.

In order to retain only those candidates for which the model fitting would be better constrained (see Section 2.3.2), we decided to focus on objects having observation in at least 2 VHS bands, which means to fit a minimum of 7 photometric bands.

This further selection criterium, along with the removal of artefacts as described in the previous section, led us to identify 606 galaxies (bottom-right panel of Figure 1). These correspond to $\sim 0.01\%$ of the whole 5-million sources DES catalogue. Template fittings and analysis have been performed on these 606 objects only, as described in the next section.

2.3 Determining Redshift and Physical Properties

2.3.1 Template Fitting Procedure

In order to confirm candidate $z \sim 4$ massive galaxies, the redshift and physical properties of the sources selected up to this stage were calculated. This was done using the photometric redshift code HyperZ (Bolzonella et al. 2000) combined with ancillary scripts for the calculation of the stellar

⁶ The VHS photometry, in the Vega magnitude system, was converted to the AB system to match the DES one according to the following relations: $J_{AB} = J_{Vega} + 0.916$, $H_{AB} = H_{Vega} + 1.366$, and $K_{sAB} = K_{sVega} + 1.827$. Source: <http://casu.ast.cam.ac.uk/surveys-projects/vista/technical/filter-set>

⁷ https://www.noao.edu/meetings/decam/media/DECam_Technical_specifications.pdf

⁸ <https://www.eso.org/sci/facilities/paranal/telescopes/vista.html>

mass, as in our previous works (Daddi et al. 2005; Maraston et al. 2006). HyperZ compares model spectral energy distributions of stellar populations (which are referred to as templates) to observed photometric data, and selects the best models using a χ^2 minimisation method. HyperZ outputs the photometric redshift, the best-fitting template, and a reduced χ^2 value (χ_r^2) for the best-fitting template, calculated as $\chi^2/(N-1)$, where N is the number of filters.

Additionally, a series of input parameters can be modified in order to more finely control the way HyperZ operates. These are: age limits, magnitude limits, redshift range and binning, reddening law, and template setup. We discuss them later. We have explored different combinations for fitting and model setup, which we now describe. We should say in advance that the final results are robust against these parameter variations.

Each galaxy spectral energy distribution model (the template) is calculated assuming a star formation history (SFH, detailing the mode of star formation, e.g. single burst, exponentially-declining star formation, etc.), an age (t parameter, which runs from the start of star formation at $t = 0$ through the galaxy evolution, at logarithmic time steps from 1 Myr to the age of the Universe at the given redshift and assumed cosmology), a chemical composition, and a reddening by dust. Each model is redshifted at various values of redshift and a χ_r^2 is calculated for each redshifted model.

The redshift range we explored here varied from 0 to 6 in steps of 0.05, consistently for each fitting run. A variegated selection of 32 sets of model spectral energy distributions based on the Maraston (2005) evolutionary population synthesis models (M05) was used at each run, spanning a wide variety of star formation histories (SFHs; as in Maraston et al. 2006). These include single-bursts simple stellar populations, τ (exponentially declining), truncated (constant until an instantaneous decline to zero, to simulate rapid quenching), and constant SFHs, each of them calculated for a grid of 221 ages and four metallicities ranging between 1/5 to twice solar. All the runs were repeated for two reddening laws: the so-called ‘SMC’ law (Prevot et al. 1984; Bouchet et al. 1985) and the well-known ‘Calzetti’ law (Calzetti et al. 2000). For each the extinction parameter A_V was allowed to vary between 0 and 3, in steps of 0.5. These two reddening laws were selected because they are maximally different among the options offered by HyperZ and they are appropriate for different classes of high-*z* galaxies. Maraston et al. (2006), by exploring all options in HyperZ, concluded that these two are those identifying the best fits in most cases of $z \sim 2$ galaxies, and that while Calzetti’s law is calibrated with starbursts, the SMC seems to be more appropriate for passive galaxies (as also concluded by Kriek & Conroy 2013). We assumed a Salpeter (1955) IMF for all model options. Furthermore, we used an age cut to retain only solutions older than 0.1 Gyr, which is commonly used in order to avoid age-dust degeneracy pushing the fits towards low ages; we have tested that our results, as far our best candidates are concerned, do not depend on this choice (see Section 3.4.4). Lastly, we ran the code with loose absolute magnitude limits (i.e. between -12 and -30) for all sources as we found that thanks to using at least 7 photometric bands (DES + VHS) we would instead obtain stable results and also avoid the risk of over-fitting.

Relevant to this work, we have expanded the public

version of HyperZ by adding the calculation of the redshift probability distribution function (PDF; see also Pforr et al., 2018 *in press*). HyperZ provides the probabilities associated with the χ^2 of all the fitted models. We calculate the PDF for the photometric redshift by summing up all the probabilities for each redshift step (0 to 6, in this case) and then normalising by the number of models (32). The sum of the discrete probabilities of each model over the redshift range equals to one. As we use the same redshift bin (0.05) throughout the explored redshift range (0 to 6) for all fitting runs and the model templates contain the same number of ages (221) we should be minimising the risk of artificially favouring particular solutions.⁹ The photometric redshift PDF is critical in order to distinguish high-probability high-redshift from lower-redshift distributions. We shall use PDFs, among other indicators, in order to determine the robustness of our final candidates.

2.3.2 Visualisation and Analysis of the Results

For each candidate, we then analysed simultaneously both the best-fit result (the photometric data along with the best-fitting model) as well as the photometric redshift PDF. Examples are shown in the top two panels of Figure 3.

In the model fitting plot (left-hand side) the photometric data (red) are matched to the template fluxes (blue), corresponding to the best fitted model (solid black line) when adjusted for the response function of the telescope camera in each band. The physical parameters of the best fitting model, the age (in Gyr), the stellar mass (in M_\odot) and the χ_r^2 are labelled. Axis labels include observed and emitted wavelengths.

The probability distribution of photometric redshifts is shown in the upper right-hand panel (in red for the curve relative to the fit in the top-left panel), where a vertical line is drawn at the value corresponding to the best-fitting model.

In some cases, the most probable solution (i.e. the peak of the curve) may not correspond to the redshift of the best fitted model. This happens when several less probable solutions (model fits with worse χ_r^2) have similar redshift value and therefore sum up to show a higher peak in the PDF plots. It can happen that the less likely, but numerous solutions sum up such as to create another maximum which competes with the one of the best-fitted solution. As it will be described later, we only accept as massive high-*z* galaxies those for which the best fitted model’s redshift matches the most probable solution (i.e. peak of the curve).

Additionally, we also indicate the value of the z_{BPZ} as calculated by the DES pipeline (dotted-dashed vertical blue line). It is important to stress again that the DES z_{BPZ} was trained with sources up to $z \sim 1.3$ therefore this procedure could not produce any solution at higher redshift.

For each candidate, we further tested the effect of assuming the DES BPZ redshift as its true redshift, and explored the resulting quality of fit and the derived physical parameters. To this aim we run a different version of HyperZ

⁹ We note, however, that as galaxy colours may vary non-linearly, the colour-space may not be evenly sampled in spite of an homogeneous age sampling in all templates.

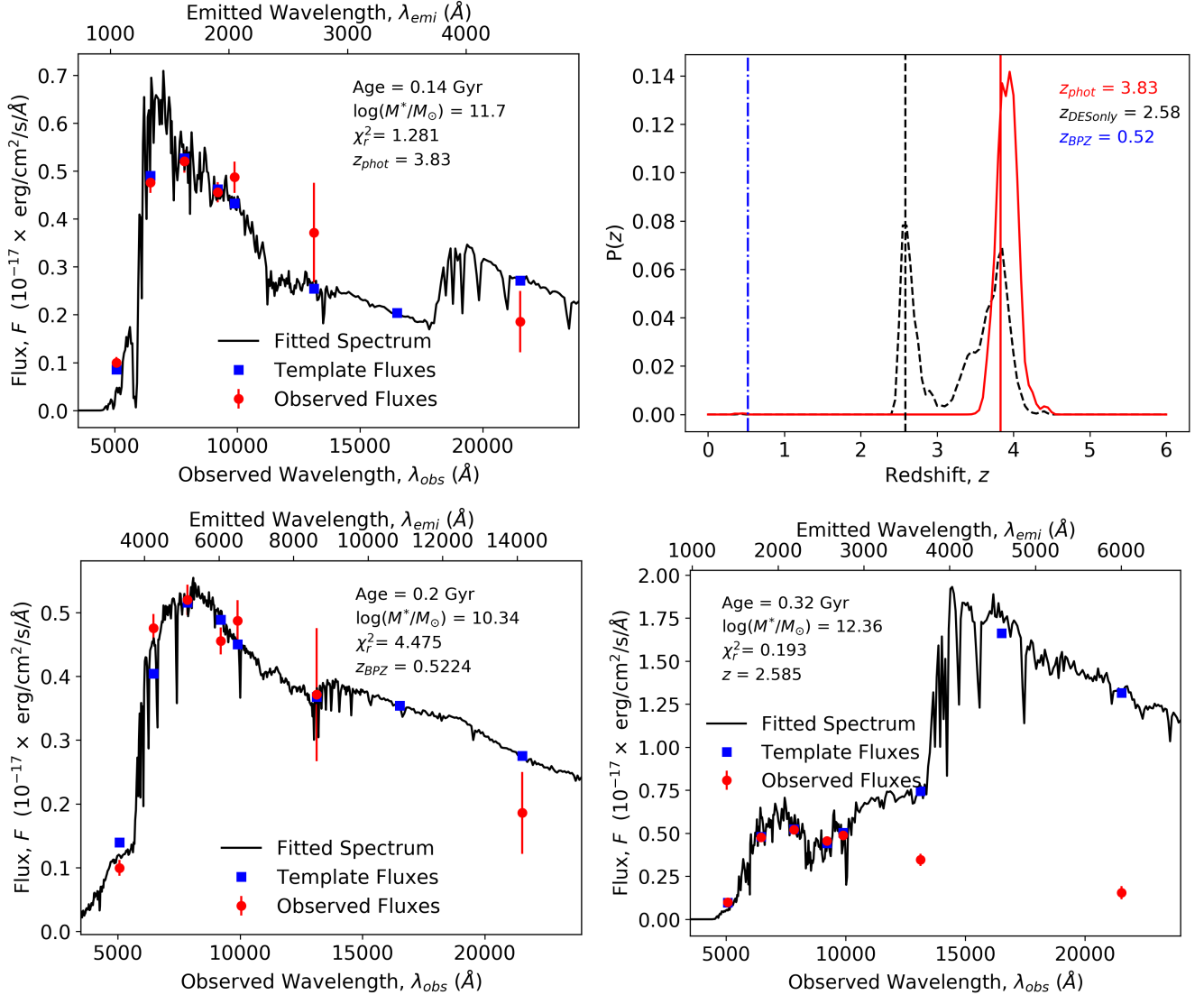


Figure 3. A comprehensive display of template fitting results (for object with ID 494790027 as an example). **Top-left:** Template fitting showing the best fitting model spectrum (solid black line) with overlaid data (red circles) with error bars, and the template fluxes (blue squares) to which the data have been fit. The derived properties age (Gyr) and stellar mass (in log and solar units) are labelled, along with the reduced χ^2 and redshift of the best fitting model. **Top-right:** The PDF of the template-fitting redshift is shown as a solid red line (the best result is marked by a vertical red line), the same for the case of only using DES bands for the fitting is shown in dashed black, and the DES BPZ value in dotted-dashed blue. **Bottom-left:** Template fitting having fixed the redshift to the value of z fixed according to the DES BPZ. This results in a considerably worse fit than when the redshift is allowed to vary (top-left), suggesting that the most likely solution is the high-redshift one. **Bottom-right:** Fitting as in top-left, but only for the DES bands while the VHS bands are plotted for reference; the redshift result confirms a high redshift (i.e. 3.28 instead of 3.80), but it can be seen that, since the overlaid VHS band fluxes are far from the model template fluxes, the result does not represent the correct template.

(named HyperZ-spec), which fixes the redshift to a known value, and repeated the fitting runs keeping the stellar population model setup as before. The result for the same high- z candidate can be seen in Figure 3 (bottom-left). In this case we must compare absolute and not reduced χ^2 values as the χ_r^2 figures are calculated in the same way in both codes (as $\chi^2/(N-1)$), but in HyperZ-spec the redshift is fixed.

We find that the absolute χ^2 of the fit at the fixed DES BPZ redshift is considerably larger than the one obtained leaving the redshift free (26.850 vs 7.686). The $\Delta\chi^2$ in this example (~ 19) implies that the low-redshift solution is in-

consistent with the best-fit high-redshift solution at the $> 2\sigma$ confidence level. The best fit corresponding to the DES BPZ redshift is also visually less convincing. The physical properties (lower mass and older age) are consistent with a low-redshift solution.

Lastly, we tested the effect of fitting only DES data vs fitting DES+VHS data. An example is shown in Figure 3 (bottom-right). The fit obtained without VHS bands (hence with the 5 DES bands only) is different in terms of physical parameters (compared to the top-left panel fit, in which VHS bands were fit as well) and the very low χ_r^2 value (0.045) indicates that DES-only fits are prone to over-fitting due to

the low number of bands. When the same galaxy is fitted with the additional VHS bands (top-left panel) we verify, as we saw earlier, that the ‘only-DES’ fitting did not correspond to the real solution, showing the importance of extending the photometric data to, in this case, the near-IR (see Section 3.3 for a quantitative evaluation on the effects of using the VHS bands in model fitting). The PDF of this type of fit is plotted in black on the top-right panel plot.

In Figure 4, as an illustration, we show the effect of the assumed reddening prescription on the fitting results. For this specific galaxy, the fit performed with the SMC-law releases a slightly lower redshift and χ_r^2 value, along with minor changes in terms of mass and age, compared to the results obtained using the Calzetti-law. A similar trend is seen in the correspondent PDFs. The PDFs referred to the fits with only DES bands are somewhat broader, but still peak at high redshift.

3 RESULTS

Starting from ~ 5 million sources, the exclusion of stars, blended sources, galaxies with uncertain data (large errors) and objects lacking VHS photometry was followed by a filtering with the theoretical colour-colour selection maps and a final visual inspection, which left us with 606 candidate massive high- z galaxies. These candidates were submitted to stellar population model fitting.

Since we focus on the high-redshift population in this paper, we proceed with a series of selection cuts (described in the next section) in order to identify the best high- z , massive galaxy candidates. In future studies, we shall explore the wider zoology of all sources falling into the selection box.

3.1 Selection of the Best Candidates

From now on, we consider the results from HyperZ runs for all 606 sources as obtained with the two reddening laws mentioned earlier. This results in two fitting results for each object. We then proceed to select the most secure sub-sample of galaxies at $z \geq 3$. To this aim, we performed three additional cuts, namely: i) we excluded those galaxies with unphysical stellar mass ($\log_{10}(M^*/M_\odot) > 12.5$); ii) we excluded objects whose fits have $\chi_r^2 > 3$ (this value was chosen considering the number of fitted bands and values typical of high- z galaxies, e.g. Maraston et al. 2006); iii) we excluded objects for which the probability of a $z \geq 3$ solution is less than 95% (corresponding to a 2σ confidence level), determined by looking at the PDFs of each object.

The number of individual galaxies passing all selection cuts is 233. With respect to the adopted reddening, 109 fitting results pass our selection criteria when using the SMC law and 203 with the Calzetti law case. This means that some galaxies satisfy the selection criteria for both reddening laws and therefore have been selected twice. The sample of 233 galaxies constitutes our *best candidate* pool. Their fitting properties are given in full in Appendix A.

The redshift distribution before and after all the cuts described above is shown in Figure 5 (here we also show template-fitting photometric redshift results for galaxies at $z < 3$) for the SMC-type of runs and the Calzetti-type in the left-hand and right-hand panels, respectively. The 606

sources from the $z \sim 4$ selection box of Figure 1 (bottom-right panel) are shown by the solid black line; the objects with $\log_{10}(M^*/M_\odot) > 12.5$ are identified by a grey shaded area; the red hatching indicates galaxies with $\chi_r^2 > 3$; the shaded orange area finally highlights the sources with high- z probability of at least 95% (note again that the best redshift solution may not correspond to the most probable one). The cuts are applied in series, as shown.

If we consider an average mass value of $\sim 10^{11.7} M_\odot$, the expected counts according to De Lucia et al. (2006) galaxy formation models, as plotted in Figure 1 of D13, are ~ 1000 at completion of DES. For our case (~ 2.7 million sources, when including star-galaxy separation and error cuts, instead of the expected value of 300 million upon completion, i.e. 1%) this would mean ~ 10 objects. We find 233 candidates, a value which lies an order of magnitude above the prediction of those models. Before drawing conclusions, however, we intend to spectroscopically confirm our best candidates.

We should also stress again that we have been very conservative for this initial paper. For example, galaxies with non-detections in VHS bands could still be high- z objects perhaps dominated by very young stars and faint in rest-frame optical, and objects with potential blending issues are not necessarily low-redshift interlopers. It will be the subject of future work to study the excluded objects.

3.1.1 On AGN contamination

A further source of uncertainty is the random presence of AGNs in the best candidates, whose effect could be to make some magnitudes brighter thereby possibly affecting the derived stellar mass. On the other hand, the AGN can be obscured and buried in the centre of the galaxy host which would not affect our template-fitting results. High- z galaxies dominated by AGNs are expected to look like point-like sources (even though not all point-like sources are expected to host an AGN and not all galaxies hosting an AGN would have their flux dominated by it). A way to quantify the point-likeness of a source is to compare the magnitudes of the object over an extended aperture with its PSF magnitude, as for a pure AGN these two quantities are the same. For all our best candidates we have evaluated a parameter, dubbed σ_{AGN} , which is meant to quantify this magnitude difference and is defined as:

$$\sigma_{AGN} = \left| \frac{i - i_{PSF}}{\sqrt{i_{err}^2 + i_{PSF}^2}} \right|, \quad (1)$$

where i and i_{PSF} are an object extended and PSF i -band magnitudes, respectively, and err are their respective errors.

Figure 6 show the results, by plotting the magnitude difference to the PSF vs the PSF magnitude, with each object being coloured according to the σ_{AGN} parameter, a 0 value of which means a complete point-like case. We also plot as blue crosses three, randomly selected objects from the COMMODORE catalogue with $\sim 100\%$ probability of being stars. They do lie precisely at the PSF zero-level (dashed line), as expected.

We see that our candidates span a range in ‘extension’, but several lie on the point-source line although they have been classified as galaxies rather than stars by the DES

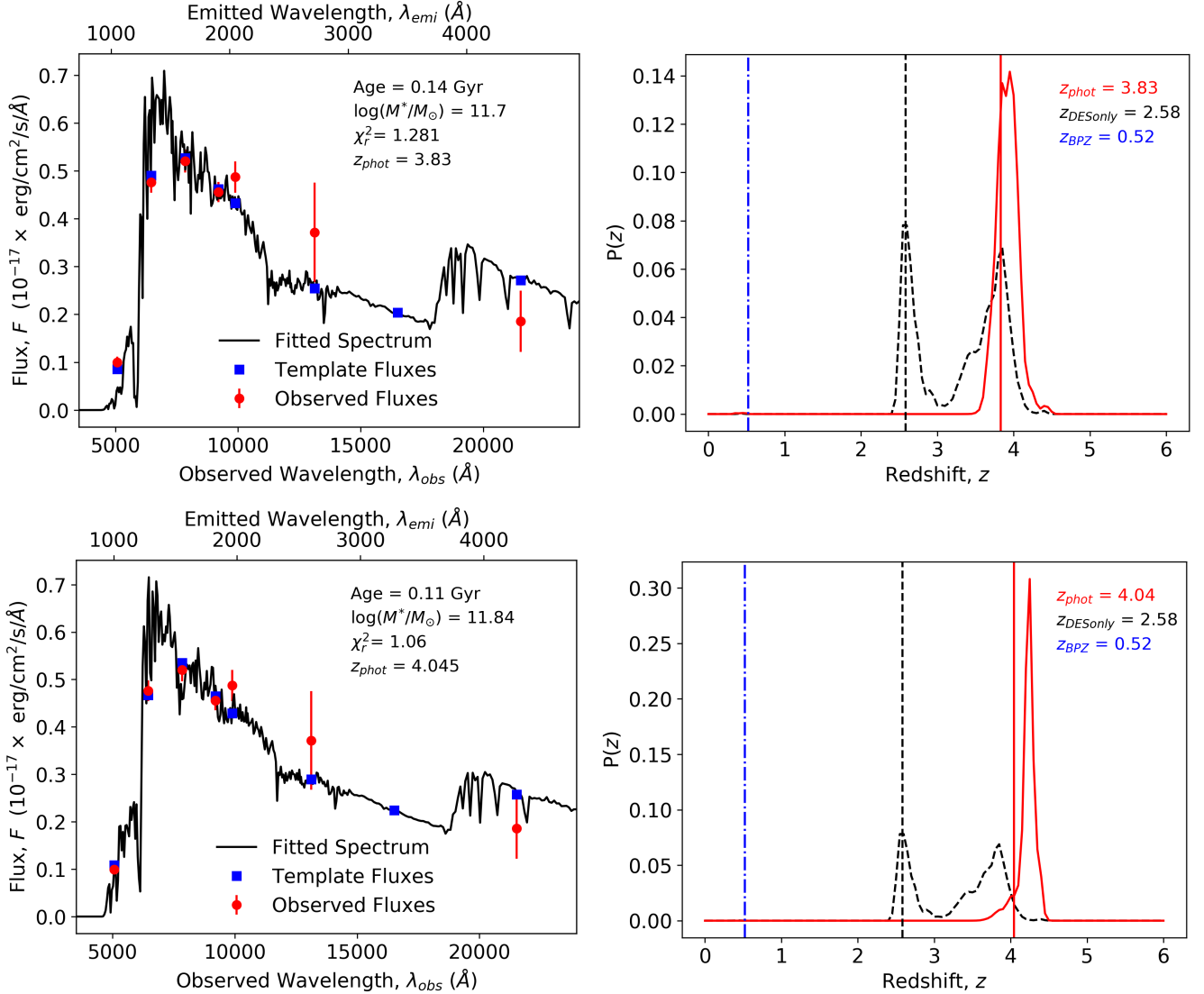


Figure 4. Legend as Figure 3. Fittings and PDFs for a high- z candidate for the various reddening laws (one in each row respectively), from top to bottom: SMC law, and Calzetti law. Compared to the SMC result for this object, the solution obtained with the Calzetti law has got a negligibly higher redshift and lower χ_r^2 , and displays minor changes in mass and age. ID of object shown here: 494790027.

pipeline. This may imply that they lie at very high redshift or that they host an AGN or a combination of both. As using this information in any quantitative way would be completely arbitrary, we just provide the σ_{AGN} values in the data tables along with all other template-fitting results (Appendix A), but we do not include it in our selection process.

3.2 Properties of the Best Candidates

The fitting results for the best candidates are given in Tables A1 and A2 for the two reddening laws, respectively. The results include, along with the photometric redshift, mass, and age, the star formation history (SFH) and its corresponding metallicity, Z/H (Z_\odot), of the best-fit template, and the absolute magnitude in the i band as calculated by HyperZ. All the outlined results are obtained using the photometry, with relevant errors, reported in Table B1.

Figure 7 shows all relevant plots for one candidate as an example. The same plots for the other candidates can be downloaded at this [link](#).

First we show image cutouts in the various photometric bands available, with a green circle indicating the galaxy position. Notice how, as expected, the galaxy is barely visible in the bluest band (g band), which is the drop-out band at these redshifts. We also point out when bands are not available. The panels below the tiles display: the spectrophotometric model fitting (upper-left), the redshift PDFs (upper-right), the spectrophotometric model fitting obtained when the redshift is fixed to the z_{BPZ} value (bottom-left), and when only the DES bands are used (bottom-right).

In the spectrophotometric model fitting plots (similar to what was shown before in Figure 3), the black line shows the best-fitting model spectrum, the blue squares are the fluxes of that model in the DES and VHS filters and the red points are the observed data in the same filters. Some key parameters

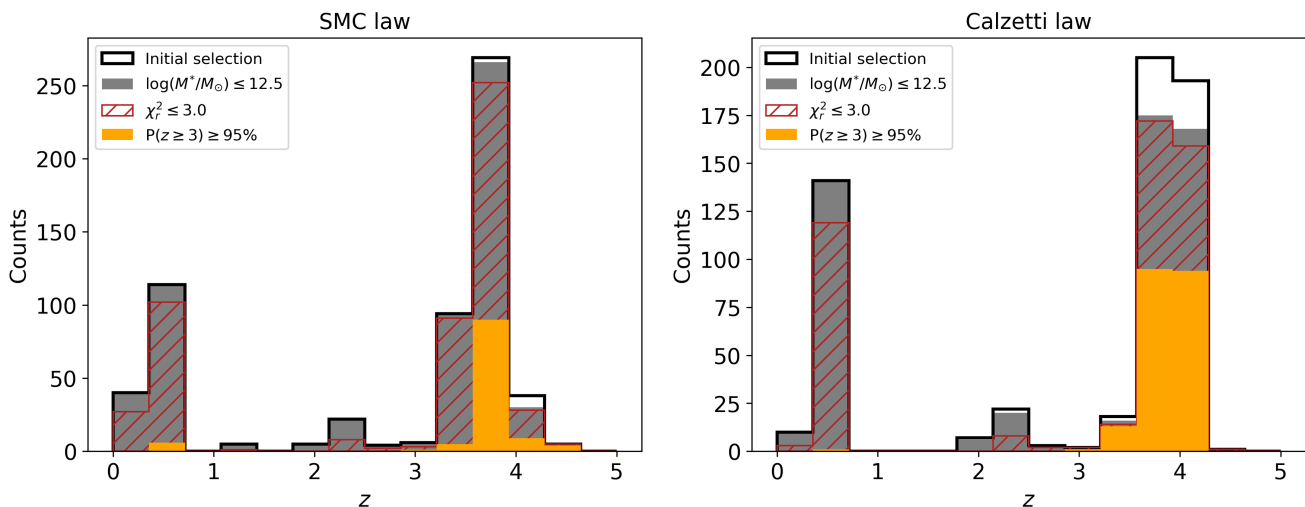


Figure 5. Redshift distribution for the 606 galaxies as found in the selection box of Figure 1 (bottom-right panel). The different cuts, applied in series, shown on the histograms illustrate our selection procedure, namely: all fitted galaxies (solid black line); those with a physical mass (filled grey bars); those fitted with a $\chi_r^2 \leq 3.0$ (hatched red); those passing our photometric redshift PDF criteria (orange bars). The two panels display the cases of SMC law on the left and Calzetti law on the right.

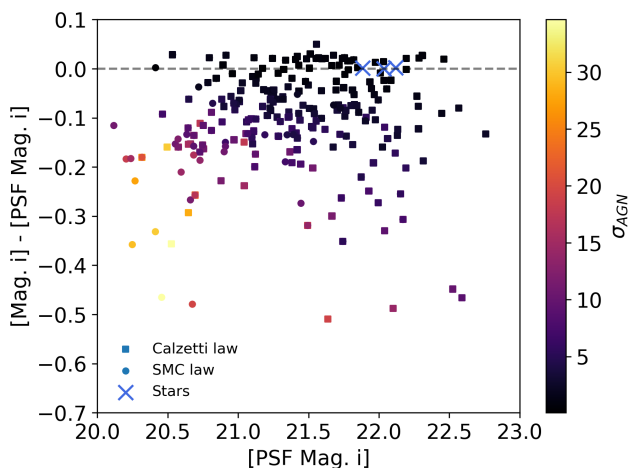


Figure 6. Difference between measured magnitude (MAG_DETMODEL) and PSF magnitude in the i band for the best candidates (distinguishing between those found with the SMC or the Calzetti law) plotted against the PSF i magnitude. Symbols are coloured by their σ_{AGN} values (see text). The further away a galaxy is from the zero-level (dashed line), the brighter it is compared to the PSF magnitude, suggesting that it is resolved and less likely to be an AGN. Three stars are also plotted as blue crosses and they lie on the zero-level line, as expected for clear point sources.

of the model¹⁰ are printed on the plot, the age (in Gyr) and the stellar mass (in $\log M_\odot$), along with the χ_r^2 .

The upper right plot shows the photometric redshift PDF using all available bands (red), DES only bands (black), and the best redshift from the DES pipeline run of BPZ (blue). Not surprisingly, the DES BPZ redshift favours lower

solutions, typically around 0.3. In order to probe the type of fitting we would obtain had we assumed the low- z solution as the correct one, we use the DES BPZ value as the true redshift and run HyperZ-spec, keeping all other parameters identical.

The result for this type of run is shown, for instance, in the bottom-left panel of Figure 7 (and at this URL for other objects). As expected due to the small redshift, the model fitting results in a lower mass galaxy ($\log M \sim 10.3 M_\odot$), though with a similar age, and generally a worse fit. The bottom-right panel instead shows the fit for the case when only DES bands have been used to run HyperZ. We can see that the fit remains good, but as a very small portion of the spectrum is fitted (corresponding to the rest-frame UV at these redshift) the physical solution differs from the one obtained when fitting all available bands. Interestingly, the photometric redshift remains high (although not as much), which reinforces the use of DES-only bands in D13 as a discriminator of high- z , massive galaxies. This can be appreciated by looking at Figure 8. Here, all best candidate galaxies' three types of redshifts ($z_{DES+VHS}$, $z_{DESonly}$, and z_{BPZ}) are shown as red, black, and blue histograms, respectively. In Section 3.3 we shall discuss in more detail how the addition of VHS data to the DES data affects our fitting results.

We summarise the properties of our best candidate galaxies in Figure 9, in comparison with the initial sample of 606 galaxies (among these here we only show galaxies at $z \geq 3$). The solid orange bars show the distribution of stellar masses, ages, and the goodness of these fits (i.e. χ_r^2), for the best candidates. Objects from 606 at $z > 3.0$ are distributed according to the solid black line, with those having physical mass $\log_{10}(M^*/M_\odot) \leq 12.5$ shown by the filled grey bars. The cut in $\chi_r^2 \leq 3.0$ is highlighted by hatched red bars. Furthermore, the PDF cut (probability of at least 95% of being at $z \geq 3$) shrinks the distribution in what is shown with the filled orange bars which match also correspond to the best candidates. The final histograms show that the many

¹⁰ The other model parameters are given in Table A1

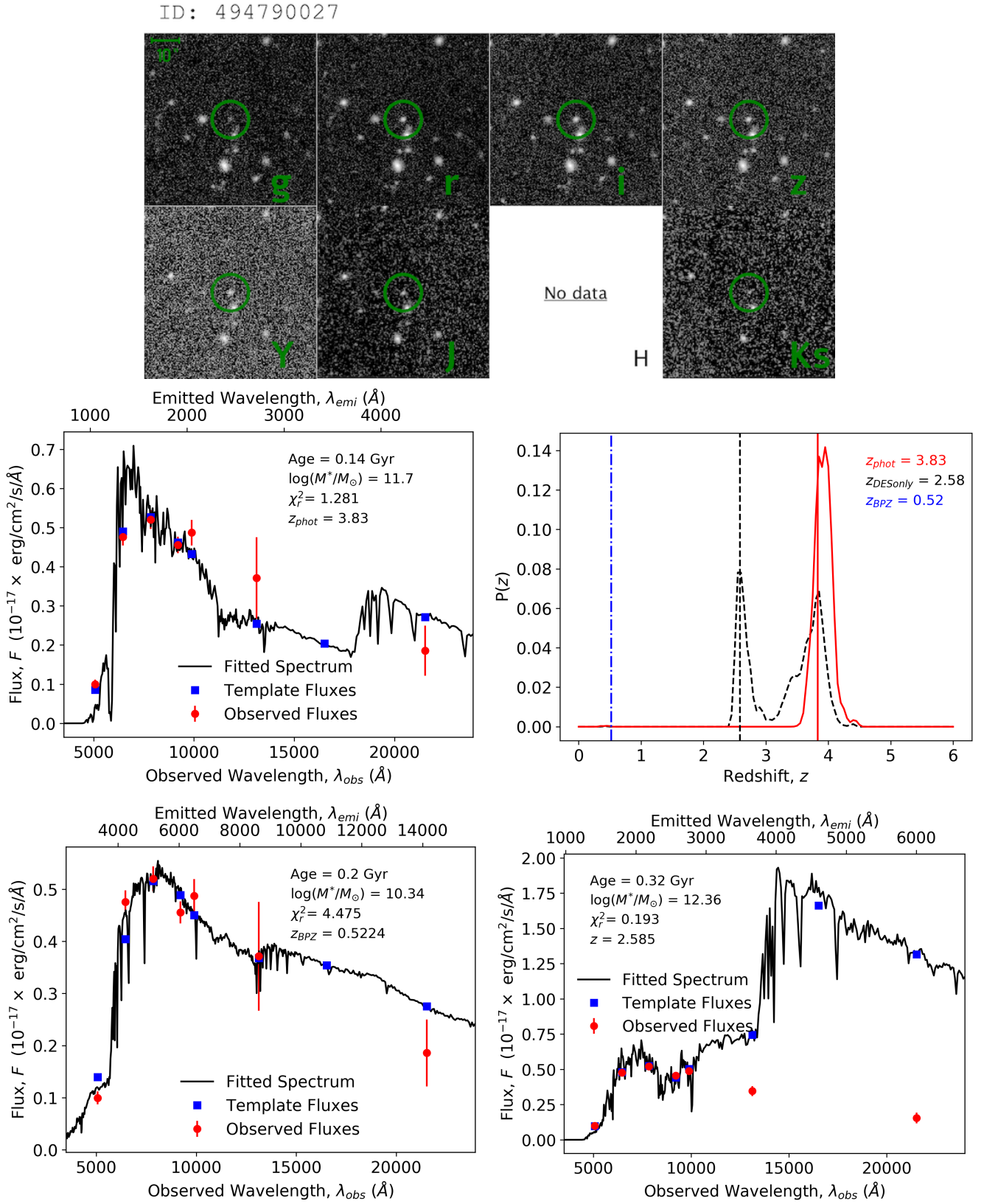


Figure 7. The observation images for all available bands (DES and VHS), the best fit, the PDF, the fit with fixed redshift according to z_{BPZ} , and the fit only using DES bands for one of our best candidates. For the galaxy images the green circles indicate the sky position of the galaxy; if the circle is red it means that the photometry is not available for that given filter. If VHS observations are not available, for one or more filters, the image is replaced by text saying so. For the plots below the images (bottom four panels) the legend is the same as in Figure 3. The rest of the best candidate plots and images can be found following this [link](#).

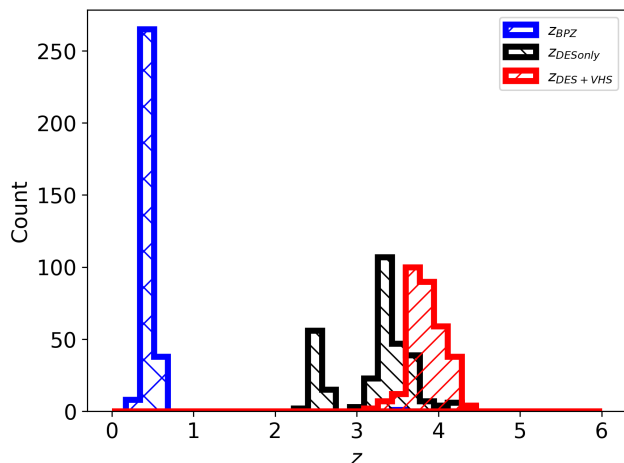


Figure 8. The distributions of $z_{DES+VHS}$, $z_{DESonly}$, and z_{BPZ} for the best candidate galaxies are plotted as red, black, and blue histograms, respectively. It can be seen that even when using only DES bands to fit these galaxies, the results still tend to be at high- z and relatively close to the $z_{DES+VHS}$ ones; on the other hand, as explained earlier, z_{BPZ} values stay below $z = 1$.

quality cuts we apply do not distort the initial distribution of galaxies. More quantitatively, performing a K-S test, we find that we cannot reject the null hypothesis that the distributions are the same with p-values, on average for the two reddening options, of 0.27, 0.29, and 0.24, respectively for mass, age, and χ^2 . Even the objects with poorer fits trace similar galaxy physical properties. All the cuts are applied in series, one after the other.

Our best candidate galaxies have large stellar masses $10^{11.5} \leq M/M_\odot \leq 10^{12.5}$, ages ~ 0.1 Gyr, have been forming stars following a rapid mode generally consistent with an exponentially-declining mode with short e -folding time, $\tau = 0.1 - 0.3$ Gyr, or a truncated model with similarly short timescales. Metallicity is generally high ($Z > Z_\odot$). Our derived ages tend to cluster around the lower age limit set in HyperZ (0.1 Gyr). This is to be expected as - in χ^2 minimisation fitting of stellar populations containing young components - the best-fitting model tend to be associated to the youngest possible age, especially when only UV/optical bands are fitted. When this happens, as the energy emission of young stellar populations is order of magnitudes higher than that of older populations, the youngest models will dominate the fit, an effect that is known as ‘over-shining’ (Maraston et al. 2010). Hence, if we allow the fitting procedure to use any value of age, rather than an age estimate for the whole galaxy, we tend to obtain the age of the last generation of stars, which may contribute very little by mass. This over-shining effect may hamper us to recover realistic galaxy stellar population properties, in particular making stellar mass estimates unreliable. In order to circumvent this problem, it is common to adopt a lower age limit in the fitting procedure (e.g. Daddi et al. 2005), which is usually set to an age (0.1 Gyr) when the most massive stars are already dead (for passive models). It is not guaranteed that such a limit ensures fully realistic ages for all galaxies, which may still be biased low. If this is the case, our stellar mass estimates will be lower limits of the true stellar mass.

In Section 3.4.4 we shall assess the effect of this assumption on the two main properties we are interested in, namely the photometric redshift and the stellar mass.

Results are summarised in Table A1 and A2. The results of the model fitting are also consistent with the simulations of D13 and with being a younger version of the stellar populations inhabiting the most massive galaxies in the local universe (Thomas et al. 2010).

Looking in more detail at the redshift and physical properties of the best candidates we can see that, compared to the assumption of an SMC law, the use of the Calzetti law often pushes redshifts and masses to higher values. All this information is summarised in Figure 10, where we show fractional distributions for each reddening law (hatched dark red for SMC law and deep pink solid line for Calzetti law) in terms of redshift, mass, and age, respectively.

The SFHs of these candidates also allow us to create a visual representation of the mass assembly and SFR of such galaxies. These are shown for two different types of SFH in Figure 11, which represent the vast majority of the best candidates. They are: $t_{trunc} = t$ and $e^{-t/\tau}$ (red and blue, respectively), plotted in the left panel for the mass assembly and in the right one for the SFR. These rapid timescales point to formation redshifts close to $z \sim 5$, which is in agreement with what is deduced from the fossil record of local high stellar mass galaxies (we shall return to this point in the discussion). Note that even if these SFRs appear extreme, values of tens of thousands of solar masses per year have already been recorded in the literature (e.g. Rowan-Robinson et al. 2016). The results from both reddening options are plotted together.

Let us conclude with a comment on the population model effect. Here we assume Maraston’s models, while results in the literature are usually based on Bruzual & Charlot (BC) models. As is well known, ages derived with Maraston models for high- z galaxies are smaller than those based on BC models, which results in smaller stellar masses M^* by e.g. ~ 0.2 dex (depending on the fitted ages). This is due to the different prescriptions for the thermally pulsing asymptotic giant branch (TP-AGB) and to the different onset age for the RGB assumed in the underlying stellar tracks (see Maraston et al. 2006). Hence, our estimates of age and M^* lie likely on the lower side than what we would obtain had we used BC-type models.

In Section 4 we shall discuss the results we obtain when we re-fit some of the galaxies recently reported in the literature, including the Glazebrook et al. (2017) object, with Maraston models and our fitting procedure.

3.3 The Effects of Fitting DES-only vs. DES+VHS Bands

Given our database and modelling, we are in the best position of quantitatively assessing the effect of using only DES bands and DES+VHS bands on the results of template fitting. Figure 12 summarises the results. Here we plot photometric redshifts (left-hand panel) and stellar masses (right-hand panel) for all 606 sources as determined via template fittings using only DES bands (y-axis) or DES+VHS bands (x-axis). The best candidates are highlighted in dark red and deep pink, also distinguishing those obtained when as-

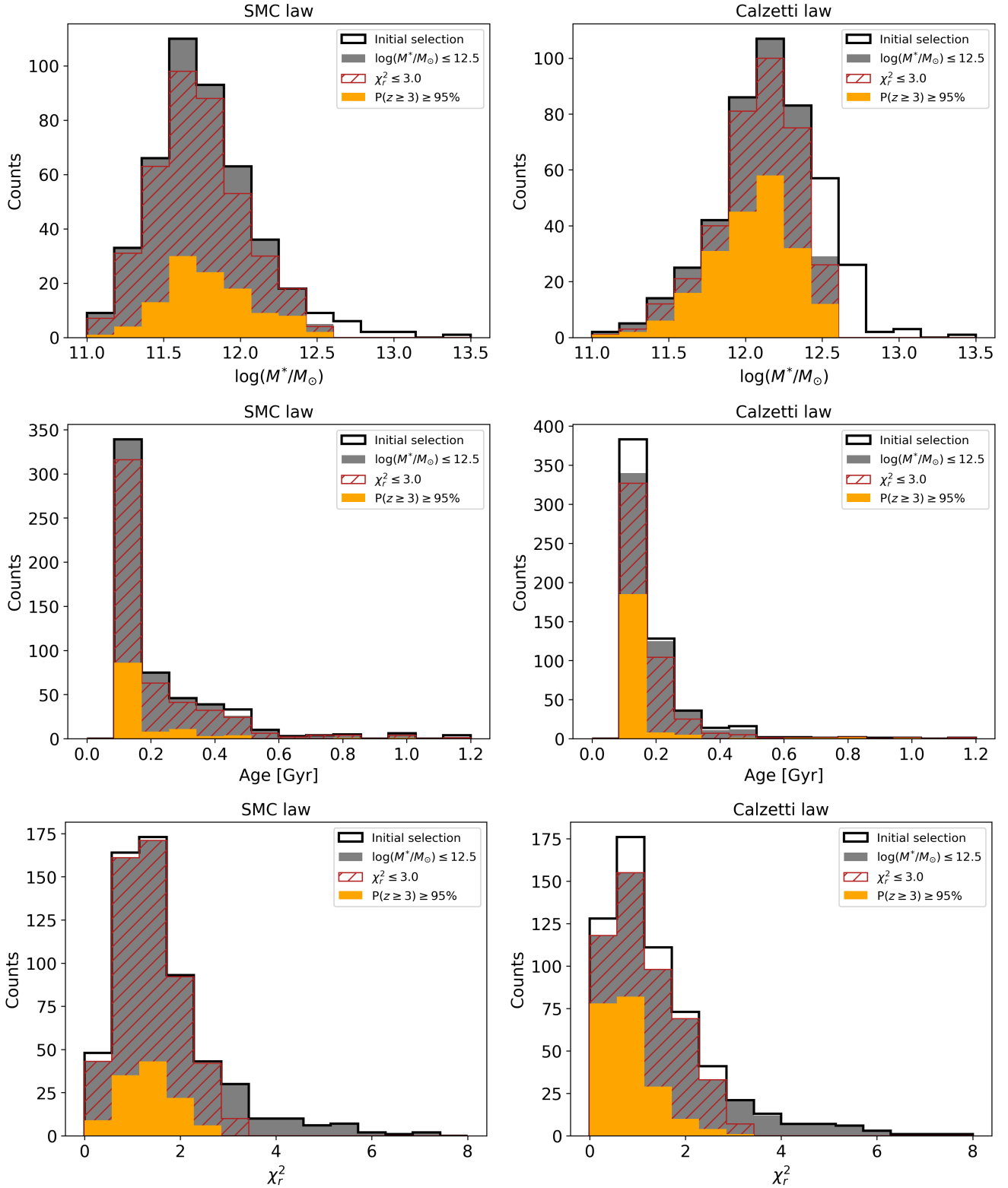


Figure 9. M^* , age, and χ_r^2 for the $z > 3$ candidates within the sample of 606 sources from the colour selection box. Legend as in Figure 5 (except for redshift cut (i.e. $z \geq 3$) applied to the initial selection). This is shown for all two reddening options (SMC law and Calzetti law) in the first and second columns, respectively.

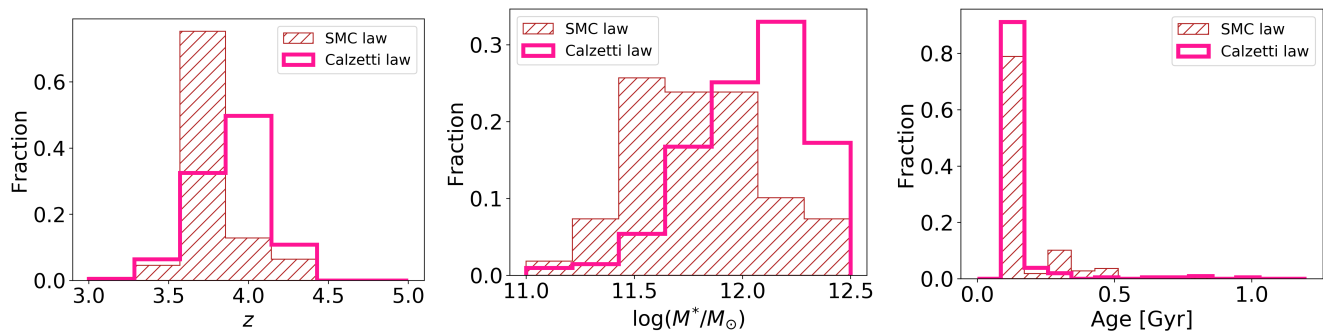


Figure 10. Distributions of (from left to right) photometric redshift, stellar mass, and age in terms of fraction for the best candidates found with the two different reddening laws: SMC law (hatched dark red bars) and Calzetti law (solid deep pink line).

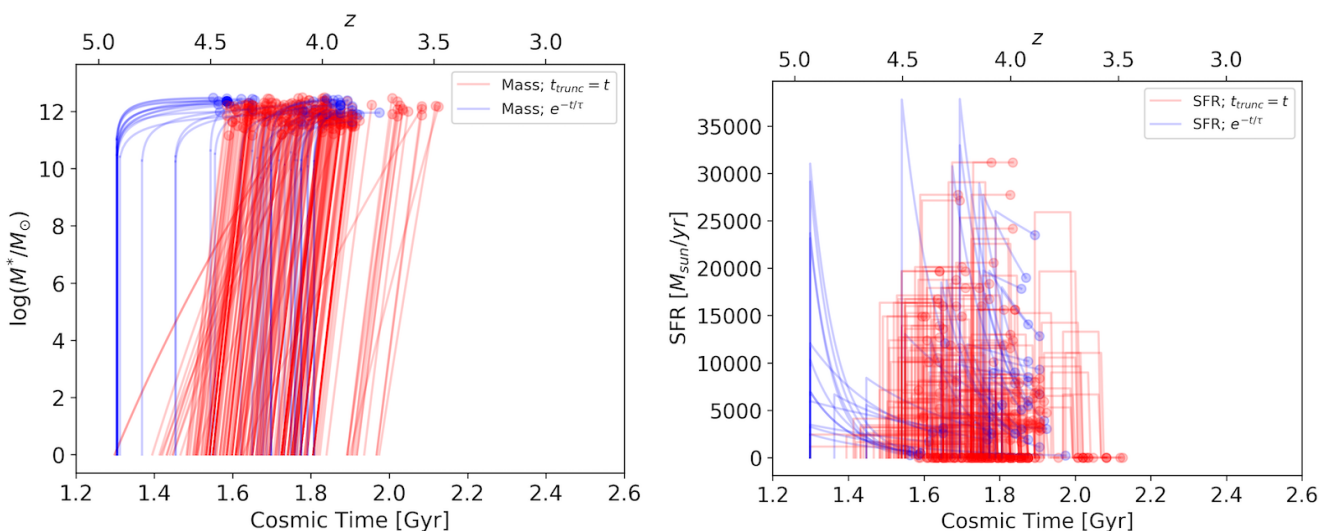


Figure 11. Galaxy mass assembly derived for the best candidate galaxies. Typical SFHs as $t_{trunc} = t$ and $e^{-t/\tau}$ are plotted in red and blue respectively for the mass assembly (left panel) and for the SFR (right panel). A few candidates with SFHs different from those two laws have not been plotted. Candidates from all two reddening options have been plotted together.

suming SMC (circles) or Calzetti (squares) reddening types, respectively.

The fitting performed with DES bands gives photometric redshifts that are always larger than 2 and very high, possibly unphysical stellar masses ($\log_{10}(M^*/M_{\odot}) > 12.5$), for $\sim 60\%$ of the galaxies. The inclusion of VHS bands in the fitting pushes the photometric redshift down to values below 2 for 25% of the sample (150 galaxies, independently of the reddening law) and their stellar masses also become lower. More generally, the addition of VHS bands results in a healthier distribution of stellar masses overall ($9 < \log_{10}(M^*/M_{\odot}) < 12.5$), with only $\sim 2\%$ of objects having $\log_{10}(M^*/M_{\odot}) > 12.5$. This confirms the notion that by fitting a wider wavelength range in the data we recover the physical properties of galaxies (as shown, for example, by Pforr et al. 2012, 2013).

More importantly for the present work, we find that the subsample of galaxies (~ 233) defining our best candidate sample remain at high redshift and with a large stellar mass independently of whether we fit only DES bands or DES+VHS bands. This confirms that our selection cut based on DES-only bands (as in Davies et al. 2013) plus the ad-

ditional criteria put forward in this paper (goodness of fits, unimodal PDF of redshift and the addition of VHS bands) are effective at selecting a robust sample of very massive, high-redshift galaxies. The combination of DES and VHS allows us to obtain more robust galaxy properties and to limit the number of low- z contaminants.

3.4 Caveats and Reliability Tests

In this section we test the reliability of our method and results. In 3.4.1 we quantify the number of low- z contaminants we found after performing spectral fitting and in 3.4.2 we comment on the number of sources expected to scatter in and out of the colour map selection box because of photometric errors. In the remaining subsections we test the effect of various parameters on photometric fitting results.

3.4.1 Contamination in the Selection Box

Colour selection based on models is a commonly adopted method to prioritise the galaxies one would like to obtain before performing the (time consuming) model fitting (e.g.

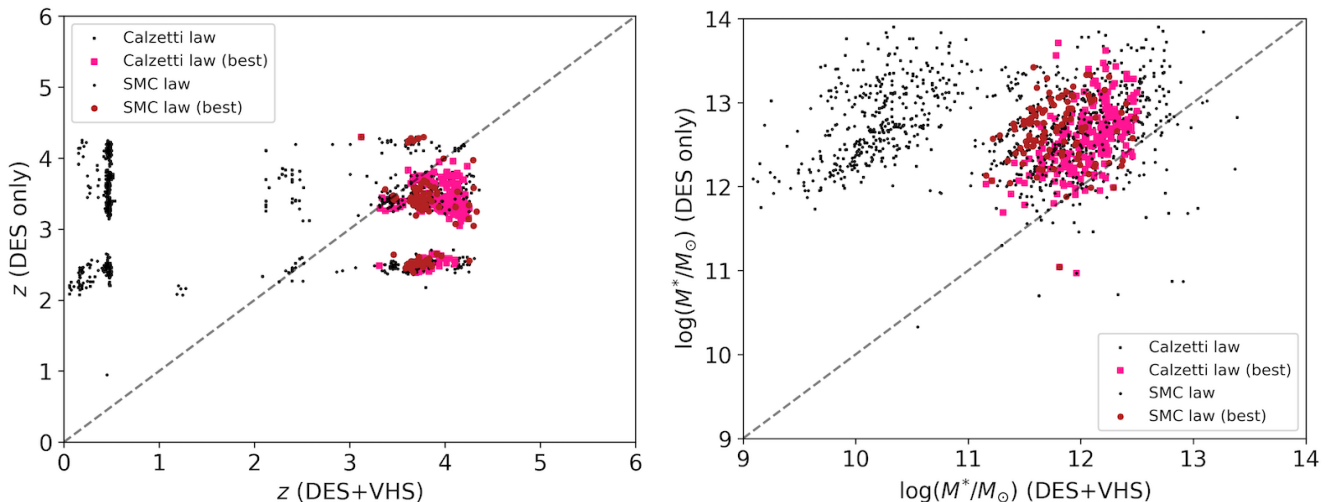


Figure 12. Comparison of the results for photometric redshift (left panel) and stellar mass (right panel) of the 606 template-fitted galaxies depending on the use of DES+VHS photometry versus the DES only data option. This is shown for both the SMC law (circles) and the Calzetti law (squares). The best candidates are highlighted in dark red and deep pink for the two reddening types, respectively, with the other sources being plotted in black. It can be appreciated that near-IR data is essential to successfully recover the true photometric redshift and mass of lower-redshift galaxies.

Daddi et al. 2005). A certain level of contaminants of various kind is expected due to various types of objects having similar colours.

D13 quantify and discuss the types of expected contaminants using DES galaxy simulations as well as real objects, and find that contamination in the $z \sim 4$ box is mostly due to intermediate-redshift galaxies (of similar colour because of their Balmer/4000 break) and quasars (D13, Figure 7). Using both DES galaxy simulations as well as real data from the MUltiwavelength Survey by Yale-Chile (MUSYC; Gawiser et al. 2006), D13 find (their Figure 11) that the $z < 2.5$ contamination in the $z \sim 4$ selection box should be 38% (consistent with the previous study by Douglas et al. 2009). Here we have the possibility of checking the D13 prediction with the real DES data after model fitting is performed. After fitting the 606 sources selected in the box, we find 34% and 32% lower-redshift galaxies for the SMC-type and Calzetti-type runs, respectively. These figures are in excellent agreement with the D13 estimates.

In conclusion, it seems unlikely that undetected lower redshift contaminants pass through the further best candidate selection cuts (in particular the redshift PDF and χ^2_r cuts), while the PSF cut should prune most pure quasars (see Figure 6).

3.4.2 Number of Sources Scattered Into the Selection Box

Photometric errors may affect the position of galaxies on our colour selection plot (specifically of the ~ 2.7 million sources without large errors and stellar contamination, see top-right panel of Figure 1). If we perturb the position (i.e. the colors) of the 3243 sources found within the $z \sim 4$ selection box according to their photometric errors in the g , r , and i bands and assuming a normal distribution, we find that $\sim 29\%$ of these sources scatter outside the box.

We can conclude therefore that of the 606 galaxies from the selection box, around 176 (or around 68 of the 233 best

candidates) could have gone unselected purely because of their random error, while the rest sits well inside the box within their error. On the other hand, it is also possible that galaxies that would be truly outside the selection box have scattered inside, which is non-trivial to model because of the non-gaussianity of the distribution. Overall, however, we stress that the colour selection served purely as a way to prioritise the galaxies to fit using stellar population models. It would be unlikely that all fitted photometric bands for the 606 sources would be affected by their errors in such a way to spuriously produce high- z massive galaxy candidates in such numbers (i.e. 233 candidates out of 606 fitted galaxies in total). Future simulation work could investigate these uncertainties quantitatively.

3.4.3 Detections vs. VHS Magnitude Limits

As mentioned before, several objects do not have VHS detections, but this does not mean they do not lie at high- z . Figure 13 shows the expected VHS J , H , K_s magnitudes, and the survey limits at 5σ confidence, for a given i DES magnitude in the case of a passively evolving model with redshift between 2 and 5 and an age of 0.1 Gyr (to represent the most common value found for our objects). Our best candidate sources (when available for a given band) are shown as dots with errors. As expected, the majority of points lie below the survey detection limits. The K_s points lying above the relative limit refer to sources with magnitudes in the other bands within the detection limits to which a K_s magnitude was assigned via force-photometry. The difference between the points and the model lines can be accounted for by the varying age, stellar mass and SFH compared to the single model shown here, which should be taken as indicative. We shall use upper limits during model fitting for these non-detections in a forthcoming paper exploiting the whole DES database.

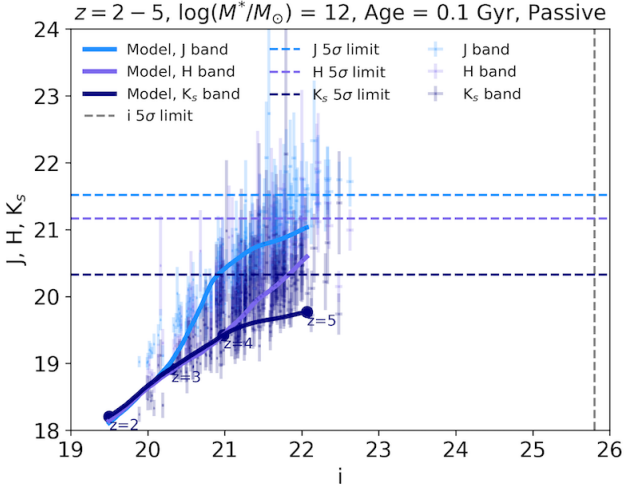


Figure 13. Expected J, H, K_s VHS magnitude for given i DES magnitude plotted as solid light blue, purple, and dark blue lines (with 5σ limits shown as dashed lines), respectively, for a passive M05 model with redshift between 2 and 5 and an age of 0.1 Gyr. Best candidate galaxies (for all reddening laws used) are plotted as dots for the available bands of each given source.

3.4.4 Age Limits in Photometric Fittings

In our model fitting we set a minimum age of 0.1 Gyr, which is larger than the minimum M05 model age (1 Myr). The setting of this limit is common practice in the literature (e.g. Daddi et al. 2005; Maraston et al. 2010) in order to contain the so-called ‘over-shining’ effect (Maraston et al. 2010) by which low levels of star formation generate luminosities that are so high that any older populations remain undetected. This effect leads to very low fitted ages, which translates into huge star formation rates and a general underestimation of the stellar mass (see discussion in Maraston et al. 2010). It should be noted that the over-shining effect is a threat mainly for a robust calculation of M^* and not for the photometric redshift, which is regulated by the SED shape. This is exactly what we find when we compare the photometric redshift and stellar masses we derive from a fitting run without an age limit (Figure 14) to our results. The plot includes results for all the 606 sources initially selected from the colour selection maps, as black dots, and for our best candidates, as larger symbols. The test shows that changing the age limit has no effect on the derived photometric redshifts (top panel) and little influence on M^* (~ -0.35 dex on average; bottom panel) as far as our best candidates are concerned.

4 COMPARISON WITH THE LITERATURE

In Section 4.1 we re-fit data from Straatman et al. (2014) to assess whether our fitting procedure recover their results. Moreover, we compare the results for our best candidates with recent literature in Section 4.2.

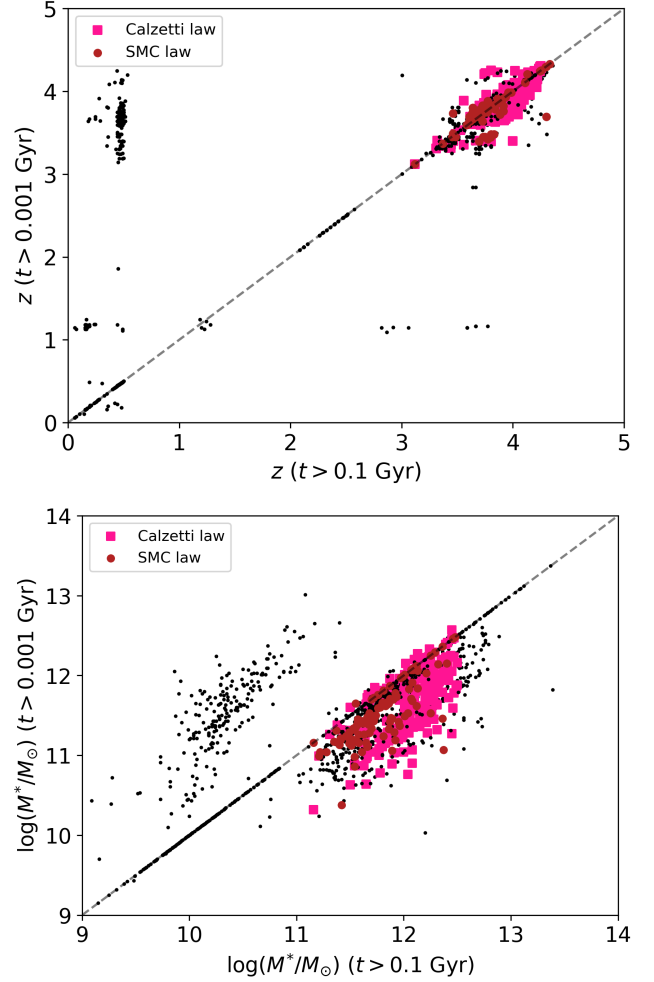


Figure 14. Effect of the minimum age allowed in the fitting (0.1 Gyr vs 1 Myr) on photometric redshifts (top panel) and stellar masses (bottom panel) of the 606 $z \sim 4$ selection box high- z candidates (black dots). Best candidates are plotted as dark red circles and deep pink squares depending on the reddening option used in the fitting (SMC law and Calzetti law, respectively). Even though redshift and masses of objects may change, our robust candidates are relatively unaffected.

4.1 Re-fitting Past Literature

As is well known (e.g. Maraston 2005; Maraston et al. 2006; Pforr et al. 2012) the results of spectro-photometric model fitting to data depend on the adopted stellar population model, the fitting setup, the fitting code, and any assumptions made (e.g. the IMF, the fitting age grid, etc.). In order to compare our results with similar ones obtained in the literature, it is useful to also adopt our fitting framework on literature data. Here we present results for the galaxies from Straatman et al. (2014). One of these objects (ZF-COSMOS-13172) is the spectroscopically confirmed $z = 3.717$ galaxy published in Glazebrook et al. (2017)¹¹. Results are summarised in Table 1, which also reports the literature values.

¹¹ This object is now named ZF-COSMOS-20115 in Glazebrook et al. (2017).

Table 1. Properties of the [Straatman et al. \(2014\)](#), ‘S14’, sample of *quiescent* (according to their own classification) galaxies compared to the values we obtain (‘us’) using our fitting setup and those bands matching our DES+VHS photometry. For each object we obtain two results according to the assumed reddening option, whose χ_r^2 is given in the last column. Note that the [Straatman et al. \(2014\)](#) stellar masses refer to a Chabrier IMF, while ours to a Salpeter IMF. The latter are ~ 0.2 dex larger, hence the [Straatman et al. \(2014\)](#) values should be increased by +0.2 dex to ensure a meaningful comparison with our derived values.

ID	z_{phot}	z_{phot}	$\log_{10}(M^*/M_{\odot})$	$\log_{10}(M^*/M_{\odot})$	Age [Gyr]	Age [Gyr]	Reddening	χ_r^2
	(S14)	(us)	(S14)	(us)	(S14)	(us)	(us)	(us)
ZF-COSMOS-13129	3.81 ± 0.17		11.25		1.58			
		4.65		11.39		0.64	SMC	0.000
		5.28		12.27		0.51	Calzetti	0.000
ZF-COSMOS-13172	3.55 ± 0.06		11.16		0.79			
		2.88		11.85		0.20	SMC	1.693
		4.13		11.82		1.02	Calzetti	4.016
ZF-COSMOS-13414	3.57 ± 0.19		10.64		1.00			
		3.84		10.77		0.64	SMC	4.103
		3.80		11.47		1.28	Calzetti	0.702
ZF-CDFS-5657	3.56 ± 0.07		10.88		1.26			
		2.71		10.50		0.51	SMC	3.786
		2.81		10.76		0.51	Calzetti	3.489
ZF-CDFS-403	3.660 (z_{spec})		11.06		0.79			
		1.76		10.62		1.80	SMC	0.034
		2.42		10.76		0.14	Calzetti	0.000
ZF-CDFS-209	3.56 ± 0.05		10.88		0.63			
		2.01		10.83		2.60	SMC	0.054
		2.05		10.53		0.29	Calzetti	0.005
ZF-CDFS-4907	3.46 ± 0.16		10.60		0.40			
		2.89		10.31		0.32	SMC	1.297
		2.89		10.31		0.32	Calzetti	1.297
ZF-CDFS-4719	3.59 ± 0.14		10.65		1.00			
		2.92		10.84		1.68	SMC	0.093
		2.83		10.90		1.43	Calzetti	0.091
ZF-UDS-885	3.99 ± 0.41		10.78		0.40			
		5.42		11.83		0.81	SMC	2.411
		3.95		12.02		1.14	Calzetti	0.410
ZF-UDS-1236	3.58 ± 0.08		10.78		0.50			
		4.27		11.41		0.64	SMC	8.198
		3.45		11.30		0.51	Calzetti	6.397

Table 1 – *continued*

ID	z_{phot}	z_{phot}	$\log_{10}(M^*/M_{\odot})$	$\log_{10}(M^*/M_{\odot})$	Age [Gyr]	Age [Gyr]	Reddening	χ_r^2
	(S14)	(us)	(S14)	(us)	(S14)	(us)	(us)	(us)
ZF-UDS-2622	3.77 ± 0.10		10.94		0.63			
		3.81		11.00		0.72	SMC	1.611
		3.87		11.41		0.90	Calzetti	0.962
ZF-UDS-3112	3.53 ± 0.06		10.63		1.26			
		3.99		10.95		0.57	SMC	6.044
		3.99		10.95		0.57	Calzetti	6.044
ZF-UDS-5418	3.53 ± 0.07		10.64		0.79			
		3.37		11.00		1.61	SMC	4.306
		3.22		10.91		1.28	Calzetti	2.806
ZF-UDS-6119	4.05 ± 0.27		10.74		0.50			
		3.91		10.84		1.02	SMC	2.040
		4.13		11.48		1.02	Calzetti	1.368
ZF-UDS-9526	3.97 ± 0.18		10.95		0.63			
		2.67		10.33		1.43	SMC	0.128
		2.67		10.33		1.43	Calzetti	0.128
ZF-UDS-10401	3.91 ± 0.38		10.58		0.25			
		3.96		10.62		0.72	SMC	0.013
		3.25		10.64		0.57	Calzetti	0.000
ZF-UDS-10684	3.95 ± 0.48		10.93		1.26			
		3.78		10.51		0.64	SMC	4.681
		3.67		10.90		1.61	Calzetti	4.526
ZF-UDS-11483	3.63 ± 0.32		11.01		1.00			
		1.20		10.25		2.10	SMC	0.000
		1.80		10.45		1.80	Calzetti	0.000

It is important to note that the [Straatman et al. \(2014\)](#) results have been obtained using 36-band photometry (with wavelength range of 3000–80000) while our DES+VHS combination grants us 8 bands at most. Hence, in order to mimic our fitting, we selected the same bands from the [Straatman et al. \(2014\)](#) database, and therefore the results of Table 1 refer to fits with these bands.

We find results that are similar in both photometric redshift and mass. Note that the χ_r^2 for most results lie slightly above our adopted cut of $\chi_r^2 < 3$ (on the other hand, one object has $\chi_r^2 = 0$ as the available photometry is made up of 3 bands out of the 8 we considered and they align with the

best fitted model). Overall, however, our method with only a few bands allows us to obtain a similar picture of galaxy evolution at high redshift.

Most interestingly, for the [Glazebrook et al. \(2017\)](#) object we obtain a best solution which includes dust and a younger age than the one reported in their paper. Our result is consistent with [Simpson et al. \(2017\)](#), who find - using ALMA and SCUBA data - dust detection in the same source, thereby questioning the quiescent nature of that galaxy. On the other hand, [Schreiber et al. \(2018\)](#) show that only 3.1 kpc away from that galaxy there is a massive, extremely obscured galaxy that they identify as the origin of the sub-mm

emission observed by [Simpson et al. \(2017\)](#). In this paper, we have not applied any particular prior on the nature of the galaxy before fitting and we provide fitting solutions with and without dust. These will be useful to potentially perform ALMA follow-ups of our candidates.

4.2 Further Comparisons with the Literature

In [Figure 15](#) we show the median values of stellar mass and redshift of the 57 galaxies from [Spitler et al. \(2014\)](#), the 7 galaxies by [Marsan et al. \(2017\)](#), the 16 galaxies by [Nayyeri et al. \(2014\)](#), and the 10 galaxies by [Merlin et al. \(2018\)](#), as a black hexagon, pentagon, triangle and a plus, respectively. The latter two studies focus on what they call ‘passive galaxies’, while we do not take any particular prior here. For comparison we also plot our best candidates (with the two usual shape and colour schemes for SMC and Calzetti laws) as well as the [Straatman et al. \(2014\)](#) sources as re-fitted by us (as light blue circles and dark blue squares for SMC law and Calzetti law, respectively).

It can be appreciated that our candidates are of typically higher redshifts and stellar masses than these previous studies and expand the envelope of results for high- z massive galaxies.

5 COMPARISON WITH MODEL GALAXIES

We use the Millennium Simulation Database¹² (volume: $(500\text{Mpc}/h)^3$) and extract the number density of galaxies with stellar masses above $\sim 10^{11}$ from different semi-analytical models, at the snapshots corresponding to $z = 3.9$ and $z = 4.1$. We find co-moving densities of $1.6 \times 10^{-5} \text{Mpc}^{-3}$ for the model described in [Gonzalez-Perez et al. \(2014\)](#), $5.2 \times 10^{-7} \text{Mpc}^{-3}$ for model galaxies from [Henriques et al. \(2015\)](#) and $5 \times 10^{-6} \text{Mpc}^{-3}$ for the model described in [Lacey et al. \(2016\)](#). These densities compare to a value of $5 \times 10^{-5} \text{Mpc}^{-3}$ for [De Lucia et al. \(2006\)](#); it is important to note that large density variations for the massive end are found in the literature (e.g. [Knebe et al. 2018](#)).

At $z = 3.9$, no galaxies from the [Gonzalez-Perez et al. \(2014\)](#) or [Lacey et al. \(2016\)](#) models have a mass above $10^{11.5}$. The same is true for the model described in [Croton et al. \(2016\)](#)¹³. This lack of galaxies with masses above $10^{11.5} M_{\odot}$ at high redshift is shown in [Figure 16](#) for [Gonzalez-Perez et al. \(2014\)](#), while most of our high-redshift candidates have masses above this limit.

Some galaxies from the [Henriques et al. \(2015\)](#) model are indeed expected to have masses above $10^{11.5}$ at $z = 3.9$, but they are rare, with a density of $7.3 \times 10^{-9} \text{Mpc}^{-3}$. This last model was designed to match the evolution of the stellar mass function up to $z = 3$ mainly by allowing the reincorporation timescale of wind ejecta to vary with cosmic time. The other two semi-analytical models do not reproduce the observed evolution of the galaxy stellar mass function above $z \sim 1$, predicting a too rapidly evolving high mass end. Moreover, models assuming warm dark matter produce more massive galaxies at high redshifts than standard cold

dark matter cosmologies ([Wang et al. 2016](#)). Thus, redshift and physical properties of galaxies in place above $z = 2$ provide crucial information to help constrain our understanding of galaxy evolution within a cosmological context. We shall compare number densities in models and data when the DES observations are complete.

In this paper we take a first glance at the physical properties - namely, colours vs. stellar mass - of massive galaxies in simulations compared to our best candidates. [Figure 16](#) presents the comparison for the [Gonzalez-Perez et al. \(2014\)](#) model run using the version based on the stellar population synthesis model from [Maraston \(2005\)](#). This was chosen as, currently, it is the only model of the five explored that provides magnitudes for the DES bands. The observed-frame $r - i$ colour of the data are consistent with a subset of model galaxies at the appropriate redshift, possibly suggesting compatible star formation histories. The model galaxies have, however, too low a stellar mass with respect to those inferred from the observational data.

As stated above, very few massive model galaxies are found above $z = 3.9$. Thus, these galaxies have the potential to change the way we understand galaxy formation, once their redshifts are spectroscopically confirmed and data for the whole DES survey are analysed.

6 CONCLUSIONS AND DISCUSSION

We have used data from the first three years of Dark Energy Survey (DES) operations together with the Science Verification (SV) catalogue, to probe the existence of high-redshift ($z \sim 4$), massive ($M \sim 10^{12} M_{\odot}$) galaxies down to the nominal full survey depth, and to study their nature. This analysis was motivated by our previous forecast (D13) according to which DES would be one of the very few surveys (the only one, at time of writing) that has the right combination of area (5000 deg. sq. at completion) and depth ($i = 24.3$) to allow for these rare objects to be detected, should they exist. In turn, these galaxies are key probes of the galaxy formation process within a cosmological framework, as they form from the largest primordial density fluctuations. Their number and characterisation vary substantially between cosmological simulations, and extrapolations of local and intermediate-redshift mass functions predict a large variation in the number density of these objects (see D13, [Figure 1](#)). In a similar fashion, DES data have been recently used to search for high-redshift quasars ([Banerji et al. 2015b](#); [Reed et al. 2017](#)).

We have applied a rigorous identification method, using theoretical maps as well as visual inspection of ~ 600 potential sources, along with data cleaning (artefacts, error cuts, and star/galaxy separation). We have then performed spectro-photometric template fitting, using a large variety of models and reddening assumptions, to minimise potential biases in the determination of photometric redshifts and galaxy properties. Critical to the model fitting, we extended our DES data g, r, i, z, Y baseline with near-IR J, H, K data from the VHS survey. After model fitting, we further applied other quality cuts in order to extract the most promising sample of high-redshift, massive galaxies, namely: goodness of fit ($\chi_r^2 < 3$); unimodal redshift probability distribution function showing a clear high- z solution; physical mass.

¹² <http://virgo.dur.ac.uk>

¹³ <https://tao.asvo.org.au/tao/>

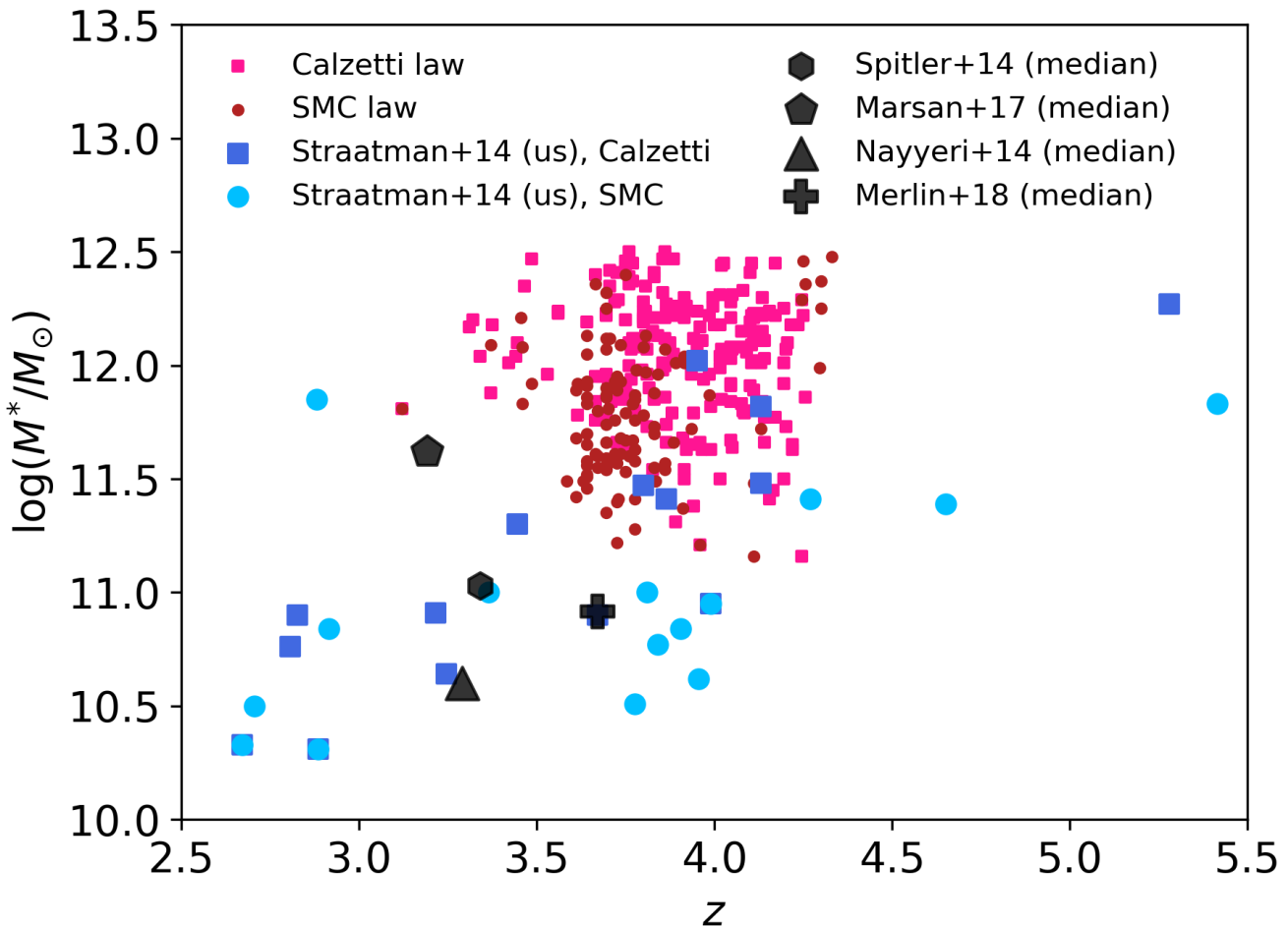


Figure 15. Stellar mass vs redshift for our candidates (large symbols for various reddening laws) compared to the median value for 57 galaxies by [Spitler et al. \(2014\)](#) (black hexagon), 7 galaxies by [Marsan et al. \(2017\)](#) (black pentagon), 16 galaxies by [Nayyeri et al. \(2014\)](#) (black triangle), 10 galaxies by [Merlin et al. \(2018\)](#) (black plus), and to the 18 values we obtain for the galaxies by [Straatman et al. \(2014\)](#) with our fitting set-up and their data (blue symbols labelled as [Straatman et al. \(2014\)](#)).

Our final result is a sample of 233 galaxies that are $z \sim 4$ candidates, with large stellar masses ($10^{11.5} \leq M/M_{\odot} \leq 10^{12.5}$) and ages of ~ 0.1 Gyr, some of which are on the verge of becoming passive. Their average star formation rates are of the order of thousands of solar masses per year and place them among the most extreme objects found so far (as in [Rowan-Robinson et al. \(2016\)](#)). This number of objects should be regarded as a lower limit due to our very conservative selection. Our best candidates, when paired with our PSF comparison consideration, constitutes an excellent sample for spectroscopic and ALMA follow-ups.

The properties of our objects make them the most likely progenitors of the most massive elliptical galaxies studied in the local universe ([Thomas et al. 2005, 2010](#)). The existence of such a class of mature, massive galaxies in the early universe pose unprecedented constraints to our understanding of galaxy formation and evolution in a cosmological context. An initial test of galaxy formation simulations reveals that galaxies with such large masses are absent in cold dark matter-based cosmologies.

Our work extends the hunt for massive galaxies at $z \sim 4$

by almost an order of magnitude in stellar mass, following the studies performed, for instance, in [Straatman et al. \(2014\)](#), [Spitler et al. \(2014\)](#), [Marsan et al. \(2017\)](#), [Nayyeri et al. \(2014\)](#), and [Merlin et al. \(2018\)](#). Our tests on the [Straatman et al. \(2014\)](#) data also confirm that even though we use a limited amount of photometric bands for the fitting, we obtain results that are similar to those obtained with 36-band photometry or even spectroscopy. This is because in order to constrain a model matching galaxy spectra what is important is the wavelength baseline covered by the data rather than the density of bands over a narrower wavelength span.

We show we are able to recover the properties of one object with a spectroscopic redshift of 3.717 reported by ([Glazebrook et al. 2017](#)), and in particular we provide solutions including the possible presence of dust.

One is then tempted to push our method to even higher redshifts. Photometric techniques similar to ours have also been used in studies based on the Hubble Frontier Fields (HFF) programme (e.g. [Laporte et al. 2016b,a](#)). HFF is a survey aimed at imaging six massive clusters at moderate

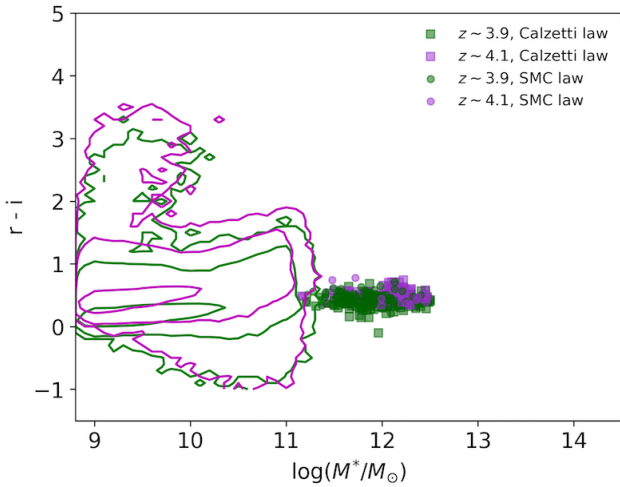


Figure 16. Observed-frame $(r-i)$ versus stellar mass for our best candidate galaxies, compared to galaxy distributions at $z \sim 3.9$ and $z \sim 4.1$ (colour-code in green and magenta respectively) from the [Gonzalez-Perez et al. \(2014\)](#) model, assuming the stellar population synthesis model from [Maraston \(2005\)](#). The model galaxies are shown as contours with the outermost one outlining the end of such a distribution, while the best candidates are plotted as scatter plot. Both observed and model galaxies include the effect of dust attenuation. The model stellar masses have been corrected to a Salpeter IMF ([Lagos et al. 2014](#); [Lacey et al. 2016](#)) for consistency with our fitting assumptions. No model galaxies are found with masses above $\sim 10^{11.5}$ at these redshifts.

redshift in order to observe very high-redshift ($z > 7$) galaxies (or proto-galaxies) that are visible because they have been lensed by the foreground clusters. Studies include the discovery of several tens of Lyman-break galaxies at redshifts $z \sim 7 - 11$ (e.g. [Zheng et al. 2014](#); [Jauzac et al. 2015](#); [Coe et al. 2015](#)).

Let us finally comment on the number counts of these extreme systems. D13 calculated the predicted galaxy number counts for a variety of approaches, including fully theoretical cosmological simulations (as per the Millennium Simulation), semi-empirical predictions obtained by passively evolving the $z = 0$ and $0.5 < z < 0.7$ published mass functions to higher redshift, available high- z mass functions ([Marchesini et al. 2010](#)), and also results from abundance-matching techniques ([Behroozi et al. 2013](#)). For example, empirical mass functions do forecast the presence of ~ 7000 galaxies with $\log(M^*/M_\odot) \geq 12.0$ within the whole DES. Of these, ~ 100 will represent true $\log(M^*/M_\odot) \geq 12.0$ systems, with the rest being misidentified due to Eddington bias (e.g. [Maraston et al. 2013](#)). In summary, the predicted number counts of D13 (Figure 1) are diverse and, at completion, a survey such as DES will help discriminate among these possibilities at the massive end of the stellar mass function. As the SV-sized data we use here include only ~ 150 deg. sq and because we calculated photometric redshifts that will need to be confirmed spectroscopically, we refrain from probing the precise number counts from D13.

Finally, this manuscript outlines a new method that only uses optical bands (in the context of DES) to identify likely massive high- z galaxies. This will work as a foundation to probe such galaxies using larger and larger photometric

datasets that will be completed in the future (such as EUCLID, LSST, etc.).

ACKNOWLEDGEMENTS

We would like to thank the MNRAS anonymous referee for his/her very useful and competent report, and Micol Bolzonella for a much appreciated support with HyperZ. This paper has also gone through internal review by the DES collaboration and we would like to thank our internal referees Karl Glazebrook and Richard McMahon for their comments which greatly improved this manuscript. We are also grateful to the DES final reader Alex Kim who gave us very useful editorial suggestions. Thanks also go to Will Hartley and Manda Banerji for providing comments, to Brian Yanny for instructing us on how to get blending information for each source, to Sophie Reed for her suggestions regarding potential mismatch between DES and VHS data, to Carlotta Gruppioni for the discussions regarding potential AGN contamination, to Benjamin Mawdsley for discussions regarding the toy model simulations predicting spurious low- z objects scattering in the selection box, and to Daniel Goddard for important stylistic plotting suggestions. We also acknowledge discussions with Alvio Renzini, Emanuele Daddi, David Elbaz, and Johan Comparat.

Funding for the DES Projects has been provided by the U.S. Department of Energy, the U.S. National Science Foundation, the Ministry of Science and Education of Spain, the Science and Technology Facilities Council of the United Kingdom, the Higher Education Funding Council for England, the National Center for Supercomputing Applications at the University of Illinois at Urbana-Champaign, the Kavli Institute of Cosmological Physics at the University of Chicago, the Center for Cosmology and Astro-Particle Physics at the Ohio State University, the Mitchell Institute for Fundamental Physics and Astronomy at Texas A&M University, Financiadora de Estudos e Projetos, Fundação Carlos Chagas Filho de Amparo à Pesquisa do Estado do Rio de Janeiro, Conselho Nacional de Desenvolvimento Científico e Tecnológico and the Ministério da Ciência, Tecnologia e Inovação, the Deutsche Forschungsgemeinschaft and the Collaborating Institutions in the Dark Energy Survey.

The Collaborating Institutions are Argonne National Laboratory, the University of California at Santa Cruz, the University of Cambridge, Centro de Investigaciones Energéticas, Medioambientales y Tecnológicas-Madrid, the University of Chicago, University College London, the DES-Brazil Consortium, the University of Edinburgh, the Eidgenössische Technische Hochschule (ETH) Zürich, Fermi National Accelerator Laboratory, the University of Illinois at Urbana-Champaign, the Institut de Ciències de l’Espai (IEEC/CSIC), the Institut de Física d’Altes Energies, Lawrence Berkeley National Laboratory, the Ludwig-Maximilians Universität München and the associated Excellence Cluster Universe, the University of Michigan, the National Optical Astronomy Observatory, the University of Nottingham, The Ohio State University, the University of Pennsylvania, the University of Portsmouth, SLAC National Accelerator Laboratory, Stanford University, the University of Sussex, Texas A&M University, and the OzDES Membership Consortium.

Based in part on observations at Cerro Tololo Inter-American Observatory, National Optical Astronomy Observatory, which is operated by the Association of Universities for Research in Astronomy (AURA) under a cooperative agreement with the National Science Foundation.

The DES data management system is supported by the National Science Foundation under Grant Numbers AST-1138766 and AST-1536171. The DES participants from Spanish institutions are partially supported by MINECO under grants AYA2015-71825, ESP2015-66861, FPA2015-68048, SEV-2016-0588, SEV-2016-0597, and MDM-2015-0509, some of which include ERDF funds from the European Union. IFAE is partially funded by the CERCA program of the Generalitat de Catalunya. Research leading to these results has received funding from the European Research Council under the European Union's Seventh Framework Program (FP7/2007-2013) including ERC grant agreements 240672, 291329, and 306478. We acknowledge support from the Australian Research Council Centre of Excellence for All-sky Astrophysics (CAASTRO), through project number CE110001020, and the Brazilian Instituto Nacional de Ciência e Tecnologia (INCT) e-Universe (CNPq grant 465376/2014-2).

This manuscript has been authored by Fermi Research Alliance, LLC under Contract No. DE-AC02-07CH11359 with the U.S. Department of Energy, Office of Science, Office of High Energy Physics. The United States Government retains and the publisher, by accepting the article for publication, acknowledges that the United States Government retains a non-exclusive, paid-up, irrevocable, world-wide license to publish or reproduce the published form of this manuscript, or allow others to do so, for United States Government purposes.

REFERENCES

- Abbott T. M. C., et al., 2018, preprint, ([arXiv:1801.03181](https://arxiv.org/abs/1801.03181))
- Banerji M., et al., 2008, *MNRAS*, **386**, 1219
- Banerji M., et al., 2015a, *MNRAS*, **446**, 2523
- Banerji M., et al., 2015b, *MNRAS*, **447**, 3368
- Behroozi P. S., et al., 2013, *ApJ*, **770**, 57
- Bolzonella M., Miralles J.-M., Pelló R., 2000, *A&A*, **363**, 476
- Bouchet P., et al., 1985, *A&A*, **149**, 330
- Calzetti D., et al., 2000, *ApJ*, **533**, 682
- Caputi K. I., et al., 2012, *ApJ*, **750**, L20
- Caputi K. I., et al., 2015, *ApJ*, **810**, 73
- Cimatti A., et al., 2004, *Nature*, **430**, 184
- Cimatti A., Daddi E., Renzini A., 2006, *A&A*, **453**, L29
- Coe D., Bradley L., Zitrin A., 2015, *ApJ*, **800**, 84
- Conselice C. J., et al., 2007, *MNRAS*, **381**, 962
- Cowie L. L., Barger A. J., 2008, *ApJ*, **686**, 72
- Cowie L. L., Songaila A., Barger A. J., 1999, *AJ*, **118**, 603
- Cross N. J. G., et al., 2012, *A&A*, **548**, A119
- Croton D. J., et al., 2016, *ApJS*, **222**, 22
- Daddi E., et al., 2005, *ApJ*, **626**, 680
- Davies L. J. M., et al., 2013, *MNRAS*, **434**, 296
- De Lucia G., et al., 2006, *MNRAS*, **366**, 499
- Douglas L. S., et al., 2009, *MNRAS*, **400**, 561
- Etherington J., et al., 2017, *MNRAS*, **466**, 228
- Glazebrook K., et al., 2017, preprint, ([arXiv:1702.01751](https://arxiv.org/abs/1702.01751))
- Goddard D., et al., 2017, *MNRAS*, **466**, 4731
- Gonzalez-Perez V., et al., 2009, *MNRAS*, **398**, 497
- Gonzalez-Perez V., et al., 2014, *MNRAS*, **439**, 264
- Guo Y., 2013, UV Snapshot of Low-redshift Massive Star-forming Galaxies: Searching for the Analogs of High-redshift Clumpy Galaxies, HST Proposal
- Henriques B. M. B., White S. D. M., Thomas P. A., Angulo R., Guo Q., Lemson G., Springel V., Overzier R., 2015, *MNRAS*, **451**, 2663
- Hoyle B., et al., 2017, preprint, ([arXiv:1708.01532](https://arxiv.org/abs/1708.01532))
- Ilbert O., et al., 2013, in Cambresy L., Martins F., Nuss E., Palacios A., eds, SF2A-2013: Proceedings of the Annual meeting of the French Society of Astronomy and Astrophysics. pp 545–548
- Jauzac M., et al., 2015, *MNRAS*, **452**, 1437
- Kim E. J., et al., 2015, *MNRAS*, **453**, 507
- Knebe A., et al., 2018, *MNRAS*, **475**, 2936
- Kriek M., Conroy C., 2013, *ApJ*, **775**, L16
- Kriek M., et al., 2016, *Nature*, **540**, 248
- Lacey C. G., et al., 2016, *MNRAS*, **462**, 3854
- Lagos C. D. P., et al., 2014, *MNRAS*, **440**, 920
- Laporte N., et al., 2016a, in Reylé C., Richard J., Cambresy L., Deleuil M., Pécontal E., Tresse L., Vauglin I., eds, SF2A-2016: Proceedings of the Annual meeting of the French Society of Astronomy and Astrophysics. pp 411–415
- Laporte N., et al., 2016b, *ApJ*, **820**, 98
- Lonoce I., et al., 2015, *MNRAS*, **454**, 3912
- Mancini C., et al., 2009, *A&A*, **500**, 705
- Maraston C., 2005, *MNRAS*, **362**, 799
- Maraston C., et al., 2006, *ApJ*, **652**, 85
- Maraston C., et al., 2010, *MNRAS*, **407**, 830
- Maraston C., et al., 2013, *MNRAS*, **435**, 2764
- Marchesini D., et al., 2010, Measuring the Rest-Frame UV Properties and the Number Density of Massive Galaxies at $3 < z < 4$, NAOJ Proposal
- Marsan Z. C., et al., 2017, *ApJ*, **842**, 21
- McMahon R., 2012, in Science from the Next Generation Imaging and Spectroscopic Surveys. p. 37
- Mehlert D., Thomas D., Saglia R. P., Bender R., Wegner G., 2003, *A&A*, **407**, 423
- Melchior P., et al., 2015, *MNRAS*, **449**, 2219
- Merlin E., et al., 2018, *MNRAS*, **473**, 2098
- Mortlock A., et al., 2015, *MNRAS*, **447**, 2
- Muzzin A., et al., 2013, *ApJ*, **777**, 18
- Nayyeri H., et al., 2014, *ApJ*, **794**, 68
- Onodera M., et al., 2012, *ApJ*, **755**, 26
- Pfarr J., et al., 2012, *MNRAS*, **422**, 3285
- Pfarr J., et al., 2013, *MNRAS*, **435**, 1389
- Pipino A., et al., 2007, *ApJ*, **665**, 295
- Pozzetti L., et al., 2010, *A&A*, **523**, A13
- Prevot M. L., et al., 1984, *A&A*, **132**, 389
- Reed S. L., et al., 2017, *MNRAS*, **468**, 4702
- Ricciardelli E., Franceschini A., 2010, *A&A*, **518**, A14
- Rossetto B. M., et al., 2011, *AJ*, **141**, 185
- Rowan-Robinson M., et al., 2016, *MNRAS*, **461**, 1100
- Sánchez S. F., et al., 2012, *A&A*, **538**, A8
- Sánchez C., et al., 2014, *MNRAS*, **445**, 1482
- Santini P., et al., 2009, *A&A*, **504**, 751
- Schreiber C., et al., 2018, *A&A*, **611**, A22
- Simpson J. M., et al., 2017, *ApJ*, **844**, L10
- Spitler L. R., et al., 2014, *ApJ*, **787**, L36
- Stefanon M., et al., 2013, *ApJ*, **768**, 92
- Straatman C. M. S., et al., 2014, *ApJ*, **783**, L14
- The Dark Energy Survey Collaboration 2005, ArXiv Astrophysics e-prints,
- Thomas D., et al., 2005, *ApJ*, **621**, 673
- Thomas D., et al., 2010, *MNRAS*, **404**, 1775
- Wake D. A., et al., 2006, *MNRAS*, **372**, 537
- Wang L., et al., 2016, preprint, ([arXiv:1612.04540](https://arxiv.org/abs/1612.04540))
- Whitaker K. E., et al., 2013, *ApJ*, **770**, L39
- White S. D. M., Rees M. J., 1978, *MNRAS*, **183**, 341

Yan H., et al., 2004, *ApJ*, 616, 63

Zheng W., et al., 2014, *ApJ*, 795, 93

APPENDIX A: FITTING RESULTS FOR THE BEST CANDIDATES

Here we provide the stellar population properties and photometric redshift for all best candidate galaxies. As usual, fits are performed for two reddening options: SMC law and Calzetti law.

APPENDIX B: PHOTOMETRY OF ALL CANDIDATES

The full DES+VHS photometry, and RA and Dec coordinates (J2000) are provided for all galaxies matching the best candidate criteria.

Table A1. Properties of the best candidates for the SMC law case, from left to right: object ID, z_{phot} , χ_r^2 , stellar mass M^* , absolute magnitude, age, star formation history, metallicity, the number σ 's used to estimate potential AGN contamination, photometric redshift found by fitting DES only bands, redshift from the DES pipeline, extinction as $E(B - V)$. Errors refer to the 99% confidence level.

ID	z_{phot}	χ_r^2	$\log_{10}(M^*/M_{\odot})$	Abs. Mag. (i)	Age (Gyr)	SFH	[Z/H] (Z_{\odot})	σ_{AGN}	$z_{DESonly}$	z_{BPZ}	E (B-V)
100600870	$3.67^{+0.16}_{-0.23}$	1.224	$11.8^{+0.03}_{-0.0}$	-27.02	0.1	$t_{trunc} = 1.0$	1	0.16	3.37	0.38	0.18
102002089	$3.77^{+0.47}_{-0.3}$	2.019	$11.28^{+0.71}_{-0.06}$	-25.63	0.1	$t_{trunc} = 1.0$	2	5.59	3.37	0.51	0.18
102009403	$3.64^{+0.19}_{-0.19}$	1.578	$11.7^{+0.02}_{-0.01}$	-26.69	0.1	$t_{trunc} = 1.0$	2	1.71	4.25	0.35	0.18
102009835	$3.77^{+0.17}_{-0.1}$	1.632	$11.83^{+0.0}_{-0.05}$	-27.01	0.1	$t_{trunc} = 0.1$	2	10.86	2.47	0.47	0.18
102009849	$3.73^{+0.23}_{-0.14}$	1.007	$11.93^{+0.04}_{-0.25}$	-27.24	0.1	$t_{trunc} = 0.1$	2	12.22	3.58	0.47	0.18
102031864	$3.77^{+0.16}_{-0.14}$	1.978	$11.67^{+0.01}_{-0.07}$	-26.6	0.1	$t_{trunc} = 0.1$	2	3.34	2.48	0.5	0.18
132987082	$3.7^{+0.14}_{-0.26}$	1.522	$11.57^{+0.42}_{-0.02}$	-26.54	0.1	CONSTANT	1/2	7.21	2.52	0.37	0.18
133572897	$3.46^{+0.12}_{-0.08}$	1.792	$12.21^{+0.05}_{-0.04}$	-27.52	0.11	$t_{trunc} = 0.1$	2	1.77	3.48	0.49	0.18
136067262	$3.73^{+0.12}_{-0.16}$	2.073	$12.09^{+0.0}_{-0.24}$	-27.66	0.1	$t_{trunc} = 0.1$	2	15.27	2.54	0.4	0.18
137806706	$3.78^{+0.55}_{-0.28}$	0.338	$11.98^{+0.21}_{-0.17}$	-26.6	0.4	$t_{trunc} = 0.3$	1	0.06	3.69	0.49	0.0
164738198	$3.67^{+0.16}_{-0.19}$	2.642	$12.36^{+0.28}_{-0.01}$	-27.76	0.29	$t_{trunc} = 1.0$	2	19.48	2.39	0.49	0.18
287114376	$3.73^{+0.26}_{-0.32}$	1.54	$11.89^{+0.27}_{-0.13}$	-26.76	0.13	$e^{-t/0.1}$ Gyr	2	2.52	3.4	0.41	0.18
396223342	$3.69^{+0.11}_{-0.26}$	0.891	$11.59^{+0.04}_{-0.02}$	-26.59	0.1	$t_{trunc} = 1.0$	1/2	4.44	3.34	0.37	0.18
396276124	$3.69^{+0.18}_{-0.26}$	1.022	$11.66^{+0.02}_{-0.23}$	-26.66	0.1	$t_{trunc} = 0.1$	1	2.61	3.45	0.48	0.18
397300605	$3.83^{+0.09}_{-0.3}$	2.084	$11.73^{+0.02}_{-0.0}$	-26.93	0.1	CONSTANT	1/2	7.77	3.25	0.47	0.18
397303505	$3.69^{+0.15}_{-0.32}$	1.604	$11.54^{+0.01}_{-0.27}$	-26.29	0.11	$t_{trunc} = 1.0$	1	4.8	3.4	0.49	0.18
397554368	$3.71^{+0.35}_{-0.28}$	1.366	$12.12^{+0.0}_{-0.44}$	-27.23	0.29	SSP	1/5	3.19	2.5	0.37	0.0
397764328	$3.77^{+0.13}_{-0.27}$	2.321	$11.58^{+0.02}_{-0.04}$	-26.4	0.1	CONSTANT	2	4.27	4.3	0.54	0.18
397885462	$3.8^{+0.2}_{-0.56}$	0.709	$11.78^{+0.4}_{-0.04}$	-26.18	0.18	$t_{trunc} = 0.1$	2	1.74	3.34	0.5	0.0
398107560	$3.67^{+0.25}_{-0.2}$	1.0	$11.61^{+0.03}_{-0.2}$	-26.46	0.1	$t_{trunc} = 0.1$	2	3.3	3.34	0.45	0.18
399804681	$3.86^{+0.21}_{-0.48}$	1.764	$11.54^{+0.02}_{-0.3}$	-26.28	0.1	$t_{trunc} = 0.1$	2	1.88	2.49	0.5	0.18
399842053	$3.72^{+0.16}_{-0.25}$	0.946	$11.61^{+0.01}_{-0.03}$	-26.48	0.1	CONSTANT	2	5.7	4.28	0.43	0.18
399842613	$4.11^{+0.15}_{-0.48}$	1.443	$11.48^{+0.0}_{-0.38}$	-26.15	0.1	$t_{trunc} = 1.0$	2	0.36	3.31	0.59	0.18
400998781	$3.64^{+0.23}_{-0.17}$	0.863	$11.52^{+0.04}_{-0.08}$	-26.23	0.1	$t_{trunc} = 0.1$	2	2.2	2.53	0.47	0.18
401003476	$3.86^{+0.18}_{-0.41}$	0.666	$12.07^{+0.07}_{-0.71}$	-26.72	1.02	$t_{trunc} = 1.0$	2	1.37	2.48	0.39	0.0
404788215	$3.61^{+0.19}_{-0.2}$	1.098	$11.68^{+0.03}_{-0.02}$	-26.65	0.1	$t_{trunc} = 1.0$	2	4.63	2.51	0.43	0.18
404798117	$3.46^{+0.38}_{-0.13}$	0.929	$12.08^{+0.26}_{-0.13}$	-27.31	0.11	$t_{trunc} = 0.1$	1/5	16.39	3.42	0.48	0.18
404886634	$3.72^{+0.15}_{-0.3}$	1.837	$11.76^{+0.02}_{-0.21}$	-26.92	0.1	$t_{trunc} = 0.1$	1	6.63	3.45	0.47	0.18
404907811	$3.61^{+0.32}_{-0.26}$	1.542	$11.89^{+0.54}_{-0.04}$	-26.86	0.23	$e^{-t/1.0}$ Gyr	1/2	6.14	4.22	0.36	0.18
405937444	$3.64^{+0.19}_{-0.2}$	1.272	$11.83^{+0.01}_{-0.02}$	-27.02	0.1	$t_{trunc} = 1.0$	2	11.74	3.42	0.42	0.18
408135057	$3.77^{+0.23}_{-0.17}$	1.411	$11.41^{+0.04}_{-0.07}$	-25.97	0.1	$t_{trunc} = 0.1$	2	0.64	3.5	0.48	0.18
408311797	$3.83^{+0.1}_{-0.19}$	2.208	$11.88^{+0.05}_{-0.01}$	-27.15	0.1	CONSTANT	2	9.19	2.52	0.48	0.18
409127588	$3.77^{+0.21}_{-0.48}$	1.367	$11.85^{+0.41}_{-0.09}$	-26.38	0.11	SSP	2	4.41	3.45	0.52	0.0
411491335	$3.69^{+0.23}_{-0.17}$	1.521	$12.32^{+0.19}_{-0.08}$	-27.84	0.13	$e^{-t/0.1}$ Gyr	2	27.57	3.19	0.43	0.18
411500732	$3.73^{+0.31}_{-0.24}$	2.43	$11.4^{+0.41}_{-0.03}$	-25.93	0.1	$t_{trunc} = 1.0$	2	0.7	3.4	0.46	0.18
412637681	$3.61^{+0.19}_{-0.25}$	2.309	$11.42^{+0.4}_{-0.01}$	-26.06	0.1	CONSTANT	1	0.49	2.48	0.46	0.18

Table A1 – continued

ID	z_{phot}	χ_r^2	$\log_{10}(M^*/M_{\odot})$	Abs. Mag. (i)	Age (Gyr)	SFH	[Z/H] (Z_{\odot})	σ_{AGN}	$z_{DESonly}$	z_{BPZ}	E (B-V)
414233666	$3.8^{+0.15}_{-0.3}$	2.121	$12.08^{+0.01}_{-0.21}$	-27.71	0.1	$t_{trunc} = 0.1$	1	11.09	3.29	0.46	0.18
414237423	$3.73^{+0.41}_{-0.29}$	1.102	$11.61^{+0.77}_{-0.22}$	-26.45	0.1	$t_{trunc} = 0.1$	2	2.3	3.58	0.43	0.18
417565185	$3.64^{+0.22}_{-0.23}$	1.051	$11.51^{+0.04}_{-0.27}$	-26.22	0.1	$t_{trunc} = 1.0$	2	1.49	2.5	0.39	0.18
431455424	$3.81^{+0.2}_{-0.24}$	1.217	$12.13^{+0.12}_{-0.09}$	-27.04	0.13	SSP	2	14.07	3.67	0.64	0.0
431827017	$3.77^{+0.16}_{-0.16}$	0.764	$11.83^{+0.04}_{-0.28}$	-27.01	0.1	$t_{trunc} = 0.1$	2	9.63	3.34	0.49	0.18
434401854	$3.69^{+0.14}_{-0.29}$	1.31	$12.25^{+0.08}_{-0.06}$	-27.82	0.16	$e^{-t/1.0}$ Gyr	1	29.43	3.42	0.44	0.18
444147103	$3.69^{+0.2}_{-0.36}$	1.289	$11.56^{+0.35}_{-0.38}$	-26.41	0.1	$t_{trunc} = 0.1$	1	4.9	3.42	0.46	0.18
470611726	$3.69^{+0.23}_{-0.47}$	1.081	$11.35^{+0.04}_{-0.29}$	-25.8	0.1	$t_{trunc} = 0.1$	2	7.27	2.5	0.5	0.18
470971747	$4.25^{+0.11}_{-0.89}$	0.739	$12.36^{+0.04}_{-0.85}$	-27.54	0.45	$e^{-t/0.1}$ Gyr	2	2.36	2.56	0.28	0.0
471600124	$3.94^{+0.49}_{-0.37}$	0.544	$11.72^{+0.36}_{-0.42}$	-26.17	0.32	$t_{trunc} = 0.3$	2	2.32	3.31	0.49	0.0
471985468	$3.64^{+0.14}_{-0.21}$	2.193	$12.13^{+0.07}_{-0.1}$	-27.32	0.11	$t_{trunc} = 0.1$	2	10.29	2.54	0.54	0.18
473133985	$3.67^{+0.22}_{-0.22}$	2.112	$11.6^{+0.43}_{-0.01}$	-26.52	0.1	$t_{trunc} = 1.0$	1	7.56	3.58	0.38	0.18
473136272	$3.64^{+0.17}_{-0.18}$	1.491	$11.91^{+0.03}_{-0.06}$	-27.16	0.1	$e^{-t/0.3}$ Gyr	2	11.56	2.52	0.41	0.18
473140970	$3.69^{+0.11}_{-0.27}$	1.047	$11.74^{+0.03}_{-0.01}$	-26.95	0.1	$t_{trunc} = 1.0$	1/2	9.56	3.34	0.42	0.18
473404298	$4.3^{+0.11}_{-0.14}$	0.554	$12.37^{+0.04}_{-0.2}$	-27.57	0.45	$e^{-t/0.1}$ Gyr	2	0.43	3.58	0.47	0.0
473408311	$3.75^{+0.16}_{-0.28}$	1.53	$11.79^{+0.39}_{-0.04}$	-27.08	0.1	$t_{trunc} = 0.1$	1/2	8.66	3.65	0.44	0.18
473411673	$3.69^{+0.22}_{-0.24}$	1.016	$11.54^{+0.02}_{-0.26}$	-26.28	0.1	$t_{trunc} = 1.0$	2	5.69	3.58	0.45	0.18
473496203	$4.3^{+0.08}_{-0.84}$	0.53	$12.25^{+0.37}_{-0.73}$	-26.98	1.28	$e^{-t/1.0}$ Gyr	2	0.37	3.05	0.38	0.0
473498930	$3.64^{+0.21}_{-0.18}$	0.992	$11.93^{+0.01}_{-0.01}$	-27.26	0.1	$t_{trunc} = 1.0$	2	20.72	3.42	0.41	0.18
473503196	$3.83^{+0.28}_{-0.18}$	0.835	$11.49^{+0.03}_{-0.26}$	-26.15	0.1	$t_{trunc} = 0.1$	2	3.37	3.5	0.59	0.18
473511031	$3.64^{+0.2}_{-0.16}$	1.643	$11.58^{+0.05}_{-0.07}$	-26.39	0.1	$t_{trunc} = 0.1$	2	1.92	2.44	0.41	0.18
473512115	$3.89^{+0.2}_{-0.34}$	2.122	$12.01^{+0.33}_{-0.37}$	-26.91	0.32	$t_{trunc} = 0.3$	2	3.44	3.58	0.43	0.0
473515263	$3.63^{+0.22}_{-0.2}$	1.616	$11.49^{+0.02}_{-0.01}$	-26.18	0.1	$t_{trunc} = 1.0$	2	2.27	3.4	0.45	0.18
473519025	$3.75^{+0.41}_{-0.35}$	1.318	$11.53^{+0.76}_{-0.36}$	-26.25	0.1	$t_{trunc} = 0.1$	2	0.81	3.4	0.5	0.18
473520285	$3.64^{+0.2}_{-0.21}$	1.199	$11.56^{+0.03}_{-0.02}$	-26.35	0.1	$t_{trunc} = 1.0$	2	3.35	3.42	0.38	0.18
473521671	$3.48^{+0.62}_{-0.13}$	1.08	$11.92^{+0.35}_{-0.16}$	-26.8	0.11	$t_{trunc} = 0.1$	2	2.5	3.45	0.58	0.18
473528868	$3.88^{+0.26}_{-0.48}$	0.686	$11.66^{+0.36}_{-0.12}$	-26.03	0.32	$t_{trunc} = 0.3$	2	1.9	3.59	0.5	0.0
473530252	$3.92^{+0.27}_{-0.31}$	1.431	$12.04^{+0.24}_{-0.36}$	-26.97	0.32	$t_{trunc} = 0.3$	2	0.76	3.5	0.46	0.0
477008049	$4.25^{+0.08}_{-0.17}$	0.681	$12.46^{+0.03}_{-0.22}$	-27.78	0.45	$e^{-t/0.1}$ Gyr	2	4.79	3.34	0.51	0.0
477008438	$3.77^{+0.19}_{-0.21}$	2.679	$11.63^{+0.01}_{-0.02}$	-26.52	0.1	$t_{trunc} = 1.0$	2	4.99	3.31	0.45	0.18
480339250	$3.86^{+0.25}_{-0.53}$	1.089	$11.57^{+0.03}_{-0.27}$	-26.37	0.1	$t_{trunc} = 0.1$	2	6.05	3.4	0.55	0.18
480995070	$3.75^{+0.16}_{-0.16}$	1.823	$11.67^{+0.0}_{-0.34}$	-26.62	0.1	$t_{trunc} = 0.1$	2	7.03	2.52	0.43	0.18
481350973	$3.67^{+0.28}_{-0.26}$	0.967	$11.55^{+0.86}_{-0.32}$	-26.48	0.1	$t_{trunc} = 1.0$	1/2	5.37	4.25	0.4	0.18
482208365	$3.69^{+0.16}_{-0.21}$	1.481	$11.86^{+0.04}_{-0.08}$	-27.03	0.1	$e^{-t/0.3}$ Gyr	2	13.71	2.5	0.44	0.18
483918716	$3.64^{+0.45}_{-0.48}$	1.28	$11.65^{+0.47}_{-0.02}$	-26.21	0.16	$e^{-t/0.1}$ Gyr	1/2	0.5	3.45	0.43	0.18
489254835	$3.83^{+0.37}_{-0.49}$	1.73	$11.55^{+0.75}_{-0.29}$	-26.31	0.1	$t_{trunc} = 0.1$	2	4.53	3.42	0.48	0.18

Table A1 – continued

ID	z_{phot}	χ_r^2	$\log_{10}(M^*/M_{\odot})$	Abs. Mag. (<i>i</i>)	Age (Gyr)	SFH	[Z/H] (Z_{\odot})	σ_{AGN}	$z_{DESonly}$	z_{BPZ}	E (B-V)
490704656	$3.73^{+0.68}_{-0.35}$	1.209	$11.22^{+1.12}_{-0.27}$	-25.49	0.1	$t_{trunc} = 1.0$	2	0.75	3.4	0.51	0.18
494789087	$3.96^{+0.48}_{-0.38}$	1.445	$11.21^{+0.55}_{-0.1}$	-25.38	0.11	$t_{trunc} = 0.1$	2	0.73	2.63	0.4	0.0
494790027	$3.83^{+0.31}_{-0.19}$	1.281	$11.7^{+0.6}_{-0.08}$	-26.22	0.14	$t_{trunc} = 0.1$	2	3.18	2.58	0.52	0.0
494790169	$4.29^{+0.12}_{-0.62}$	0.598	$11.99^{+0.35}_{-0.11}$	-26.76	0.29	$e^{-t/0.1} \text{ Gyr}$	2	1.53	3.98	0.42	0.0
494792459	$4.11^{+0.36}_{-0.34}$	1.167	$11.16^{+1.68}_{-0.65}$	-25.27	0.11	$t_{trunc} = 0.1$	2	0.36	3.08	0.44	0.0
494793098	$3.98^{+0.29}_{-0.25}$	0.383	$11.87^{+0.25}_{-0.11}$	-26.55	0.32	$t_{trunc} = 0.3$	2	0.33	4.0	0.48	0.0
494800805	$4.25^{+0.1}_{-1.22}$	0.196	$12.29^{+0.26}_{-0.5}$	-27.19	0.81	$e^{-t/0.3} \text{ Gyr}$	2	0.64	3.15	0.39	0.0
494801634	$3.37^{+0.5}_{-0.3}$	0.437	$12.09^{+0.1}_{-0.01}$	-27.08	0.45	$t_{trunc} = 0.3$	1/5	0.95	3.56	0.35	0.0
495323159	$3.91^{+0.42}_{-0.31}$	1.903	$11.37^{+0.68}_{-0.08}$	-25.66	0.14	$t_{trunc} = 0.1$	1/5	0.54	2.65	0.41	0.0
495342175	$3.64^{+0.2}_{-0.23}$	2.408	$11.46^{+0.38}_{-0.27}$	-26.09	0.1	$t_{trunc} = 1.0$	2	0.81	2.46	0.4	0.18
495566911	$3.12^{+0.21}_{-0.15}$	0.438	$11.81^{+0.03}_{-0.11}$	-26.12	0.16	SSP	2	0.56	4.29	0.54	0.0
497171956	$3.72^{+0.24}_{-0.11}$	1.868	$11.93^{+0.04}_{-0.05}$	-27.26	0.1	$t_{trunc} = 0.1$	2	6.9	3.56	0.44	0.18
501217876	$3.69^{+0.16}_{-0.22}$	1.175	$11.87^{+0.01}_{-0.03}$	-27.11	0.1	CONSTANT	2	14.42	2.5	0.42	0.18
501218097	$3.84^{+0.11}_{-0.29}$	1.961	$11.96^{+0.09}_{-0.35}$	-26.78	0.32	$t_{trunc} = 0.3$	2	5.96	3.61	0.38	0.0
501524910	$3.92^{+0.25}_{-0.46}$	1.41	$12.01^{+0.36}_{-0.12}$	-26.91	0.32	$t_{trunc} = 0.3$	2	4.02	3.53	0.4	0.0
501577492	$3.69^{+0.15}_{-0.14}$	1.59	$12.12^{+0.01}_{-0.07}$	-27.73	0.1	$t_{trunc} = 0.1$	2	34.62	2.5	0.45	0.18
503984762	$3.77^{+0.27}_{-0.28}$	0.479	$11.76^{+0.36}_{-0.1}$	-26.28	0.32	$t_{trunc} = 0.3$	2	0.27	2.54	0.38	0.0
504038042	$3.73^{+0.22}_{-0.12}$	1.172	$11.95^{+0.04}_{-0.06}$	-27.3	0.1	$t_{trunc} = 0.1$	2	10.92	3.29	0.48	0.18
504056183	$3.76^{+0.18}_{-0.53}$	1.519	$11.6^{+0.0}_{-0.32}$	-26.51	0.1	$t_{trunc} = 0.1$	1	5.42	3.27	0.43	0.18
504194446	$3.77^{+0.25}_{-0.09}$	2.009	$11.87^{+0.03}_{-0.05}$	-27.1	0.1	$t_{trunc} = 0.1$	2	9.77	3.4	0.48	0.18
504330828	$3.58^{+0.11}_{-0.21}$	2.148	$11.49^{+0.03}_{-0.03}$	-26.32	0.1	CONSTANT	1/2	4.25	2.45	0.35	0.18
505028285	$3.69^{+0.26}_{-0.13}$	1.048	$11.9^{+0.04}_{-0.06}$	-27.18	0.1	$t_{trunc} = 0.1$	2	17.04	3.56	0.47	0.18
506017320	$3.77^{+0.19}_{-0.14}$	0.719	$11.63^{+0.03}_{-0.07}$	-26.5	0.1	$t_{trunc} = 0.1$	2	4.07	3.37	0.49	0.18
506345182	$3.73^{+0.44}_{-0.47}$	1.044	$11.41^{+0.78}_{-0.31}$	-25.97	0.1	$t_{trunc} = 0.1$	2	1.09	3.4	0.53	0.18
506534457	$3.64^{+0.18}_{-0.13}$	1.484	$11.86^{+0.03}_{-0.06}$	-27.08	0.1	$t_{trunc} = 0.1$	2	8.97	2.49	0.4	0.18
506537406	$3.73^{+0.24}_{-0.24}$	1.615	$11.57^{+0.03}_{-0.25}$	-26.35	0.1	$t_{trunc} = 0.1$	2	4.12	2.61	0.5	0.18
507681715	$3.81^{+0.62}_{-0.41}$	1.395	$11.97^{+0.88}_{-0.04}$	-26.65	0.36	$t_{trunc} = 0.3$	1	5.25	2.56	0.41	0.0
507785363	$3.46^{+0.72}_{-0.18}$	0.872	$11.83^{+0.33}_{-0.08}$	-26.56	0.13	$t_{trunc} = 0.1$	1/2	0.67	2.64	0.48	0.18
507791066	$3.62^{+0.17}_{-0.21}$	1.08	$11.92^{+0.16}_{-0.1}$	-27.13	0.11	$e^{-t/0.1} \text{ Gyr}$	1/2	10.98	4.25	0.47	0.18
507791331	$3.75^{+0.19}_{-0.21}$	1.514	$12.4^{+0.12}_{-0.07}$	-27.95	0.14	$e^{-t/0.1} \text{ Gyr}$	2	30.31	2.5	0.48	0.18
507810919	$3.69^{+0.15}_{-0.31}$	1.282	$11.66^{+0.01}_{-0.27}$	-26.67	0.1	$t_{trunc} = 0.1$	1	9.6	2.55	0.41	0.18
507820438	$3.64^{+0.19}_{-0.2}$	0.78	$12.05^{+0.04}_{-0.08}$	-27.47	0.11	$e^{-t/1.0} \text{ Gyr}$	2	18.39	4.28	0.42	0.18
508601732	$4.13^{+0.16}_{-0.15}$	1.847	$11.72^{+0.05}_{-0.07}$	-26.74	0.1	$t_{trunc} = 0.1$	2	5.08	3.53	0.65	0.18
618652137	$3.7^{+0.17}_{-0.24}$	0.918	$11.81^{+0.0}_{-0.27}$	-27.05	0.1	$t_{trunc} = 0.1$	1	4.1	3.5	0.45	0.18
618663972	$3.69^{+0.21}_{-0.2}$	1.575	$12.07^{+0.13}_{-0.03}$	-27.31	0.11	$e^{-t/0.1} \text{ Gyr}$	2	8.83	3.53	0.52	0.18
618664093	$3.73^{+0.13}_{-0.31}$	1.132	$11.68^{+0.0}_{-0.25}$	-26.81	0.1	$t_{trunc} = 0.1$	1/2	1.29	3.4	0.47	0.18

Table A1 – *continued*

ID	z_{phot}	χ_r^2	$\log_{10}(M^*/M_\odot)$	Abs. Mag. (<i>i</i>)	Age (Gyr)	SFH	[Z/H] (Z_\odot)	σ_{AGN}	$z_{DESonly}$	z_{BPZ}	E (B-V)
618664306	$4.33^{+0.08}_{-0.12}$	1.867	$12.48^{+0.23}_{-0.16}$	-27.93	0.36	$e^{-t/0.1 \text{ Gyr}}$	2	1.62	3.25	0.41	0.0

Table A2. As in Table A1, but for the Calzetti-type reddening.

ID	z_{phot}	χ^2_r	$\log_{10}(M^*/M_\odot)$	Abs. Mag. (<i>i</i>)	Age (Gyr)	SFH	[Z/H] (Z_\odot)	σ_{AGN}	$z_{DESonly}$	z_{BPZ}	E (B-V)
100669215	$3.87^{+0.39}_{-0.38}$	0.863	$11.74^{+0.25}_{-0.28}$	-26.5	0.1	$t_{trunc} = 0.1$	2	0.04	2.65	0.47	0.25
102002089	$4.22^{+0.12}_{-0.44}$	1.209	$11.65^{+0.04}_{-0.02}$	-26.26	0.1	$t_{trunc} = 0.1$	2	5.59	3.31	0.51	0.25
102009403	$4.05^{+0.13}_{-0.38}$	2.106	$12.07^{+0.02}_{-0.33}$	-27.33	0.1	$t_{trunc} = 0.1$	2	1.71	3.75	0.35	0.25
102031864	$4.01^{+0.28}_{-0.19}$	2.487	$12.31^{+0.4}_{-0.01}$	-27.6	0.1	$t_{trunc} = 1.0$	2	3.34	3.58	0.5	0.37
105765488	$4.1^{+0.24}_{-0.47}$	1.199	$12.19^{+0.44}_{-0.28}$	-27.29	0.1	$t_{trunc} = 0.1$	2	2.41	2.56	0.51	0.37
115286147	$3.96^{+0.31}_{-0.32}$	0.35	$11.63^{+0.15}_{-0.0}$	-26.23	0.1	$t_{trunc} = 1.0$	2	0.66	3.25	0.43	0.25
132987082	$3.98^{+0.22}_{-0.21}$	0.733	$11.96^{+0.08}_{-0.04}$	-27.03	0.1	$t_{trunc} = 0.1$	2	7.21	3.64	0.37	0.25
133076071	$3.56^{+0.75}_{-0.25}$	0.926	$12.23^{+0.6}_{-0.02}$	-26.75	0.1	SSP	2	1.9	3.4	0.49	0.25
133575827	$4.11^{+0.18}_{-0.22}$	1.165	$12.23^{+0.33}_{-0.05}$	-27.4	0.1	$t_{trunc} = 0.1$	2	11.06	3.31	0.5	0.37
133592684	$3.81^{+0.65}_{-0.48}$	0.023	$12.07^{+0.62}_{-0.2}$	-26.65	0.13	$t_{trunc} = 0.1$	2	1.18	3.71	0.51	0.25
133755647	$3.73^{+0.63}_{-0.45}$	0.404	$12.41^{+0.13}_{-0.18}$	-27.14	0.18	$e^{-t/0.1}$ Gyr	2	0.38	3.75	0.33	0.37
133779875	$4.13^{+0.2}_{-0.51}$	0.978	$12.11^{+0.33}_{-0.25}$	-27.08	0.1	$t_{trunc} = 0.1$	2	4.32	3.64	0.52	0.37
133785852	$3.69^{+0.57}_{-0.38}$	0.773	$11.77^{+0.47}_{-0.03}$	-26.26	0.1	CONSTANT	2	1.44	2.46	0.46	0.37
134036466	$3.96^{+0.3}_{-0.34}$	0.829	$12.17^{+0.48}_{-0.26}$	-27.24	0.1	$t_{trunc} = 0.1$	2	1.73	3.73	0.51	0.37
134797801	$4.04^{+0.29}_{-0.76}$	1.2	$11.67^{+0.37}_{-0.17}$	-26.33	0.1	$t_{trunc} = 0.1$	2	0.82	3.15	0.48	0.25
135449486	$3.73^{+0.56}_{-0.54}$	0.707	$11.9^{+0.25}_{-0.12}$	-26.57	0.1	$t_{trunc} = 1.0$	2	2.37	3.25	0.4	0.37
135756581	$4.02^{+0.19}_{-0.2}$	0.85	$12.44^{+0.18}_{-0.01}$	-27.93	0.1	$t_{trunc} = 1.0$	2	2.51	3.35	0.53	0.37
135760809	$3.75^{+0.19}_{-0.31}$	0.731	$12.2^{+0.3}_{-0.08}$	-27.32	0.1	$t_{trunc} = 0.1$	2	1.05	3.69	0.45	0.37
135856576	$3.64^{+0.31}_{-0.32}$	1.148	$12.19^{+0.54}_{-0.03}$	-27.31	0.1	$e^{-t/0.3}$ Gyr	1	0.4	3.64	0.42	0.37
135857162	$3.86^{+0.32}_{-0.43}$	1.097	$12.0^{+0.09}_{-0.06}$	-26.82	0.1	CONSTANT	2	0.05	3.45	0.39	0.37
136034648	$4.01^{+0.37}_{-0.53}$	0.488	$11.5^{+0.52}_{-0.07}$	-25.88	0.1	$t_{trunc} = 0.1$	2	0.39	3.79	0.42	0.25
137552954	$3.8^{+0.31}_{-0.36}$	1.028	$12.21^{+0.19}_{-0.02}$	-27.36	0.1	CONSTANT	2	1.72	3.4	0.41	0.37
137650861	$3.44^{+0.61}_{-0.08}$	0.733	$12.1^{+0.66}_{-0.04}$	-26.95	0.11	$t_{trunc} = 0.1$	2	1.76	3.4	0.42	0.25
137806706	$3.94^{+0.53}_{-0.43}$	0.234	$12.12^{+0.27}_{-0.3}$	-26.84	0.32	$t_{trunc} = 0.3$	2	0.06	3.94	0.49	0.12
164738777	$3.69^{+0.53}_{-0.53}$	0.571	$12.22^{+0.15}_{-0.46}$	-26.8	0.23	$e^{-t/0.1}$ Gyr	2	1.85	2.38	0.51	0.25
285308599	$3.81^{+0.6}_{-0.52}$	0.176	$11.9^{+0.58}_{-0.01}$	-26.46	0.11	$t_{trunc} = 0.1$	2	0.37	2.58	0.4	0.25
287114376	$4.0^{+0.31}_{-0.27}$	1.173	$12.3^{+0.31}_{-0.01}$	-27.57	0.1	$t_{trunc} = 1.0$	2	2.52	3.33	0.41	0.37
287127591	$3.67^{+0.64}_{-0.42}$	0.138	$11.95^{+0.41}_{-0.09}$	-26.68	0.1	$t_{trunc} = 0.1$	2	1.94	3.73	0.4	0.37
289328303	$4.01^{+0.29}_{-0.39}$	0.6	$12.04^{+0.37}_{-0.1}$	-26.91	0.1	$t_{trunc} = 0.1$	2	0.3	2.52	0.45	0.37
289329064	$4.2^{+0.18}_{-0.45}$	0.744	$12.01^{+0.35}_{-0.23}$	-26.86	0.1	$t_{trunc} = 1.0$	2	2.4	3.69	0.54	0.37
290792079	$3.42^{+0.85}_{-0.2}$	1.864	$12.01^{+0.69}_{-0.14}$	-26.74	0.11	$t_{trunc} = 0.1$	2	2.83	3.42	0.36	0.25
395017226	$3.69^{+0.35}_{-0.33}$	0.435	$12.23^{+0.39}_{-0.07}$	-27.34	0.1	$e^{-t/0.3}$ Gyr	2	2.96	3.4	0.41	0.37
395746810	$4.04^{+0.26}_{-0.29}$	0.244	$12.28^{+0.35}_{-0.0}$	-27.54	0.1	$t_{trunc} = 1.0$	2	8.31	3.25	0.45	0.37
396223342	$4.04^{+0.17}_{-0.18}$	0.557	$11.92^{+0.32}_{-0.34}$	-26.95	0.1	$t_{trunc} = 0.3$	2	4.44	3.44	0.37	0.25
396276124	$3.85^{+0.32}_{-0.18}$	0.701	$12.32^{+0.36}_{-0.01}$	-27.63	0.1	$t_{trunc} = 1.0$	2	2.61	3.42	0.48	0.37
396551822	$3.77^{+0.54}_{-0.38}$	0.231	$12.07^{+0.06}_{-0.03}$	-27.01	0.1	$t_{trunc} = 1.0$	2	1.27	3.29	0.47	0.37

Table A2 – *continued*

ID	z_{phot}	χ_r^2	$\log_{10}(M^*/M_{\odot})$	Abs. Mag. (<i>i</i>)	Age (Gyr)	SFH	[Z/H] (Z_{\odot})	σ_{AGN}	$z_{DESonly}$	z_{BPZ}	E (B-V)
397300605	4.14 ^{+0.15} _{-0.13}	1.197	12.03 ^{+0.4} _{-0.02}	-27.23	0.1	$t_{trunc} = 1.0$	2	7.77	3.29	0.47	0.25
397303505	3.8 ^{+0.34} _{-0.34}	1.263	12.19 ^{+0.18} _{-0.02}	-27.29	0.1	CONSTANT	2	4.8	3.4	0.49	0.37
397554368	3.77 ^{+0.54} _{-0.33}	0.717	12.12 ^{+0.41} _{-0.05}	-27.09	0.11	$t_{trunc} = 0.1$	1	3.19	3.61	0.37	0.25
397885462	4.14 ^{+0.22} _{-0.67}	0.569	12.11 ^{+0.53} _{-0.18}	-27.08	0.1	$t_{trunc} = 0.1$	2	1.74	3.29	0.5	0.37
398107560	3.91 ^{+0.29} _{-0.21}	0.699	12.25 ^{+0.13} _{-0.04}	-27.46	0.1	CONSTANT	2	3.3	3.4	0.45	0.37
399842613	4.25 ^{+0.15} _{-0.16}	1.231	12.22 ^{+0.45} _{-0.02}	-27.37	0.1	$t_{trunc} = 0.1$	2	0.36	3.32	0.59	0.37
401003476	3.86 ^{+0.42} _{-0.53}	0.44	12.0 ^{+0.19} _{-0.34}	-26.54	0.16	$e^{-t/0.1}$ Gyr	2	1.37	3.4	0.39	0.25
401582291	3.7 ^{+0.6} _{-0.46}	0.259	11.91 ^{+0.35} _{-0.04}	-26.49	0.11	$t_{trunc} = 0.1$	2	2.58	2.46	0.4	0.25
404760121	3.88 ^{+0.33} _{-0.28}	0.224	11.79 ^{+0.43} _{-0.3}	-26.63	0.1	$t_{trunc} = 0.1$	2	4.56	3.61	0.4	0.25
404798494	3.92 ^{+0.17} _{-0.1}	0.823	12.02 ^{+0.04} _{-0.05}	-27.2	0.1	$t_{trunc} = 0.1$	2	7.32	3.34	0.44	0.25
404907811	3.72 ^{+0.42} _{-0.32}	0.664	12.28 ^{+0.21} _{-0.02}	-27.52	0.1	$e^{-t/1.0}$ Gyr	2	6.14	3.4	0.36	0.37
405529691	3.71 ^{+0.43} _{-0.31}	0.264	12.42 ^{+0.12} _{-0.12}	-27.72	0.11	$e^{-t/0.3}$ Gyr	2	7.91	3.42	0.41	0.37
405537460	4.2 ^{+0.18} _{-0.84}	0.301	12.07 ^{+0.52} _{-0.11}	-26.99	0.1	$t_{trunc} = 0.1$	2	7.74	3.39	0.59	0.37
405539533	3.8 ^{+0.35} _{-0.37}	0.246	12.2 ^{+0.19} _{-0.03}	-27.33	0.1	$t_{trunc} = 1.0$	2	2.12	3.45	0.46	0.37
405686502	3.99 ^{+0.32} _{-0.38}	0.789	11.63 ^{+0.15} _{-0.34}	-26.22	0.1	$t_{trunc} = 1.0$	2	1.33	3.25	0.41	0.25
405937444	4.04 ^{+0.12} _{-0.14}	1.5	12.21 ^{+0.03} _{-0.35}	-27.67	0.1	$t_{trunc} = 0.1$	2	11.74	3.4	0.42	0.25
406039218	3.76 ^{+0.37} _{-0.17}	1.012	12.5 ^{+0.15} _{-0.0}	-28.09	0.1	$t_{trunc} = 1.0$	2	22.07	3.42	0.39	0.37
406366767	3.44 ^{+0.86} _{-0.25}	0.957	12.04 ^{+0.25} _{-0.0}	-26.82	0.11	$t_{trunc} = 0.1$	2	0.03	3.29	0.43	0.25
407630148	3.88 ^{+0.38} _{-0.34}	0.985	12.05 ^{+0.16} _{-0.02}	-26.95	0.1	CONSTANT	2	2.07	3.37	0.53	0.37
408132796	3.76 ^{+0.4} _{-0.33}	1.048	12.36 ^{+0.48} _{-0.09}	-27.71	0.1	$t_{trunc} = 0.1$	2	4.01	3.34	0.46	0.37
408135057	4.08 ^{+0.24} _{-0.24}	1.633	12.08 ^{+0.42} _{-0.02}	-27.02	0.1	$t_{trunc} = 1.0$	2	0.64	3.75	0.48	0.37
409127588	4.11 ^{+0.21} _{-0.63}	1.095	12.14 ^{+0.35} _{-0.23}	-27.18	0.1	$t_{trunc} = 1.0$	2	4.41	3.48	0.52	0.37
410163990	4.11 ^{+0.22} _{-0.49}	0.959	12.22 ^{+0.26} _{-0.23}	-27.38	0.1	$t_{trunc} = 0.1$	2	0.52	2.51	0.54	0.37
411500732	4.17 ^{+0.13} _{-0.28}	1.938	11.77 ^{+0.03} _{-0.31}	-26.57	0.1	$t_{trunc} = 0.1$	2	0.7	3.37	0.46	0.25
411502452	3.94 ^{+0.28} _{-0.42}	0.828	11.96 ^{+0.46} _{-0.32}	-27.06	0.1	$t_{trunc} = 0.1$	2	2.72	3.4	0.41	0.25
412637681	3.94 ^{+0.26} _{-0.47}	1.938	11.79 ^{+0.44} _{-0.29}	-26.61	0.1	$t_{trunc} = 0.1$	2	0.49	2.48	0.46	0.25
414173316	3.67 ^{+0.5} _{-0.2}	0.421	11.76 ^{+0.31} _{-0.0}	-26.56	0.1	CONSTANT	2	2.24	3.4	0.34	0.25
414235028	4.04 ^{+0.29} _{-0.61}	0.151	12.08 ^{+0.46} _{-0.19}	-27.07	0.16	CONSTANT	2	8.39	3.29	0.35	0.25
414237423	4.0 ^{+0.31} _{-0.3}	0.331	12.26 ^{+0.17} _{-0.01}	-27.48	0.1	$t_{trunc} = 1.0$	2	2.3	3.46	0.43	0.37
414248322	3.8 ^{+0.48} _{-0.27}	0.397	12.08 ^{+0.12} _{-0.04}	-27.06	0.1	$t_{trunc} = 0.3$	1/5	4.73	3.67	0.45	0.37
415246403	3.79 ^{+0.37} _{-0.35}	1.017	11.98 ^{+0.35} _{-0.02}	-26.79	0.1	CONSTANT	2	0.17	2.46	0.49	0.37
417446833	3.86 ^{+0.51} _{-0.46}	0.283	12.12 ^{+0.39} _{-0.23}	-26.77	0.13	$t_{trunc} = 0.1$	2	0.43	3.65	0.57	0.25
417565001	3.83 ^{+0.13} _{-0.34}	2.192	11.86 ^{+0.03} _{-0.28}	-26.8	0.1	$t_{trunc} = 0.1$	2	2.01	2.42	0.37	0.25
417565185	3.83 ^{+0.41} _{-0.33}	0.801	12.21 ^{+0.08} _{-0.02}	-27.35	0.1	CONSTANT	2	1.49	3.77	0.39	0.37
417579802	3.83 ^{+0.41} _{-0.48}	0.281	12.41 ^{+0.46} _{-0.04}	-27.52	0.1	$t_{trunc} = 0.1$	2	6.89	3.5	0.51	0.49
429617726	3.92 ^{+0.33} _{-0.26}	0.289	12.3 ^{+0.44} _{-0.29}	-27.56	0.1	$t_{trunc} = 0.1$	2	5.91	3.34	0.46	0.37

Table A2 – continued

ID	z_{phot}	χ_r^2	$\log_{10}(M^*/M_{\odot})$	Abs. Mag. (<i>i</i>)	Age (Gyr)	SFH	[Z/H] (Z_{\odot})	σ_{AGN}	$z_{DESonly}$	z_{BPZ}	E (B-V)
431449768	$3.76^{+0.4}_{-0.37}$	0.636	$12.1^{+0.07}_{-0.03}$	-27.07	0.1	$t_{trunc} = 1.0$	2	3.77	3.4	0.34	0.37
431455424	$3.81^{+0.53}_{-0.24}$	1.217	$12.13^{+0.27}_{-0.09}$	-27.04	0.13	SSP	2	14.07	3.42	0.64	0.0
444147103	$3.87^{+0.34}_{-0.39}$	0.609	$12.23^{+0.18}_{-0.04}$	-27.39	0.1	$t_{trunc} = 1.0$	2	4.9	3.44	0.46	0.37
444182193	$3.89^{+0.3}_{-0.41}$	0.76	$12.26^{+0.39}_{-0.22}$	-27.47	0.1	$t_{trunc} = 0.1$	2	9.0	3.64	0.43	0.37
446501990	$4.24^{+0.17}_{-0.23}$	0.934	$12.18^{+0.36}_{-0.03}$	-27.27	0.1	$t_{trunc} = 1.0$	2	2.7	3.88	0.5	0.37
465281154	$4.13^{+0.2}_{-0.44}$	0.128	$11.84^{+0.52}_{-0.36}$	-26.75	0.1	$t_{trunc} = 0.1$	2	8.61	3.4	0.39	0.25
470611726	$3.88^{+0.38}_{-0.5}$	0.538	$12.04^{+0.27}_{-0.06}$	-26.93	0.1	$t_{trunc} = 0.1$	2	7.27	3.64	0.5	0.37
470971747	$3.83^{+0.52}_{-0.46}$	0.57	$12.39^{+0.0}_{-0.28}$	-27.22	1.02	$t_{trunc} = 1.0$	1	2.36	2.54	0.28	0.12
471106730	$4.11^{+0.27}_{-0.82}$	0.184	$12.09^{+0.02}_{-0.1}$	-26.62	0.29	$e^{-t/0.3 \text{ Gyr}}$	2	0.54	3.38	0.42	0.25
471394809	$3.88^{+0.42}_{-0.46}$	0.932	$12.22^{+0.0}_{-0.25}$	-26.89	0.32	$e^{-t/0.3 \text{ Gyr}}$	2	4.72	3.81	0.4	0.25
471566339	$3.71^{+0.3}_{-0.27}$	0.576	$11.84^{+0.38}_{-0.04}$	-26.75	0.1	$t_{trunc} = 0.1$	2	5.77	2.46	0.29	0.25
471600124	$4.14^{+0.26}_{-0.51}$	0.213	$11.77^{+0.3}_{-0.28}$	-26.36	0.14	CONSTANT	2	2.32	3.25	0.49	0.25
471612288	$3.92^{+0.33}_{-0.45}$	0.448	$11.63^{+0.39}_{-0.31}$	-26.21	0.1	$t_{trunc} = 0.1$	2	0.92	3.29	0.39	0.25
471703164	$3.83^{+0.43}_{-0.46}$	0.273	$11.54^{+0.26}_{-0.19}$	-26.0	0.1	CONSTANT	2	0.51	3.46	0.36	0.25
473133985	$4.01^{+0.18}_{-0.28}$	0.903	$11.99^{+0.16}_{-0.29}$	-27.11	0.1	$t_{trunc} = 0.1$	2	7.56	3.58	0.38	0.25
473140970	$3.96^{+0.19}_{-0.09}$	0.896	$12.11^{+0.29}_{-0.28}$	-27.43	0.1	$t_{trunc} = 0.1$	2	9.56	3.43	0.42	0.25
473404298	$3.85^{+0.53}_{-0.45}$	0.14	$11.98^{+0.42}_{-0.15}$	-26.76	0.1	$e^{-t/1.0 \text{ Gyr}}$	2	0.43	3.69	0.47	0.37
473408311	$4.08^{+0.14}_{-0.13}$	0.674	$12.15^{+0.26}_{-0.28}$	-27.51	0.1	$t_{trunc} = 0.1$	2	8.66	3.65	0.44	0.25
473411673	$4.1^{+0.15}_{-0.33}$	0.533	$11.91^{+0.26}_{-0.35}$	-26.91	0.1	$t_{trunc} = 0.1$	2	5.69	3.61	0.45	0.25
473496203	$4.16^{+0.22}_{-0.55}$	0.383	$11.41^{+0.51}_{-0.16}$	-26.07	0.1	$t_{trunc} = 0.1$	1	0.37	3.05	0.38	0.12
473498930	$4.05^{+0.13}_{-0.08}$	1.032	$12.31^{+0.03}_{-0.04}$	-27.91	0.1	$t_{trunc} = 0.1$	2	20.72	3.53	0.41	0.25
473503196	$4.13^{+0.23}_{-0.25}$	0.547	$12.15^{+0.43}_{-0.01}$	-27.19	0.1	$t_{trunc} = 1.0$	2	3.37	3.31	0.59	0.37
473511031	$3.86^{+0.34}_{-0.19}$	1.458	$12.21^{+0.36}_{-0.04}$	-27.36	0.1	CONSTANT	2	1.92	2.44	0.41	0.37
473512115	$4.11^{+0.18}_{-0.29}$	1.324	$12.01^{+0.51}_{-0.37}$	-27.16	0.1	$t_{trunc} = 0.1$	2	3.44	3.62	0.43	0.25
473514761	$4.2^{+0.14}_{-0.47}$	1.842	$12.25^{+0.23}_{-0.45}$	-27.03	0.72	$e^{-t/1.0 \text{ Gyr}}$	2	3.02	3.15	0.46	0.12
473515047	$3.81^{+0.41}_{-0.37}$	0.625	$12.35^{+0.03}_{-0.15}$	-27.31	0.26	$e^{-t/0.3 \text{ Gyr}}$	2	3.13	3.4	0.37	0.25
473515263	$4.08^{+0.17}_{-0.16}$	0.998	$11.8^{+0.16}_{-0.01}$	-26.65	0.1	CONSTANT	2	2.27	3.34	0.45	0.25
473519025	$4.01^{+0.29}_{-0.31}$	0.714	$12.18^{+0.15}_{-0.02}$	-27.27	0.1	$t_{trunc} = 1.0$	2	0.81	3.46	0.5	0.37
473520285	$3.8^{+0.37}_{-0.18}$	1.077	$12.24^{+0.34}_{-0.0}$	-27.44	0.1	CONSTANT	2	3.35	3.4	0.38	0.37
473520601	$4.14^{+0.19}_{-0.38}$	0.503	$12.23^{+0.22}_{-0.1}$	-27.41	0.1	$t_{trunc} = 1.0$	2	2.05	3.55	0.56	0.37
473521671	$4.13^{+0.14}_{-0.18}$	0.866	$12.3^{+0.02}_{-0.03}$	-27.57	0.1	$t_{trunc} = 0.1$	2	2.5	3.45	0.58	0.37
473528868	$4.05^{+0.31}_{-0.57}$	0.208	$11.64^{+0.37}_{-0.31}$	-26.24	0.1	$t_{trunc} = 0.1$	2	1.9	3.63	0.5	0.25
473530252	$4.11^{+0.22}_{-0.26}$	0.371	$12.02^{+0.82}_{-0.3}$	-27.2	0.1	$t_{trunc} = 0.1$	2	0.76	3.75	0.46	0.25
473532585	$4.04^{+0.22}_{-0.31}$	0.523	$11.91^{+0.43}_{-0.35}$	-26.91	0.1	$t_{trunc} = 0.1$	2	0.78	3.33	0.43	0.25
476998818	$3.76^{+0.38}_{-0.37}$	1.496	$12.39^{+0.07}_{-0.27}$	-27.81	0.1	$t_{trunc} = 1.0$	2	8.94	3.46	0.33	0.37
477008049	$3.8^{+0.52}_{-0.58}$	0.339	$12.28^{+0.2}_{-0.13}$	-27.18	0.2	CONSTANT	1	4.79	3.45	0.51	0.37

Table A2 – *continued*

ID	z_{phot}	χ_r^2	$\log_{10}(M^*/M_{\odot})$	Abs. Mag. (<i>i</i>)	Age (Gyr)	SFH	[Z/H] (Z_{\odot})	σ_{AGN}	$z_{DESonly}$	z_{BPZ}	E (B-V)
477008438	4.2 ^{+0.08} _{-0.14}	2.353	11.92 ^{+0.03} _{-0.02}	-26.95	0.1	CONSTANT	2	4.99	3.29	0.45	0.25
479472291	3.83 ^{+0.49} _{-0.52}	0.957	11.85 ^{+0.57} _{-0.05}	-26.44	0.1	$t_{trunc} = 0.1$	2	0.38	2.4	0.56	0.37
479999051	3.46 ^{+0.81} _{-0.06}	0.255	12.35 ^{+0.43} _{-0.12}	-27.57	0.11	$t_{trunc} = 0.1$	2	3.53	3.4	0.36	0.25
480008436	3.48 ^{+0.82} _{-0.2}	0.365	12.47 ^{+0.67} _{-0.15}	-27.89	0.11	$t_{trunc} = 0.1$	2	10.76	3.29	0.41	0.25
480339250	4.13 ^{+0.19} _{-0.53}	0.613	12.3 ^{+0.53} _{-0.07}	-27.57	0.1	$t_{trunc} = 0.1$	2	6.05	3.34	0.55	0.37
481065880	3.87 ^{+0.43} _{-0.29}	1.102	12.27 ^{+0.31} _{-0.01}	-27.51	0.1	$t_{trunc} = 1.0$	2	4.82	2.64	0.5	0.37
481350973	3.97 ^{+0.33} _{-0.35}	0.275	11.94 ^{+0.39} _{-0.34}	-26.98	0.1	$t_{trunc} = 0.1$	2	5.37	3.64	0.4	0.25
481989803	3.76 ^{+0.62} _{-0.47}	0.543	12.0 ^{+0.59} _{-0.03}	-26.71	0.11	$t_{trunc} = 0.1$	2	3.48	3.29	0.43	0.25
481994767	4.2 ^{+0.25} _{-0.63}	0.245	11.5 ^{+0.54} _{-0.25}	-25.89	0.1	$t_{trunc} = 0.1$	2	0.98	3.49	0.51	0.25
482001634	3.88 ^{+0.38} _{-0.56}	1.609	12.04 ^{+0.01} _{-0.29}	-26.44	0.32	$e^{-t/0.3}$ Gyr	2	0.04	3.34	0.44	0.25
483918716	4.11 ^{+0.25} _{-0.83}	0.701	12.45 ^{+0.06} _{-0.38}	-27.28	0.64	$e^{-t/1.0}$ Gyr	2	0.5	3.37	0.43	0.25
489254835	4.11 ^{+0.25} _{-0.39}	0.866	12.21 ^{+0.42} _{-0.11}	-27.34	0.1	$t_{trunc} = 1.0$	2	4.53	3.75	0.48	0.37
490689649	4.1 ^{+0.11} _{-0.33}	1.02	12.41 ^{+0.07} _{-0.1}	-27.88	0.11	$e^{-t/0.1}$ Gyr	2	23.72	3.25	0.42	0.25
490704656	4.17 ^{+0.21} _{-0.71}	0.896	12.45 ^{+0.13} _{-0.38}	-27.31	0.45	$e^{-t/0.3}$ Gyr	2	0.75	3.29	0.51	0.25
492431224	4.17 ^{+0.19} _{-0.8}	0.868	12.22 ^{+0.74} _{-0.05}	-27.36	0.1	$t_{trunc} = 0.1$	2	7.22	3.29	0.54	0.37
492605523	3.77 ^{+0.33} _{-0.12}	0.595	11.8 ^{+0.36} _{-0.27}	-26.64	0.1	$t_{trunc} = 0.1$	2	5.57	3.75	0.41	0.25
493212188	4.08 ^{+0.18} _{-0.37}	0.799	11.83 ^{+0.32} _{-0.34}	-26.72	0.1	$t_{trunc} = 0.1$	2	3.81	3.5	0.4	0.25
493739755	4.21 ^{+0.21} _{-0.45}	0.94	12.1 ^{+0.43} _{-0.24}	-27.07	0.1	$t_{trunc} = 0.3$	2	4.09	3.15	0.5	0.37
493882026	3.69 ^{+0.4} _{-0.46}	0.421	11.96 ^{+0.19} _{-0.14}	-26.71	0.1	$e^{-t/1.0}$ Gyr	2	1.0	2.46	0.44	0.37
494789087	3.96 ^{+0.48} _{-0.38}	1.445	11.21 ^{+0.55} _{-0.1}	-25.38	0.11	$t_{trunc} = 0.1$	2	0.73	2.63	0.4	0.0
494790027	4.04 ^{+0.35} _{-0.38}	1.06	11.84 ^{+0.36} _{-0.05}	-26.62	0.11	$t_{trunc} = 0.1$	2	3.18	2.58	0.52	0.12
494790169	4.08 ^{+0.32} _{-0.39}	0.243	11.79 ^{+0.55} _{-0.06}	-26.66	0.1	CONSTANT	1/5	1.53	3.96	0.42	0.25
494790792	3.95 ^{+0.44} _{-0.65}	0.243	12.24 ^{+0.38} _{-0.05}	-27.49	0.1	$t_{trunc} = 0.1$	1	4.72	3.26	0.5	0.37
494791393	3.75 ^{+0.61} _{-0.4}	0.724	11.65 ^{+0.14} _{-0.21}	-25.82	0.13	SSP	2	0.52	3.4	0.59	0.0
494792459	4.25 ^{+0.2} _{-0.42}	0.761	11.16 ^{+1.67} _{-0.63}	-25.36	0.1	$t_{trunc} = 0.1$	2	0.36	3.15	0.44	0.12
494793098	4.02 ^{+0.4} _{-0.32}	0.179	11.85 ^{+0.34} _{-0.1}	-26.65	0.11	$t_{trunc} = 0.1$	2	0.33	3.81	0.48	0.12
494793167	4.09 ^{+0.24} _{-0.47}	0.229	11.8 ^{+0.38} _{-0.35}	-26.64	0.1	$t_{trunc} = 0.1$	2	2.53	3.75	0.41	0.25
494800805	4.25 ^{+0.1} _{-1.22}	0.196	12.29 ^{+0.26} _{-0.5}	-27.19	0.81	$e^{-t/0.3}$ Gyr	2	0.64	3.15	0.39	0.0
494801634	3.34 ^{+0.53} _{-0.26}	0.373	12.04 ^{+0.61} _{-0.06}	-26.95	0.1	SSP	1/2	0.95	3.44	0.35	0.12
495323159	3.92 ^{+0.41} _{-0.48}	1.814	11.5 ^{+0.22} _{-0.07}	-25.9	0.11	$t_{trunc} = 0.1$	1/5	0.54	2.65	0.41	0.12
495325646	3.74 ^{+0.58} _{-0.45}	0.378	11.85 ^{+0.25} _{-0.16}	-26.45	0.1	$t_{trunc} = 1.0$	2	0.18	3.29	0.48	0.37
495342175	3.75 ^{+0.29} _{-0.25}	1.587	12.2 ^{+0.38} _{-0.05}	-27.32	0.1	$t_{trunc} = 0.1$	2	0.81	2.46	0.4	0.37
495508558	4.25 ^{+0.11} _{-0.18}	1.819	11.86 ^{+0.4} _{-0.06}	-26.79	0.1	$t_{trunc} = 0.3$	2	0.02	3.29	0.39	0.25
495566911	3.12 ^{+0.21} _{-0.15}	0.438	11.81 ^{+0.03} _{-0.11}	-26.12	0.16	SSP	2	0.56	4.29	0.54	0.0
496787409	4.14 ^{+0.23} _{-0.49}	0.246	11.77 ^{+0.53} _{-0.34}	-26.58	0.1	$t_{trunc} = 0.1$	2	4.22	3.19	0.45	0.25
497171956	4.16 ^{+0.1} _{-0.08}	0.851	12.24 ^{+0.04} _{-0.29}	-27.75	0.1	$t_{trunc} = 0.1$	2	6.9	3.75	0.44	0.25

Table A2 – continued

ID	z_{phot}	χ_r^2	$\log_{10}(M^*/M_\odot)$	Abs. Mag. (<i>i</i>)	Age (Gyr)	SFH	[Z/H] (Z_\odot)	σ_{AGN}	$z_{DESonly}$	z_{BPZ}	E (B-V)
497174314	3.94 ^{+0.47} _{-0.89}	0.17	11.38 ^{+0.92} _{-0.15}	-25.58	0.11	$t_{trunc} = 0.1$	1	1.76	2.56	0.59	0.12
498898550	3.67 ^{+0.56} _{-0.34}	0.39	11.84 ^{+0.25} _{-0.02}	-26.42	0.1	$t_{trunc} = 1.0$	2	2.18	2.44	0.41	0.37
499908069	3.37 ^{+0.85} _{-0.21}	0.565	11.88 ^{+0.25} _{-0.14}	-26.41	0.11	$t_{trunc} = 0.1$	2	0.89	3.42	0.41	0.25
499909599	4.14 ^{+0.26} _{-0.47}	0.595	11.66 ^{+0.36} _{-0.35}	-26.29	0.1	$t_{trunc} = 0.1$	2	2.04	3.21	0.43	0.25
500048125	3.75 ^{+0.64} _{-0.45}	0.585	11.87 ^{+0.83} _{-0.18}	-26.37	0.13	SSP	2	2.17	3.25	0.49	0.0
500110571	3.99 ^{+0.26} _{-0.55}	0.655	11.82 ^{+0.36} _{-0.32}	-26.7	0.1	$t_{trunc} = 0.1$	2	3.83	3.71	0.41	0.25
500571685	3.38 ^{+0.88} _{-0.09}	0.985	12.18 ^{+0.08} _{-0.28}	-27.17	0.11	$t_{trunc} = 0.1$	2	14.94	3.26	0.4	0.25
500910602	4.22 ^{+0.15} _{-0.55}	0.558	11.63 ^{+0.6} _{-0.09}	-26.23	0.1	$t_{trunc} = 0.1$	2	1.08	3.25	0.51	0.25
501218097	4.11 ^{+0.22} _{-0.14}	0.666	11.89 ^{+0.43} _{-0.02}	-26.89	0.1	$t_{trunc} = 1.0$	2	5.96	3.6	0.38	0.25
501511673	4.2 ^{+0.13} _{-0.37}	0.806	11.73 ^{+0.04} _{-0.4}	-26.46	0.1	$t_{trunc} = 0.1$	2	0.23	3.25	0.49	0.25
501524910	4.13 ^{+0.2} _{-0.32}	0.38	12.01 ^{+0.42} _{-0.36}	-27.17	0.1	$t_{trunc} = 0.1$	2	4.02	3.79	0.4	0.25
501665859	3.91 ^{+0.37} _{-0.48}	1.302	11.68 ^{+0.42} _{-0.0}	-26.4	0.1	$t_{trunc} = 0.1$	1/5	2.39	2.65	0.29	0.25
502431214	3.67 ^{+0.28} _{-0.29}	0.805	12.4 ^{+0.24} _{-0.01}	-27.8	0.1	$e^{-t/1.0 \text{ Gyr}}$	2	7.24	3.67	0.42	0.37
502433292	3.92 ^{+0.33} _{-0.39}	1.378	12.21 ^{+0.38} _{-0.04}	-27.35	0.1	$t_{trunc} = 1.0$	2	4.44	3.4	0.45	0.37
502449004	3.71 ^{+0.11} _{-0.18}	2.397	12.35 ^{+0.05} _{-0.0}	-27.69	0.1	CONSTANT	2	5.02	2.46	0.45	0.37
503482151	3.68 ^{+0.59} _{-0.32}	0.318	11.95 ^{+0.08} _{-0.0}	-26.71	0.1	CONSTANT	2	5.9	3.7	0.46	0.37
503811408	3.88 ^{+0.28} _{-0.13}	0.809	12.47 ^{+0.22} _{-0.06}	-28.0	0.1	$t_{trunc} = 0.1$	2	11.55	3.34	0.47	0.37
503973856	4.03 ^{+0.29} _{-0.61}	1.435	12.45 ^{+0.77} _{-0.01}	-27.93	0.1	$t_{trunc} = 0.1$	2	3.56	3.35	0.61	0.37
503973990	3.73 ^{+0.38} _{-0.37}	0.86	11.66 ^{+0.41} _{-0.14}	-26.3	0.1	$t_{trunc} = 0.1$	2	2.25	2.4	0.56	0.25
503984762	3.81 ^{+0.3} _{-0.46}	0.301	11.73 ^{+0.05} _{-0.26}	-26.37	0.11	$t_{trunc} = 0.1$	2	0.27	2.54	0.38	0.12
503985134	3.85 ^{+0.4} _{-0.39}	0.257	12.01 ^{+0.12} _{-0.23}	-26.84	0.1	$t_{trunc} = 0.1$	2	0.82	3.48	0.48	0.37
504051667	4.0 ^{+0.24} _{-0.64}	1.718	12.18 ^{+0.54} _{-0.25}	-27.06	0.26	CONSTANT	2	1.42	3.25	0.39	0.25
504056183	3.92 ^{+0.33} _{-0.25}	0.944	12.26 ^{+0.18} _{-0.01}	-27.48	0.1	$t_{trunc} = 1.0$	2	5.42	3.4	0.43	0.37
504194446	4.21 ^{+0.09} _{-0.26}	1.142	12.18 ^{+0.05} _{-0.38}	-27.59	0.1	$t_{trunc} = 0.1$	2	9.77	3.48	0.48	0.25
504330828	3.86 ^{+0.14} _{-0.1}	1.841	11.86 ^{+0.02} _{-0.37}	-26.8	0.1	$t_{trunc} = 0.1$	2	4.25	2.45	0.35	0.25
504394690	3.56 ^{+0.59} _{-0.29}	1.649	12.24 ^{+0.61} _{-0.1}	-27.31	0.11	$t_{trunc} = 0.1$	2	1.57	3.34	0.37	0.25
504825888	4.04 ^{+0.28} _{-0.38}	0.31	12.03 ^{+0.22} _{-0.19}	-26.89	0.18	$t_{trunc} = 0.3$	2	1.46	3.3	0.37	0.25
505013250	3.86 ^{+0.3} _{-0.16}	1.22	12.5 ^{+0.0} _{-0.0}	-28.07	0.1	$t_{trunc} = 1.0$	2	12.17	3.35	0.46	0.37
505018776	3.31 ^{+0.65} _{-0.29}	0.523	12.17 ^{+0.75} _{-0.13}	-26.68	0.23	$t_{trunc} = 0.1$	1/5	0.29	2.48	0.42	0.25
505028285	4.13 ^{+0.11} _{-0.32}	0.528	12.22 ^{+0.36} _{-0.35}	-27.68	0.1	$t_{trunc} = 0.1$	2	17.04	3.48	0.47	0.25
506153545	3.96 ^{+0.32} _{-0.59}	1.414	11.66 ^{+0.38} _{-0.29}	-26.29	0.1	$t_{trunc} = 0.1$	2	2.61	3.29	0.38	0.25
506329583	3.77 ^{+0.6} _{-0.45}	0.399	11.94 ^{+0.87} _{-0.25}	-26.72	0.11	$t_{trunc} = 0.1$	1/2	1.72	2.56	0.4	0.25
506345182	4.02 ^{+0.29} _{-0.53}	0.485	12.07 ^{+0.39} _{-0.13}	-27.01	0.1	$t_{trunc} = 1.0$	2	1.09	3.4	0.53	0.37
506383847	4.17 ^{+0.3} _{-0.55}	0.3	11.45 ^{+0.76} _{-0.18}	-25.95	0.1	$t_{trunc} = 0.1$	1/2	4.16	3.12	0.5	0.25
506534457	3.86 ^{+0.1} _{-0.15}	1.624	12.49 ^{+0.05} _{-0.01}	-28.06	0.1	CONSTANT	2	8.97	2.49	0.4	0.37
506537406	3.98 ^{+0.35} _{-0.25}	1.501	12.22 ^{+0.05} _{-0.01}	-27.37	0.1	CONSTANT	2	4.12	2.59	0.5	0.37

Table A2 – *continued*

ID	z_{phot}	χ_r^2	$\log_{10}(M^*/M_{\odot})$	Abs. Mag. (<i>i</i>)	Age (Gyr)	SFH	[Z/H] (Z_{\odot})	σ_{AGN}	$z_{DESonly}$	z_{BPZ}	E (B-V)
506572275	$3.81^{+0.44}_{-0.35}$	0.905	$12.24^{+0.59}_{-0.1}$	-27.42	0.1	$t_{trunc} = 0.1$	2	2.15	3.75	0.49	0.37
506589633	$3.73^{+0.39}_{-0.29}$	0.252	$12.29^{+0.27}_{-0.08}$	-27.53	0.1	$t_{trunc} = 0.1$	2	0.77	2.55	0.43	0.37
506646930	$3.62^{+0.37}_{-0.17}$	0.67	$11.78^{+0.36}_{-0.01}$	-26.62	0.1	$t_{trunc} = 1.0$	2	13.77	3.83	3.5	0.25
506674710	$3.92^{+0.35}_{-0.6}$	0.793	$11.54^{+0.4}_{-0.05}$	-26.0	0.1	$t_{trunc} = 0.1$	2	4.77	3.29	0.45	0.25
506674855	$3.75^{+0.46}_{-0.33}$	0.231	$11.91^{+0.12}_{-0.24}$	-26.43	0.14	$e^{-t/0.1}$ Gyr	2	4.12	2.48	0.35	0.25
506674909	$3.53^{+0.22}_{-0.58}$	2.948	$11.96^{+0.04}_{-0.62}$	-26.35	0.81	$e^{-t/0.3}$ Gyr	2	4.29	3.31	0.41	0.0
506675198	$3.95^{+0.19}_{-0.1}$	1.455	$12.07^{+0.17}_{-0.05}$	-27.31	0.1	$t_{trunc} = 0.1$	2	13.62	3.3	0.39	0.25
507681715	$3.81^{+0.57}_{-0.37}$	1.116	$11.96^{+0.59}_{-0.04}$	-26.72	0.13	$t_{trunc} = 0.1$	2	5.25	2.56	0.41	0.12
507691551	$3.87^{+0.36}_{-0.43}$	0.75	$11.66^{+0.16}_{-0.05}$	-26.3	0.1	$e^{-t/1.0}$ Gyr	2	3.45	3.34	0.38	0.25
507780409	$3.84^{+0.16}_{-0.4}$	0.874	$12.13^{+0.15}_{-0.07}$	-27.07	0.13	$e^{-t/0.1}$ Gyr	2	1.67	3.65	0.36	0.25
507785363	$3.88^{+0.58}_{-0.44}$	0.37	$12.1^{+0.57}_{-0.29}$	-26.95	0.11	$t_{trunc} = 0.1$	2	0.67	2.64	0.48	0.25
507791066	$3.75^{+0.41}_{-0.21}$	0.553	$12.42^{+0.22}_{-0.02}$	-27.88	0.1	CONSTANT	2	10.98	3.7	0.47	0.37
507791530	$3.77^{+0.53}_{-0.31}$	0.702	$12.45^{+0.08}_{-0.02}$	-27.62	0.1	$t_{trunc} = 0.3$	2	2.4	2.6	0.54	0.49
507803985	$3.83^{+0.35}_{-0.38}$	0.62	$12.15^{+0.19}_{-0.03}$	-27.21	0.1	CONSTANT	2	1.63	3.5	0.4	0.37
507810919	$3.77^{+0.21}_{-0.21}$	0.563	$12.37^{+0.09}_{-0.04}$	-27.73	0.1	$t_{trunc} = 0.1$	2	9.6	2.55	0.41	0.37
508217521	$3.89^{+0.37}_{-0.73}$	0.38	$11.31^{+0.4}_{-0.18}$	-25.41	0.1	$t_{trunc} = 0.1$	2	1.41	3.4	0.45	0.25
618652137	$3.85^{+0.3}_{-0.18}$	0.711	$12.47^{+0.19}_{-0.0}$	-28.01	0.1	CONSTANT	2	4.1	3.34	0.45	0.37
618654757	$3.94^{+0.35}_{-0.27}$	0.554	$11.65^{+0.16}_{-0.02}$	-26.28	0.1	$t_{trunc} = 1.0$	2	0.64	3.27	0.43	0.25
618660654	$3.77^{+0.38}_{-0.19}$	1.199	$12.12^{+0.19}_{-0.0}$	-27.45	0.1	$t_{trunc} = 1.0$	2	27.05	3.37	0.27	0.25
618664093	$4.08^{+0.14}_{-0.42}$	0.811	$12.33^{+0.11}_{-0.02}$	-27.45	0.26	CONSTANT	2	1.29	3.34	0.47	0.25
618664306	$4.09^{+0.25}_{-0.24}$	0.964	$12.06^{+0.25}_{-0.02}$	-27.38	0.1	$t_{trunc} = 0.1$	1	1.62	3.21	0.41	0.25
618667069	$3.75^{+0.2}_{-0.45}$	1.662	$12.46^{+0.1}_{-0.24}$	-27.48	0.14	$e^{-t/0.1}$ Gyr	2	0.76	2.42	0.49	0.37
618667272	$3.32^{+0.94}_{-0.05}$	2.294	$12.2^{+0.67}_{-0.03}$	-27.14	0.14	$t_{trunc} = 0.1$	2	0.4	3.29	0.4	0.12

This paper has been typeset from a $\text{T}_{\text{E}}\text{X}/\text{L}^{\text{A}}\text{T}_{\text{E}}\text{X}$ file prepared by the author.

Table B1. Photometry for all galaxies matching the best candidate criteria (as in Section 3.1).

ID	RA	Dec	<i>g</i>	<i>r</i>	<i>i</i>	<i>z</i>	<i>Y</i>	<i>J</i>	<i>H</i>	<i>K_s</i>
100600870	342.30182	-45.078395	22.6555 ± 0.0389	20.8248 ± 0.0107	20.4152 ± 0.0091	20.0676 ± 0.017	20.0109 ± 0.0434	19.5742 ± 0.1168	///	19.1676 ± 0.1954
100669215	342.03479	-44.585222	23.4434 ± 0.0705	21.6989 ± 0.0216	21.3218 ± 0.0203	21.1502 ± 0.0362	20.8496 ± 0.1093	20.3986 ± 0.2289	///	20.0326 ± 0.2853
102002089	342.83733	-44.098439	24.601 ± 0.1949	22.4569 ± 0.0323	21.8981 ± 0.0313	21.4884 ± 0.0422	21.5888 ± 0.1419	22.069 ± 0.6841	///	20.7842 ± 0.5095
102009403	342.92415	-44.216238	23.0138 ± 0.0534	21.1502 ± 0.0133	20.7563 ± 0.0117	20.3417 ± 0.0217	20.2165 ± 0.0552	20.2064 ± 0.2059	///	19.8197 ± 0.4318
102009835	342.78469	-44.222644	23.2401 ± 0.0574	21.2488 ± 0.0128	20.7316 ± 0.0108	20.3393 ± 0.0172	20.0885 ± 0.0449	19.9653 ± 0.1708	///	19.5771 ± 0.301
102009849	343.07164	-44.222642	22.9057 ± 0.0415	20.9317 ± 0.0096	20.4301 ± 0.0082	20.0647 ± 0.0132	19.9559 ± 0.0384	19.5375 ± 0.1272	///	18.8814 ± 0.1611
102031864	342.67377	-44.586054	23.7029 ± 0.0824	21.6185 ± 0.0158	21.166 ± 0.0131	20.6985 ± 0.0243	20.559 ± 0.069	20.3562 ± 0.1998	///	20.0655 ± 0.3812
105765488	343.14792	-44.73924	24.547 ± 0.186	22.2931 ± 0.0307	21.679 ± 0.0248	21.3457 ± 0.0381	20.9561 ± 0.1048	20.5069 ± 0.2779	///	19.9714 ± 0.3972
115286147	346.7354	-54.15315	23.6712 ± 0.072	21.8732 ± 0.0187	21.5055 ± 0.0216	21.2711 ± 0.0271	21.2205 ± 0.1017	21.0654 ± 0.3385	20.4333 ± 0.3563	20.7988 ± 0.5508
132987082	352.71081	-56.175512	23.1963 ± 0.0604	21.3267 ± 0.0138	20.936 ± 0.0128	20.6552 ± 0.0213	20.4853 ± 0.0558	20.4962 ± 0.3287	20.2877 ± 0.326	19.9255 ± 0.2908
133076071	352.25228	-54.44832	25.4926 ± 0.3086	23.1365 ± 0.0578	22.627 ± 0.0485	22.0704 ± 0.0467	22.0912 ± 0.182	21.7161 ± 0.3706	20.9951 ± 0.3085	///
133572897	352.63464	-55.347821	23.438 ± 0.0723	21.2476 ± 0.0132	20.6824 ± 0.0148	20.2945 ± 0.0123	20.1462 ± 0.0443	19.777 ± 0.1121	19.3033 ± 0.1181	18.9962 ± 0.1502
133575827	352.67649	-55.400238	24.4783 ± 0.198	22.2043 ± 0.0323	21.6132 ± 0.0291	21.1491 ± 0.0318	21.1862 ± 0.1105	20.9814 ± 0.3641	19.8677 ± 0.2136	19.8708 ± 0.2773
133592684	351.76774	-55.706425	25.4775 ± 0.4146	22.9885 ± 0.0455	22.3547 ± 0.054	22.0122 ± 0.066	21.8248 ± 0.1865	21.5672 ± 0.4797	21.0576 ± 0.3478	///
133755647	351.91336	-53.493204	24.4042 ± 0.1861	22.4897 ± 0.039	22.062 ± 0.0436	21.6709 ± 0.0432	21.4716 ± 0.129	21.6099 ± 0.414	20.5935 ± 0.3413	///
133779875	352.71218	-56.397366	24.934 ± 0.265	22.5784 ± 0.0335	21.9448 ± 0.0276	21.5152 ± 0.0376	21.2576 ± 0.0928	21.511 ± 0.4189	20.7446 ± 0.4251	20.2463 ± 0.3848
133785852	352.18188	-56.500569	24.3457 ± 0.1665	22.4928 ± 0.0368	22.2019 ± 0.0372	21.7933 ± 0.0578	21.7324 ± 0.1663	21.8538 ± 0.528	21.3977 ± 0.4754	///
134036466	352.37636	-53.819372	24.223 ± 0.1449	22.1393 ± 0.0323	21.605 ± 0.0203	21.27 ± 0.028	21.0453 ± 0.0917	20.2741 ± 0.2098	20.7209 ± 0.4705	19.8545 ± 0.29
134797801	353.7305	-54.894179	24.0588 ± 0.1346	22.1215 ± 0.0328	21.6522 ± 0.0369	21.4115 ± 0.051	21.437 ± 0.1785	20.5483 ± 0.2525	20.1579 ± 0.2536	20.4186 ± 0.3508
135449486	353.25806	-53.740368	24.0972 ± 0.1317	22.256 ± 0.0245	21.8684 ± 0.025	21.5708 ± 0.037	21.5983 ± 0.1506	20.6018 ± 0.2768	///	20.2794 ± 0.3621
135756581	353.7427	-55.810608	23.3406 ± 0.0691	21.3252 ± 0.023	20.8207 ± 0.0213	20.3921 ± 0.0167	20.3421 ± 0.0519	19.7828 ± 0.2156	19.4258 ± 0.1912	19.1619 ± 0.1735
135760809	353.74692	-55.88496	23.588 ± 0.0759	21.7434 ± 0.025	21.3865 ± 0.0304	20.9549 ± 0.0351	20.8349 ± 0.0815	20.1222 ± 0.2272	20.1289 ± 0.2668	19.4991 ± 0.2475
135856576	353.29081	-55.221638	23.1259 ± 0.0632	21.434 ± 0.018	21.1319 ± 0.0191	20.8609 ± 0.029	20.729 ± 0.0756	19.8682 ± 0.1669	20.0908 ± 0.2622	19.2495 ± 0.1864
135857162	353.45976	-55.233363	24.1318 ± 0.1085	22.1671 ± 0.0264	21.7816 ± 0.0302	21.3856 ± 0.0349	21.3156 ± 0.1054	21.1737 ± 0.4544	20.1333 ± 0.2346	20.3493 ± 0.3292
136034648	353.68277	-54.057979	24.4399 ± 0.123	22.5119 ± 0.0313	22.0482 ± 0.027	21.8656 ± 0.0407	21.7545 ± 0.1699	21.1021 ± 0.258	21.1659 ± 0.4415	21.0203 ± 0.4616
136067262	352.86591	-54.565938	22.4776 ± 0.0329	20.5077 ± 0.0077	20.055 ± 0.0083	19.7252 ± 0.0083	19.4739 ± 0.0236	19.1608 ± 0.0844	18.8353 ± 0.0815	18.5181 ± 0.0889
137552954	354.14324	-53.680157	23.4352 ± 0.0772	21.5577 ± 0.0173	21.2035 ± 0.0199	20.7824 ± 0.0228	20.7397 ± 0.0852	20.0006 ± 0.1948	20.2114 ± 0.36	19.6497 ± 0.3023
137650861	354.24639	-55.389564	23.5837 ± 0.0773	21.779 ± 0.0219	21.4551 ± 0.0323	21.0314 ± 0.0309	21.049 ± 0.0851	20.508 ± 0.2074	20.1826 ± 0.2531	19.5486 ± 0.1901
137806706	354.36219	-54.375504	24.7472 ± 0.2121	22.5005 ± 0.0355	21.8507 ± 0.0285	21.5693 ± 0.0312	21.4401 ± 0.1208	21.9481 ± 0.6971	20.7374 ± 0.3222	19.7515 ± 0.2184
164738198	358.90161	-54.818986	22.4492 ± 0.0527	20.5963 ± 0.0152	20.1956 ± 0.0165	19.776 ± 0.0202	19.3846 ± 0.0736	19.1157 ± 0.1568	19.3069 ± 0.2075	18.3731 ± 0.189
164738777	358.75276	-54.83057	23.8034 ± 0.1519	22.1184 ± 0.0473	21.8647 ± 0.0596	21.4598 ± 0.0756	21.0705 ± 0.2825	21.2516 ± 0.4482	20.556 ± 0.3502	19.8052 ± 0.2597
285308599	14.414781	-48.804004	24.7676 ± 0.2334	22.7232 ± 0.0415	22.2136 ± 0.0395	21.9378 ± 0.073	21.5997 ± 0.178	21.3909 ± 0.3709	21.1189 ± 0.4607	///
287114376	15.20774	-49.788143	23.6629 ± 0.1105	21.6639 ± 0.0206	21.1472 ± 0.0223	20.6945 ± 0.021	20.6482 ± 0.0625	21.0043 ± 0.4252	20.005 ± 0.3234	19.3694 ± 0.2374
287127591	14.834417	-50.057703	24.0709 ± 0.101	22.278 ± 0.0287	21.8705 ± 0.0376	21.5943 ± 0.0422	21.3773 ± 0.1198	20.9281 ± 0.2765	20.8242 ± 0.4541	///
289328303	14.893991	-48.693727	24.7251 ± 0.169	22.5617 ± 0.0361	21.9878 ± 0.0314	21.6397 ± 0.0474	21.367 ± 0.106	20.7427 ± 0.3011	20.8539 ± 0.3599	20.3699 ± 0.439
289329064	15.312428	-48.706967	25.0449 ± 0.2507	22.6631 ± 0.0372	22.0102 ± 0.0359	21.6065 ± 0.0423	21.4101 ± 0.1157	20.875 ± 0.3671	21.2675 ± 0.5009	20.5554 ± 0.3884
290792079	16.25137	-49.77414	23.7461 ± 0.0919	21.9562 ± 0.0302	21.6583 ± 0.038	21.1624 ± 0.0467	21.4474 ± 0.189	21.039 ± 0.3194	20.3046 ± 0.3015	///
395017226	74.586265	-58.313936	23.2962 ± 0.0743	21.5345 ± 0.0202	21.1771 ± 0.0232	20.8012 ± 0.0234	20.7718 ± 0.0792	20.3102 ± 0.1374	///	19.4084 ± 0.2242
395746810	74.445041	-44.532828	23.8575 ± 0.1305	21.7522 ± 0.0161	21.198 ± 0.0142	20.8371 ± 0.0216	20.752 ± 0.0812	20.2545 ± 0.2339	///	19.5169 ± 0.2744
396223342	73.654576	-53.700542	23.1074 ± 0.0432	21.3073 ± 0.0138	20.8929 ± 0.0132	20.5505 ± 0.0186	20.5346 ± 0.0786	20.1705 ± 0.299	20.0543 ± 0.3993	19.9464 ± 0.416
396276124	74.967618	-48.454857	23.2672 ± 0.0618	21.3685 ± 0.0149	20.9423 ± 0.0173	20.58 ± 0.0236	20.4901 ± 0.0503	20.1177 ± 0.1443	///	19.5708 ± 0.2546
396551822	75.118785	-56.433087	23.7063 ± 0.0999	21.866 ± 0.029	21.4662 ± 0.0184	21.1487 ± 0.0288	21.0696 ± 0.1015	20.9235 ± 0.3866	///	20.0047 ± 0.3445
397300605	74.061341	-51.962462	23.0718 ± 0.0482	21.1513 ± 0.0107	20.6845 ± 0.0113	20.2851 ± 0.0154	20.281 ± 0.0626	20.3177 ± 0.3422	20.6818 ± 0.6108	19.4903 ± 0.3249
397303505	74.450771	-52.010571	23.4739 ± 0.0603	21.6514 ± 0.0155	21.2691 ± 0.0192	20.7807 ± 0.0235	20.8044 ± 0.0696	20.791 ± 0.3929	20.2137 ± 0.3405	19.739 ± 0.3198
397554368	75.356969	-50.873063	23.7775 ± 0.0869	21.8318 ± 0.0203	21.4502 ± 0.0201	21.1724 ± 0.0298	20.9651 ± 0.097	20.4776 ± 0.2366	21.1366 ± 0.7077	19.2596 ± 0.2286

Table B1 – continued

ID	RA	Dec	g	r	i	z	Y	J	H	K_s
397764328	74.890797	-52.347374	23.5908 ± 0.0918	21.6711 ± 0.0211	21.2131 ± 0.0219	20.6847 ± 0.0255	20.5936 ± 0.0656	20.8524 ± 0.2944	19.809 ± 0.257	20.0628 ± 0.3292
397885462	73.562242	-59.48389	24.9502 ± 0.2252	22.5626 ± 0.0249	21.9313 ± 0.0258	21.5111 ± 0.0346	21.5167 ± 0.1147	21.4336 ± 0.469	///	20.1094 ± 0.3602
398107560	74.313676	-51.699346	23.5493 ± 0.0617	21.6321 ± 0.014	21.1804 ± 0.0144	20.7587 ± 0.0196	20.6536 ± 0.0679	20.6748 ± 0.27	20.1912 ± 0.3498	19.5987 ± 0.2567
399804681	74.814022	-51.10434	24.2284 ± 0.1626	22.166 ± 0.0331	21.604 ± 0.0277	21.032 ± 0.0389	20.9641 ± 0.1101	///	21.3539 ± 0.8698	19.7706 ± 0.38
399842053	74.771454	-51.68691	23.36 ± 0.0647	21.5027 ± 0.0156	21.0551 ± 0.0165	20.6205 ± 0.0208	20.5097 ± 0.0549	20.2867 ± 0.2367	20.8851 ± 0.7733	19.7016 ± 0.3453
399842613	75.053674	-51.696081	24.9501 ± 0.2206	22.4861 ± 0.029	21.746 ± 0.0226	21.2557 ± 0.0297	21.2596 ± 0.1008	///	20.7158 ± 0.4189	20.3271 ± 0.3888
400998781	75.100601	-45.683346	23.7645 ± 0.0918	21.839 ± 0.0178	21.3687 ± 0.0167	21.0268 ± 0.0233	20.7628 ± 0.0704	20.4275 ± 0.2373	20.5278 ± 0.3386	20.3169 ± 0.5816
401003476	75.35966	-45.76118	23.9154 ± 0.1235	22.0856 ± 0.0308	21.7697 ± 0.0271	21.4402 ± 0.0393	21.3884 ± 0.164	21.2846 ± 0.302	21.2964 ± 0.5372	19.9379 ± 0.3416
401582291	64.467562	-58.898214	24.5483 ± 0.2288	22.5131 ± 0.0473	22.1264 ± 0.0501	21.7576 ± 0.0536	21.5444 ± 0.2075	21.5302 ± 0.4591	///	20.1246 ± 0.2651
404760121	64.736812	-59.604299	23.3602 ± 0.0617	21.5514 ± 0.0183	21.2555 ± 0.0152	20.9841 ± 0.0219	20.8746 ± 0.0889	20.624 ± 0.3042	///	20.0661 ± 0.3319
404788215	65.0661	-60.109331	22.9465 ± 0.0545	21.1413 ± 0.0128	20.7484 ± 0.0107	20.4236 ± 0.012	20.2369 ± 0.0494	20.0363 ± 0.2626	///	19.5802 ± 0.3211
404798117	64.63269	-60.275175	22.7971 ± 0.0477	20.9261 ± 0.0108	20.5082 ± 0.0075	20.134 ± 0.0088	20.0712 ± 0.0445	19.6986 ± 0.2053	///	18.7474 ± 0.1934
404798494	64.735582	-60.281503	22.8486 ± 0.0472	21.0882 ± 0.0127	20.7222 ± 0.0085	20.3916 ± 0.0104	20.3547 ± 0.0532	19.866 ± 0.1715	///	19.65 ± 0.3155
404886634	75.115868	-53.892735	23.0517 ± 0.0705	21.1583 ± 0.015	20.7596 ± 0.0158	20.2935 ± 0.0149	20.2824 ± 0.0602	19.5284 ± 0.1803	19.7741 ± 0.3507	19.1199 ± 0.1798
404907811	74.805477	-54.223115	23.1039 ± 0.0568	21.3026 ± 0.0133	20.9829 ± 0.0146	20.5729 ± 0.0189	20.5462 ± 0.0627	20.219 ± 0.2805	20.2028 ± 0.3399	19.1973 ± 0.2258
405529691	65.117284	-47.215187	22.9859 ± 0.0566	21.2186 ± 0.0135	20.8256 ± 0.0128	20.476 ± 0.0285	20.4139 ± 0.061	19.9611 ± 0.1815	///	19.0709 ± 0.2174
405537460	65.478563	-47.338487	25.2986 ± 0.3594	22.7805 ± 0.0411	22.0764 ± 0.0386	21.6464 ± 0.0506	21.6283 ± 0.1684	21.2757 ± 0.4063	///	20.0457 ± 0.3743
405539533	65.116222	-47.369926	23.4267 ± 0.0564	21.6028 ± 0.0149	21.1819 ± 0.0171	20.8571 ± 0.0257	20.7523 ± 0.0766	20.2255 ± 0.1939	///	19.6028 ± 0.3283
405686502	65.164352	-52.879981	23.7051 ± 0.0819	21.9415 ± 0.0233	21.5463 ± 0.0237	21.2429 ± 0.0309	21.4574 ± 0.1453	///	20.9149 ± 0.6179	20.5062 ± 0.5354
405937444	62.975669	-50.249041	22.6574 ± 0.0422	20.8067 ± 0.0097	20.4151 ± 0.0095	20.0197 ± 0.0116	19.9339 ± 0.0373	19.7463 ± 0.132	19.2522 ± 0.1818	19.134 ± 0.2049
406039218	62.191626	-50.576468	22.6071 ± 0.0332	20.7808 ± 0.0105	20.3524 ± 0.0092	20.0607 ± 0.0132	19.991 ± 0.0418	19.424 ± 0.1381	19.2638 ± 0.1886	18.9398 ± 0.1777
406366767	64.496811	-51.686919	23.7201 ± 0.1058	21.9184 ± 0.0252	21.5077 ± 0.0268	21.1835 ± 0.0334	21.4243 ± 0.1671	///	20.0413 ± 0.2778	19.8268 ± 0.2729
407630148	64.861041	-57.074594	24.0186 ± 0.1351	22.1055 ± 0.0429	21.6619 ± 0.0326	21.2322 ± 0.038	21.2625 ± 0.1413	21.4115 ± 0.552	///	20.2885 ± 0.4175
408132796	75.087803	-58.98511	23.2578 ± 0.0719	21.3597 ± 0.0177	20.952 ± 0.0188	20.5829 ± 0.022	20.5814 ± 0.0786	19.8598 ± 0.1492	///	19.1699 ± 0.221
408135057	75.239132	-59.018159	24.3785 ± 0.1205	22.3252 ± 0.023	21.7784 ± 0.025	21.3381 ± 0.0293	21.1517 ± 0.0868	21.5292 ± 0.4326	///	20.5262 ± 0.4663
408311797	76.370391	-51.127227	22.9456 ± 0.0566	21.0052 ± 0.0147	20.5265 ± 0.012	20.0224 ± 0.0178	19.8377 ± 0.0435	19.7207 ± 0.2125	19.8212 ± 0.3157	19.3971 ± 0.2453
409127588	76.164078	-53.361555	24.6746 ± 0.3113	22.1943 ± 0.0363	21.6538 ± 0.0346	21.1917 ± 0.0454	21.2397 ± 0.1598	21.0225 ± 0.3155	///	20.0819 ± 0.398
410163990	76.409332	-51.657022	24.5772 ± 0.1976	22.2201 ± 0.0338	21.6152 ± 0.0272	21.2317 ± 0.0394	20.9677 ± 0.0847	21.2381 ± 0.6188	20.2781 ± 0.3549	20.0919 ± 0.495
411491335	76.457981	-51.875177	22.439 ± 0.0278	20.5167 ± 0.007	20.0393 ± 0.0058	19.5733 ± 0.0087	19.5696 ± 0.0314	19.1866 ± 0.1195	18.7518 ± 0.1313	18.4397 ± 0.1378
411500732	76.42265	-52.014029	24.104 ± 0.1255	22.0469 ± 0.0223	21.5737 ± 0.021	21.1512 ± 0.0331	21.0509 ± 0.0991	22.7368 ± 1.9292	20.8167 ± 0.5139	20.8872 ± 0.6996
411502452	76.547769	-52.041829	23.0166 ± 0.0598	21.2702 ± 0.0143	20.893 ± 0.0146	20.5077 ± 0.0256	20.538 ± 0.0825	20.0929 ± 0.2539	20.1879 ± 0.361	19.6299 ± 0.3589
412637681	77.509814	-55.587338	23.4912 ± 0.0853	21.7185 ± 0.0212	21.3535 ± 0.0247	20.9935 ± 0.0281	20.7794 ± 0.0752	21.2144 ± 0.3166	///	20.3509 ± 0.5627
414173316	77.759211	-54.51745	22.6755 ± 0.0334	21.1531 ± 0.0118	20.9737 ± 0.014	20.7169 ± 0.0233	20.725 ± 0.083	20.7809 ± 0.3979	20.3158 ± 0.3934	20.1399 ± 0.3997
414233666	77.141751	-52.204417	22.4313 ± 0.035	20.4623 ± 0.0082	20.0013 ± 0.0073	19.5652 ± 0.0116	19.5786 ± 0.03	19.0301 ± 0.1276	18.7956 ± 0.1321	18.4607 ± 0.1602
414235028	77.228654	-52.228478	23.1905 ± 0.0504	21.3496 ± 0.0125	20.9219 ± 0.0111	20.6251 ± 0.0199	20.5805 ± 0.0544	20.4523 ± 0.2887	20.1747 ± 0.3567	///
414237423	77.311045	-52.267314	23.7765 ± 0.0811	21.723 ± 0.0165	21.2099 ± 0.0133	20.8681 ± 0.0229	20.7274 ± 0.0637	20.5735 ± 0.2637	20.3744 ± 0.4091	19.5854 ± 0.2725
414248322	77.450892	-52.451427	23.4408 ± 0.0635	21.6418 ± 0.0184	21.2592 ± 0.0181	21.0471 ± 0.0299	20.968 ± 0.0853	20.3269 ± 0.235	20.4217 ± 0.3819	19.7555 ± 0.3024
415246403	76.845921	-57.960174	23.9919 ± 0.1117	22.1305 ± 0.0279	21.7255 ± 0.0302	21.4194 ± 0.0404	21.0415 ± 0.1004	21.0782 ± 0.321	///	20.347 ± 0.3444
417446833	78.683303	-55.542744	25.3732 ± 0.2964	22.9691 ± 0.0373	22.3065 ± 0.0362	21.8995 ± 0.0516	21.6686 ± 0.1419	21.5122 ± 0.5379	///	20.2202 ± 0.4242
417565001	78.514677	-59.118784	23.1326 ± 0.0993	21.292 ± 0.0256	21.1465 ± 0.0298	20.7002 ± 0.0366	20.586 ± 0.0808	20.4386 ± 0.2725	///	19.7768 ± 0.3142
417565185	78.042549	-59.12149	23.503 ± 0.079	21.6217 ± 0.0196	21.2055 ± 0.0206	20.8387 ± 0.0271	20.6695 ± 0.099	20.7859 ± 0.3845	///	19.9382 ± 0.3777
417579802	78.892568	-59.302243	25.0052 ± 0.2943	22.689 ± 0.0433	22.1223 ± 0.0446	21.6426 ± 0.0533	21.5012 ± 0.1415	21.0526 ± 0.2719	///	19.722 ± 0.253
429617726	80.073587	-60.616957	23.7366 ± 0.1092	21.7555 ± 0.0241	21.2501 ± 0.0228	20.8693 ± 0.0338	20.8168 ± 0.1043	20.2875 ± 0.1685	///	19.511 ± 0.2726
431449768	80.455728	-58.88703	23.6336 ± 0.0945	21.786 ± 0.0229	21.4117 ± 0.0223	21.0735 ± 0.0398	21.0377 ± 0.1018	20.4183 ± 0.1879	///	19.975 ± 0.3288
431455424	81.597737	-58.959126	24.6513 ± 0.2397	21.8823 ± 0.0227	21.1749 ± 0.0156	20.7796 ± 0.0256	20.6714 ± 0.0717	20.0864 ± 0.2123	///	19.3482 ± 0.2785

Table B1 – *continued*

ID	RA	Dec	<i>g</i>	<i>r</i>	<i>i</i>	<i>z</i>	<i>Y</i>	<i>J</i>	<i>H</i>	<i>K_s</i>
431827017	81.354041	-58.057944	23.2026 ± 0.0476	21.2471 ± 0.011	20.7517 ± 0.0115	20.3163 ± 0.0167	20.152 ± 0.0392	19.8805 ± 0.1737	///	19.1435 ± 0.2499
434401854	82.755855	-59.110482	22.1099 ± 0.0321	20.2853 ± 0.008	19.8901 ± 0.0083	19.4465 ± 0.0112	19.3971 ± 0.029	19.025 ± 0.0832	///	18.2387 ± 0.1132
444147103	85.376884	-58.940568	23.5463 ± 0.0735	21.6129 ± 0.0154	21.192 ± 0.0154	20.818 ± 0.0267	20.775 ± 0.0862	20.1796 ± 0.2493	///	19.7918 ± 0.3938
444182193	85.110945	-59.440915	23.7537 ± 0.0926	21.8281 ± 0.0205	21.3662 ± 0.0227	20.8868 ± 0.0312	20.7948 ± 0.0928	20.6415 ± 0.2817	///	19.5198 ± 0.3014
446501990	85.426451	-59.886883	24.6979 ± 0.188	22.3271 ± 0.0229	21.6196 ± 0.0219	21.2602 ± 0.0285	21.088 ± 0.0768	20.4715 ± 0.2061	///	20.2923 ± 0.4367
465281154	88.694639	-60.880289	23.8226 ± 0.1104	21.8313 ± 0.0213	21.328 ± 0.0163	20.9986 ± 0.0192	20.9853 ± 0.0918	20.7884 ± 0.3129	///	20.0238 ± 0.4269
470611726	68.015452	-57.726539	24.4208 ± 0.1593	22.3445 ± 0.0275	21.8636 ± 0.0288	21.4757 ± 0.0426	21.2412 ± 0.1197	21.3266 ± 0.3366	///	20.1595 ± 0.4922
470971747	68.208929	-46.413716	24.0987 ± 0.1243	22.224 ± 0.0271	21.7986 ± 0.0315	21.5484 ± 0.0447	21.2657 ± 0.1219	21.8636 ± 0.639	20.633 ± 0.2853	///
471106730	67.806799	-48.09239	24.4546 ± 0.1494	22.5018 ± 0.0334	22.012 ± 0.0311	21.6765 ± 0.0431	21.6995 ± 0.1584	21.3476 ± 0.4082	///	20.3634 ± 0.414
471394809	68.225794	-49.845339	23.7923 ± 0.1258	22.0831 ± 0.0333	21.7222 ± 0.0397	21.3568 ± 0.0477	21.2234 ± 0.1538	21.5166 ± 0.3726	21.6085 ± 0.7613	19.8777 ± 0.3553
471566339	67.791747	-55.696441	22.863 ± 0.0353	21.2469 ± 0.0107	20.9837 ± 0.0153	20.8102 ± 0.02	20.5601 ± 0.0619	20.3447 ± 0.2166	///	19.7623 ± 0.3429
471600124	67.869581	-50.51476	24.1376 ± 0.1269	22.1467 ± 0.0252	21.6436 ± 0.0243	21.3571 ± 0.0396	21.4194 ± 0.1494	21.4962 ± 0.5654	20.9746 ± 0.5645	20.2412 ± 0.4441
471612288	68.709632	-50.703145	23.8449 ± 0.0823	22.0712 ± 0.0192	21.7054 ± 0.0212	21.3864 ± 0.0332	21.3935 ± 0.1154	20.763 ± 0.2999	20.8055 ± 0.3421	20.5186 ± 0.4057
471703164	67.76219	-58.42731	23.5709 ± 0.0907	21.937 ± 0.0255	21.6394 ± 0.0294	21.3997 ± 0.0499	21.4529 ± 0.1611	21.0869 ± 0.3356	///	20.9197 ± 0.611
471985468	68.102795	-51.605856	23.9431 ± 0.1032	21.7663 ± 0.0198	21.1723 ± 0.0183	20.6454 ± 0.0214	20.3563 ± 0.0652	20.0749 ± 0.2601	20.1773 ± 0.435	19.3967 ± 0.2487
473133985	68.278612	-59.221893	23.1876 ± 0.0564	21.2676 ± 0.0179	20.918 ± 0.0184	20.5623 ± 0.0208	20.4779 ± 0.0616	20.3628 ± 0.3244	///	19.8854 ± 0.3629
473136272	68.511645	-59.258768	22.6157 ± 0.0438	20.757 ± 0.0124	20.394 ± 0.0159	19.9438 ± 0.0164	19.811 ± 0.0456	19.567 ± 0.179	///	19.0002 ± 0.236
473140970	68.018102	-59.326386	22.7329 ± 0.0328	20.9469 ± 0.0087	20.5496 ± 0.01	20.171 ± 0.0128	20.1362 ± 0.0353	19.9709 ± 0.2354	///	19.3725 ± 0.273
473404298	69.190285	-53.57752	24.2228 ± 0.1205	22.2758 ± 0.0231	21.8083 ± 0.0265	21.5149 ± 0.0354	21.3414 ± 0.1081	21.1183 ± 0.349	20.9943 ± 0.4442	///
473408311	68.154396	-53.640567	22.899 ± 0.0414	20.9924 ± 0.0089	20.5245 ± 0.0097	20.2577 ± 0.0128	20.1052 ± 0.0392	20.1029 ± 0.2052	19.4351 ± 0.2472	19.3967 ± 0.3048
473411673	68.342642	-53.697237	23.5694 ± 0.0761	21.6306 ± 0.0165	21.1501 ± 0.0169	20.8434 ± 0.0221	20.7352 ± 0.0698	20.2406 ± 0.282	20.0624 ± 0.311	20.1277 ± 0.4122
473496203	68.212594	-52.534274	23.1208 ± 0.0483	21.32 ± 0.0153	20.948 ± 0.019	20.8536 ± 0.0234	20.8906 ± 0.103	20.7444 ± 0.28	20.0464 ± 0.3494	20.3174 ± 0.4628
473498930	68.254197	-52.584789	22.4382 ± 0.0244	20.5714 ± 0.0071	20.137 ± 0.0061	19.7813 ± 0.0081	19.7027 ± 0.0285	19.4225 ± 0.1614	19.1099 ± 0.1822	18.9732 ± 0.1685
473503196	68.909139	-52.659906	24.4077 ± 0.1486	22.2416 ± 0.0277	21.6304 ± 0.0284	21.2237 ± 0.0288	21.119 ± 0.1047	20.9983 ± 0.3423	21.0803 ± 0.6356	20.1595 ± 0.3725
473511031	68.753934	-52.795529	23.6007 ± 0.0809	21.6237 ± 0.0185	21.257 ± 0.0227	20.8359 ± 0.0276	20.6099 ± 0.1122	20.218 ± 0.2205	20.4341 ± 0.418	19.9327 ± 0.3162
473512115	68.849081	-52.81743	23.3463 ± 0.0571	21.3662 ± 0.0129	20.9137 ± 0.0147	20.6 ± 0.0171	20.4476 ± 0.0603	20.854 ± 0.3506	19.6202 ± 0.273	19.7195 ± 0.3539
473514761	68.69552	-52.864257	23.4876 ± 0.0658	21.6858 ± 0.0173	21.2713 ± 0.0206	20.9585 ± 0.0238	21.2592 ± 0.1275	21.4338 ± 0.6027	20.0219 ± 0.2868	20.1094 ± 0.3443
473515047	68.696452	-52.86959	22.9084 ± 0.0388	21.2686 ± 0.012	20.9422 ± 0.0151	20.6508 ± 0.0177	20.6624 ± 0.0729	19.9769 ± 0.2377	20.3863 ± 0.507	19.3123 ± 0.2227
473515263	68.722423	-52.873137	23.5003 ± 0.0656	21.6486 ± 0.0165	21.2154 ± 0.0192	20.8589 ± 0.0212	20.8558 ± 0.0863	20.8481 ± 0.4468	20.0665 ± 0.2988	20.8256 ± 0.7838
473519025	69.1008	-52.936476	24.0393 ± 0.1012	21.9567 ± 0.0205	21.4533 ± 0.0223	21.0557 ± 0.0245	20.9363 ± 0.0906	21.27 ± 0.5549	20.5077 ± 0.3753	19.7921 ± 0.3149
473520285	69.096087	-52.956492	23.3578 ± 0.069	21.4833 ± 0.0169	21.1118 ± 0.02	20.6784 ± 0.0245	20.6302 ± 0.0854	20.2812 ± 0.2525	20.1506 ± 0.3385	19.8298 ± 0.3216
473520601	68.931326	-52.962545	24.3092 ± 0.177	22.0243 ± 0.0249	21.4266 ± 0.0275	21.0256 ± 0.0279	20.8627 ± 0.1009	20.5927 ± 0.3115	20.1106 ± 0.3451	19.9529 ± 0.4215
473521671	69.128687	-52.981234	24.3187 ± 0.1436	22.0736 ± 0.0243	21.4911 ± 0.0283	20.9878 ± 0.0247	20.8696 ± 0.0906	20.6394 ± 0.3011	20.1737 ± 0.4037	19.8794 ± 0.3939
473528868	68.674413	-53.097801	24.1166 ± 0.1223	22.2099 ± 0.028	21.7669 ± 0.0328	21.4741 ± 0.0407	21.3384 ± 0.1279	21.5962 ± 0.6845	21.1738 ± 0.5239	20.4126 ± 0.4157
473530252	68.665468	-53.118678	23.326 ± 0.0575	21.3349 ± 0.0126	20.8245 ± 0.0183	20.5805 ± 0.0171	20.5111 ± 0.0568	20.0143 ± 0.1948	19.8325 ± 0.2459	19.5137 ± 0.2643
473532585	68.669534	-53.155561	23.4498 ± 0.0613	21.5327 ± 0.0145	21.1079 ± 0.0173	20.79 ± 0.0206	20.7767 ± 0.072	20.4669 ± 0.3203	19.8571 ± 0.2716	19.9781 ± 0.4112
476998818	80.775198	-56.96095	22.9227 ± 0.0728	21.0226 ± 0.0221	20.6496 ± 0.0176	20.3897 ± 0.0232	20.3291 ± 0.1019	19.5362 ± 0.1445	///	19.0818 ± 0.2283
477008049	80.723353	-57.106877	23.8122 ± 0.0925	21.9787 ± 0.0233	21.5891 ± 0.0195	21.2365 ± 0.0342	21.2065 ± 0.1147	21.1477 ± 0.4207	///	19.56 ± 0.2348
477008438	81.047966	-57.113178	23.4808 ± 0.0706	21.5231 ± 0.016	21.0241 ± 0.0144	20.5601 ± 0.0207	20.5961 ± 0.0637	20.4656 ± 0.2417	///	20.9803 ± 1.057
479472291	72.171121	-45.288854	24.7652 ± 0.2445	22.7269 ± 0.0468	22.3355 ± 0.0494	21.8283 ± 0.0716	21.6033 ± 0.2091	21.7642 ± 0.4696	21.3982 ± 0.5541	///
479999051	72.528332	-52.87657	23.0289 ± 0.0458	21.1696 ± 0.0115	20.8216 ± 0.0123	20.464 ± 0.0166	20.4292 ± 0.0546	20.0697 ± 0.2392	19.643 ± 0.2247	///
480008436	72.410619	-53.037279	22.7515 ± 0.0367	20.9045 ± 0.0097	20.5081 ± 0.0099	20.1442 ± 0.0134	20.1127 ± 0.0436	19.7786 ± 0.2444	19.1614 ± 0.1861	///
480339250	72.299325	-53.204044	24.2994 ± 0.1888	22.0722 ± 0.0321	21.4702 ± 0.0296	20.9923 ± 0.0313	20.999 ± 0.1264	20.3812 ± 0.2839	20.3993 ± 0.2756	///
480995070	73.093464	-60.584365	23.6004 ± 0.0912	21.6301 ± 0.0165	21.1455 ± 0.0187	20.7126 ± 0.0206	20.4067 ± 0.0573	20.2847 ± 0.1411	///	19.7413 ± 0.379
481065880	72.101555	-48.944222	23.4708 ± 0.0812	21.4922 ± 0.0152	20.9918 ± 0.0149	20.8064 ± 0.0195	20.5594 ± 0.0635	20.2096 ± 0.1334	///	19.4956 ± 0.1879

Table B1 – continued

ID	RA	Dec	<i>g</i>	<i>r</i>	<i>i</i>	<i>z</i>	<i>Y</i>	<i>J</i>	<i>H</i>	<i>K_s</i>
481350973	72.813908	-47.600626	23.1958 ± 0.0612	21.3706 ± 0.0158	20.9589 ± 0.0182	20.6744 ± 0.0213	20.5618 ± 0.0759	20.5647 ± 0.3233	///	19.9526 ± 0.5323
481989803	72.120899	-45.61534	24.4427 ± 0.1475	22.4001 ± 0.0324	21.9192 ± 0.0285	21.5902 ± 0.0425	21.6684 ± 0.1651	20.8491 ± 0.2714	20.8164 ± 0.3249	///
481994767	71.896784	-45.687727	24.8643 ± 0.2282	22.7831 ± 0.0452	22.2127 ± 0.0404	21.9062 ± 0.0618	21.8439 ± 0.2125	21.8744 ± 0.5399	22.007 ± 0.7345	///
482001634	72.307954	-45.794599	24.2255 ± 0.1234	22.5135 ± 0.0314	22.1931 ± 0.0315	21.7569 ± 0.0548	22.0476 ± 0.2355	21.3845 ± 0.3144	21.9101 ± 0.6719	///
482208365	73.320644	-51.189418	22.8554 ± 0.0359	20.9531 ± 0.0099	20.5427 ± 0.0095	20.1552 ± 0.014	20.0031 ± 0.0415	19.931 ± 0.2528	19.1732 ± 0.209	19.2358 ± 0.2245
483918716	72.085462	-48.777383	24.1798 ± 0.1091	22.2827 ± 0.0232	21.8386 ± 0.0258	21.435 ± 0.0344	21.4798 ± 0.1145	21.4635 ± 0.3782	///	19.9161 ± 0.3324
489254835	69.13225	-55.548991	24.316 ± 0.1564	22.0218 ± 0.0194	21.4483 ± 0.0165	21.0965 ± 0.0303	20.9006 ± 0.0864	20.7104 ± 0.2035	///	20.0555 ± 0.3584
490689649	69.699465	-50.470457	22.724 ± 0.0556	20.7901 ± 0.0101	20.3348 ± 0.0047	20.0119 ± 0.0048	19.9312 ± 0.0311	19.5759 ± 0.1132	19.2226 ± 0.1444	18.8934 ± 0.1221
490704656	69.206037	-50.70402	24.5856 ± 0.2029	22.52 ± 0.0384	22.0135 ± 0.0387	21.5827 ± 0.0518	21.7259 ± 0.2148	21.752 ± 0.5469	21.1371 ± 0.3792	///
492431224	72.971578	-53.024726	24.6768 ± 0.2208	22.3423 ± 0.0348	21.7108 ± 0.0311	21.2272 ± 0.0405	21.3848 ± 0.1612	20.7611 ± 0.382	20.2978 ± 0.2511	///
492605523	69.282253	-53.006647	23.105 ± 0.0616	21.4524 ± 0.0268	21.1915 ± 0.0238	20.8579 ± 0.0313	20.7097 ± 0.098	20.472 ± 0.3439	20.775 ± 0.4058	19.9658 ± 0.326
493212188	73.272104	-47.599847	23.6873 ± 0.0792	21.7956 ± 0.0184	21.3344 ± 0.0192	20.9807 ± 0.0258	20.8355 ± 0.1045	20.6709 ± 0.4332	///	20.5957 ± 0.685
493739755	70.668823	-48.194975	24.8323 ± 0.2236	22.4769 ± 0.0337	21.7691 ± 0.0326	21.4422 ± 0.0406	21.3932 ± 0.1217	20.491 ± 0.2117	///	20.4062 ± 0.5695
493882026	73.756147	-47.923077	23.8901 ± 0.1064	22.0808 ± 0.024	21.7685 ± 0.0306	21.4226 ± 0.0387	21.246 ± 0.1024	20.6618 ± 0.3157	///	19.9958 ± 0.4409
494789087	69.898546	-46.782506	23.8557 ± 0.1356	21.9308 ± 0.0361	21.5423 ± 0.0289	21.5443 ± 0.0481	21.1287 ± 0.1132	22.0732 ± 0.8393	///	21.0469 ± 0.8443
494790027	70.402136	-46.796962	24.138 ± 0.1352	21.864 ± 0.0236	21.3387 ± 0.02	21.1324 ± 0.0258	20.8994 ± 0.0731	20.6496 ± 0.3046	///	20.2624 ± 0.3745
494790169	70.575727	-46.798513	23.2371 ± 0.0465	21.3858 ± 0.0118	20.941 ± 0.0128	20.8265 ± 0.0172	20.7429 ± 0.0526	20.5034 ± 0.1831	///	20.0217 ± 0.4448
494790792	70.118141	-46.809179	23.7461 ± 0.0968	21.758 ± 0.026	21.2542 ± 0.0242	20.9573 ± 0.0278	20.8978 ± 0.0929	20.3048 ± 0.2452	///	19.3178 ± 0.2806
494791393	70.545803	-46.818298	25.8019 ± 0.5094	22.9725 ± 0.0505	22.3344 ± 0.0364	21.9215 ± 0.0508	22.0782 ± 0.2109	21.7367 ± 0.5105	///	20.8025 ± 0.6156
494792459	70.361105	-46.834652	24.2656 ± 0.1335	22.2795 ± 0.0298	21.7942 ± 0.0307	21.6362 ± 0.0434	21.7176 ± 0.1596	20.8556 ± 0.2748	///	22.1288 ± 1.8666
494793098	70.361899	-46.84422	23.9821 ± 0.1053	21.8222 ± 0.0204	21.2755 ± 0.0197	21.0539 ± 0.0263	20.9669 ± 0.0823	20.8774 ± 0.2682	///	20.2478 ± 0.5222
494793167	70.322957	-46.845463	23.8321 ± 0.0829	21.8795 ± 0.0192	21.387 ± 0.0206	21.1299 ± 0.0252	20.9922 ± 0.0774	20.6869 ± 0.2351	///	20.3403 ± 0.5394
494800805	70.223709	-46.969603	23.3453 ± 0.0791	21.6088 ± 0.0224	21.2646 ± 0.0233	21.1833 ± 0.0371	21.3461 ± 0.1833	20.9634 ± 0.4222	///	19.9742 ± 0.3398
494801634	70.204006	-46.984426	23.108 ± 0.0641	21.3465 ± 0.018	21.1355 ± 0.0166	20.9708 ± 0.0236	20.926 ± 0.0767	20.3121 ± 0.2086	///	19.2022 ± 0.2093
495323159	65.394135	-46.057881	23.4555 ± 0.0678	21.7668 ± 0.0197	21.4263 ± 0.0244	21.433 ± 0.0555	21.0016 ± 0.0969	20.7891 ± 0.3456	21.5235 ± 0.9513	20.8319 ± 0.6251
495325646	65.413155	-46.101938	24.1823 ± 0.1228	22.4046 ± 0.038	22.001 ± 0.0336	21.6707 ± 0.0519	21.7598 ± 0.2104	///	21.7652 ± 1.3242	20.4605 ± 0.5438
495342175	65.087082	-46.3792	23.6315 ± 0.0661	21.7161 ± 0.017	21.3624 ± 0.0171	21.0386 ± 0.0259	20.6991 ± 0.0633	20.9568 ± 0.4498	20.768 ± 0.6159	19.9356 ± 0.4688
495508558	64.591881	-57.810162	24.0085 ± 0.1786	21.734 ± 0.0197	21.1739 ± 0.0263	20.8205 ± 0.0317	21.0451 ± 0.1696	20.2084 ± 0.1872	///	20.4662 ± 0.4553
495566911	70.276529	-48.286447	24.379 ± 0.1996	22.23 ± 0.0356	21.6714 ± 0.0325	21.6571 ± 0.0625	21.791 ± 0.2094	20.9532 ± 0.3595	///	19.9958 ± 0.3845
496787409	63.374087	-59.79275	24.0008 ± 0.1195	22.0032 ± 0.0246	21.4945 ± 0.0205	21.1897 ± 0.033	21.2715 ± 0.1553	20.727 ± 0.2958	///	20.0388 ± 0.3226
497171956	65.710748	-58.418902	22.884 ± 0.0491	20.8448 ± 0.0097	20.3696 ± 0.0094	20.0618 ± 0.0114	19.9096 ± 0.0327	19.6361 ± 0.1176	///	18.9846 ± 0.1623
497174314	64.973407	-58.457378	24.4577 ± 0.1761	22.5676 ± 0.0456	22.1586 ± 0.0487	21.9922 ± 0.0904	21.7573 ± 0.2387	22.3304 ± 0.8953	///	20.7245 ± 0.5142
498898550	65.712873	-59.065758	24.0901 ± 0.1197	22.2997 ± 0.0353	21.9947 ± 0.0433	21.6648 ± 0.0426	21.4354 ± 0.136	21.5185 ± 0.5076	///	20.4729 ± 0.408
499908069	65.468426	-47.534492	23.8878 ± 0.0981	22.1885 ± 0.0242	21.9058 ± 0.0318	21.5545 ± 0.0485	21.6761 ± 0.1802	21.0946 ± 0.2938	///	20.1886 ± 0.3185
499909599	65.492297	-47.55904	24.3098 ± 0.1254	22.2842 ± 0.0236	21.7533 ± 0.0253	21.4982 ± 0.0397	21.6327 ± 0.1549	20.8654 ± 0.2354	///	20.4361 ± 0.4379
500048125	66.429253	-56.267392	24.9981 ± 0.311	22.4494 ± 0.026	21.7672 ± 0.0244	21.3979 ± 0.0352	21.466 ± 0.1457	20.7618 ± 0.3188	///	19.8518 ± 0.3352
500110571	70.92143	-58.350365	23.5309 ± 0.0876	21.6786 ± 0.0192	21.2638 ± 0.0178	20.9827 ± 0.0324	20.7802 ± 0.0892	20.4678 ± 0.2583	///	20.3056 ± 0.5442
500571685	65.734516	-47.379303	23.1512 ± 0.0701	21.4725 ± 0.018	21.1271 ± 0.0229	20.7555 ± 0.0351	20.9316 ± 0.1251	20.5235 ± 0.2618	///	19.4581 ± 0.2056
500910602	71.460323	-46.202889	24.5877 ± 0.1886	22.4886 ± 0.0312	21.914 ± 0.0343	21.5586 ± 0.0428	21.6458 ± 0.1791	21.7584 ± 0.4942	20.7106 ± 0.3438	20.6049 ± 0.5369
501217876	66.041527	-52.819775	22.6725 ± 0.0419	20.8092 ± 0.0101	20.3847 ± 0.0101	19.9921 ± 0.0153	19.8369 ± 0.0438	20.0441 ± 0.3983	19.1979 ± 0.2433	19.0833 ± 0.2217
501218097	65.762156	-52.821932	23.3563 ± 0.0535	21.4202 ± 0.0166	20.969 ± 0.0122	20.7017 ± 0.0207	20.5805 ± 0.0659	///	20.7299 ± 0.4663	20.3083 ± 0.5642
501511673	67.243745	-60.378716	24.3018 ± 0.1113	22.2241 ± 0.0241	21.6714 ± 0.0206	21.2992 ± 0.0242	21.3162 ± 0.1111	20.6496 ± 0.2486	///	20.9327 ± 0.8991
501524910	66.697138	-60.5957	23.3954 ± 0.0716	21.3984 ± 0.0152	20.8981 ± 0.0123	20.6364 ± 0.0167	20.5033 ± 0.0732	19.9998 ± 0.2457	///	19.5555 ± 0.2512
501577492	65.529485	-57.087743	22.2891 ± 0.0412	20.4103 ± 0.0083	19.9915 ± 0.0091	19.5186 ± 0.0116	19.3548 ± 0.0362	19.0141 ± 0.0798	///	18.6395 ± 0.1814
501665859	71.672277	-47.591956	23.1878 ± 0.0515	21.4964 ± 0.0157	21.1655 ± 0.0188	21.1146 ± 0.0246	20.8241 ± 0.0756	20.7005 ± 0.2542	///	20.1931 ± 0.3165

Table B1 – *continued*

ID	RA	Dec	<i>g</i>	<i>r</i>	<i>i</i>	<i>z</i>	<i>Y</i>	<i>J</i>	<i>H</i>	<i>K_s</i>
502431214	65.942299	-46.553076	22.7071 ± 0.0379	20.9606 ± 0.0099	20.6372 ± 0.0112	20.2516 ± 0.0176	20.1892 ± 0.0442	19.9818 ± 0.1994	19.2778 ± 0.1497	19.0157 ± 0.1745
502433292	66.409402	-46.568465	23.6993 ± 0.0929	21.727 ± 0.0198	21.2826 ± 0.0206	20.8858 ± 0.0303	20.9898 ± 0.115	20.1812 ± 0.2583	19.8842 ± 0.263	19.974 ± 0.3567
502449004	65.844648	-46.707587	22.8891 ± 0.0412	21.0685 ± 0.0131	20.7778 ± 0.0151	20.474 ± 0.0207	20.146 ± 0.0553	19.8829 ± 0.12	///	19.5314 ± 0.3161
503482151	66.649327	-58.546895	23.8134 ± 0.1008	22.062 ± 0.0256	21.6794 ± 0.0291	21.3887 ± 0.0404	21.189 ± 0.1058	21.1799 ± 0.2995	///	20.2835 ± 0.3403
503811408	70.787127	-52.978216	23.2053 ± 0.0594	21.28 ± 0.0135	20.8055 ± 0.0143	20.3545 ± 0.0178	20.2962 ± 0.055	20.1231 ± 0.2981	19.3309 ± 0.218	19.1173 ± 0.2316
503973856	71.227329	-44.778327	23.6823 ± 0.1294	21.5272 ± 0.0331	20.9504 ± 0.0298	20.6236 ± 0.0319	20.6429 ± 0.1169	19.6565 ± 0.1644	///	18.9792 ± 0.2099
503973990	71.217655	-44.780499	23.3519 ± 0.0959	21.6747 ± 0.0375	21.5158 ± 0.0491	21.1546 ± 0.0515	21.0994 ± 0.1777	21.2706 ± 0.4969	///	20.2714 ± 0.3984
503984762	71.018342	-44.948031	23.7379 ± 0.0742	21.7577 ± 0.0188	21.4376 ± 0.0183	21.2233 ± 0.0361	21.0102 ± 0.0878	20.9198 ± 0.3497	///	19.8396 ± 0.354
503985134	71.013934	-44.953898	24.331 ± 0.1115	22.389 ± 0.023	21.9089 ± 0.023	21.5687 ± 0.041	21.4623 ± 0.127	20.7513 ± 0.2782	///	20.2006 ± 0.3825
504038042	71.39045	-52.049047	22.8125 ± 0.0375	20.8787 ± 0.0102	20.4005 ± 0.0098	19.9239 ± 0.012	19.8667 ± 0.0352	19.8114 ± 0.2304	19.2146 ± 0.1916	18.9377 ± 0.1799
504051667	72.349051	-52.272785	23.322 ± 0.0564	21.5095 ± 0.0165	21.0965 ± 0.0145	20.8096 ± 0.0196	20.8302 ± 0.064	19.9785 ± 0.2024	19.7234 ± 0.2235	19.7586 ± 0.2747
504056183	71.339025	-52.34761	23.5642 ± 0.0655	21.6291 ± 0.018	21.1479 ± 0.0177	20.7422 ± 0.0222	20.8139 ± 0.0927	20.1137 ± 0.2159	///	19.504 ± 0.2264
504194446	66.099016	-51.118123	23.2181 ± 0.0612	21.0982 ± 0.0136	20.5919 ± 0.0111	20.255 ± 0.0145	20.0988 ± 0.0477	19.7879 ± 0.2517	19.4747 ± 0.2418	19.3972 ± 0.2774
504330828	67.145378	-50.373978	23.1291 ± 0.047	21.4316 ± 0.0119	21.097 ± 0.0127	20.813 ± 0.02	20.5226 ± 0.0553	20.6876 ± 0.3383	20.9076 ± 0.58	19.8315 ± 0.3205
504394690	66.525615	-49.260798	23.4748 ± 0.084	21.5242 ± 0.0237	21.1626 ± 0.0202	20.7947 ± 0.022	20.8201 ± 0.1049	19.8222 ± 0.1774	///	19.3278 ± 0.2493
504825888	66.295589	-60.190845	23.4268 ± 0.0619	21.5766 ± 0.0192	21.1377 ± 0.0204	20.8464 ± 0.0219	20.8598 ± 0.0862	20.3412 ± 0.2711	///	19.793 ± 0.2894
505013250	72.080434	-51.480723	22.8535 ± 0.0334	20.9016 ± 0.0095	20.4941 ± 0.0088	20.1545 ± 0.0115	20.0737 ± 0.0361	19.4464 ± 0.185	19.2072 ± 0.1731	19.0424 ± 0.1933
505018776	71.922491	-51.553863	24.6871 ± 0.151	22.8295 ± 0.0404	22.481 ± 0.0474	22.1188 ± 0.0708	21.8956 ± 0.1942	///	20.1492 ± 0.2341	19.7364 ± 0.3091
505028285	72.117204	-51.713201	22.8788 ± 0.0383	20.914 ± 0.0103	20.4363 ± 0.0104	20.0759 ± 0.0153	19.9913 ± 0.0502	19.7034 ± 0.2184	19.5768 ± 0.2826	19.0487 ± 0.2171
506017320	70.104975	-51.684777	23.7955 ± 0.0866	21.7769 ± 0.0226	21.2558 ± 0.0231	20.8174 ± 0.0265	20.6396 ± 0.0907	20.352 ± 0.255	20.2845 ± 0.3382	19.886 ± 0.2878
506153545	71.440457	-48.468766	23.8422 ± 0.0748	22.0488 ± 0.0183	21.6804 ± 0.0228	21.2587 ± 0.0364	21.3952 ± 0.0943	21.1499 ± 0.3377	///	20.2704 ± 0.3557
506329583	66.656908	-51.464977	23.8578 ± 0.1753	22.0277 ± 0.0259	21.6374 ± 0.0301	21.468 ± 0.0503	21.1333 ± 0.136	21.0297 ± 0.3731	20.9004 ± 0.4895	///
506345182	66.967637	-55.747027	24.3794 ± 0.1524	22.2277 ± 0.0236	21.7105 ± 0.0249	21.3227 ± 0.0318	21.2297 ± 0.1161	21.075 ± 0.3798	///	20.231 ± 0.475
506383847	71.82706	-49.119781	24.5496 ± 0.1903	22.52 ± 0.034	21.9882 ± 0.0337	21.8294 ± 0.049	21.8817 ± 0.2167	21.1532 ± 0.3435	///	20.7714 ± 0.4408
506534457	66.516394	-59.392889	22.8638 ± 0.0421	20.9491 ± 0.0089	20.5583 ± 0.0132	20.1807 ± 0.0111	19.9464 ± 0.0325	19.7133 ± 0.1204	///	19.0525 ± 0.1728
506537406	67.81106	-59.441728	23.8835 ± 0.108	21.8331 ± 0.0224	21.2802 ± 0.024	21.0069 ± 0.0313	20.6972 ± 0.0676	20.7452 ± 0.2988	///	20.0631 ± 0.4094
506572275	67.113463	-56.408528	23.6338 ± 0.0742	21.7324 ± 0.019	21.2609 ± 0.0186	20.9633 ± 0.0232	20.8565 ± 0.0851	19.8368 ± 0.2241	///	19.4777 ± 0.352
506589633	67.51748	-56.684982	23.3492 ± 0.0663	21.5182 ± 0.0151	21.0862 ± 0.0146	20.7987 ± 0.0234	20.5561 ± 0.077	20.2118 ± 0.2368	///	19.4276 ± 0.3205
506646930	70.326828	-50.439845	22.5345 ± 0.035	21.0373 ± 0.0109	20.8922 ± 0.0076	20.6646 ± 0.0092	20.5195 ± 0.0734	20.5782 ± 0.2394	20.1755 ± 0.3336	20.3265 ± 0.4575
506674710	70.499013	-50.804827	24.0668 ± 0.111	22.2647 ± 0.0309	21.9204 ± 0.0175	21.5804 ± 0.0188	21.7134 ± 0.1519	20.9526 ± 0.3146	///	20.5681 ± 0.3619
506674855	70.492258	-50.807343	23.6095 ± 0.0811	21.9397 ± 0.0226	21.6659 ± 0.0135	21.4152 ± 0.0157	21.2002 ± 0.104	21.2213 ± 0.4521	///	20.1676 ± 0.3064
506674909	70.483191	-50.807614	22.6307 ± 0.0341	21.71 ± 0.0187	21.8107 ± 0.0162	21.5835 ± 0.019	22.261 ± 0.2839	20.7457 ± 0.3673	///	20.1191 ± 0.3587
506675198	70.515975	-50.811698	22.8002 ± 0.04	21.0193 ± 0.0105	20.6184 ± 0.0057	20.322 ± 0.0062	20.3049 ± 0.0482	19.5661 ± 0.1436	19.7694 ± 0.2368	19.4277 ± 0.2112
507681715	67.217708	-53.525888	24.1343 ± 0.2575	21.8899 ± 0.0466	21.3924 ± 0.0455	21.2145 ± 0.0623	20.7942 ± 0.1663	20.4294 ± 0.2097	20.8157 ± 0.4821	///
507691551	68.038665	-53.69669	23.405 ± 0.0675	21.6883 ± 0.0188	21.4028 ± 0.0239	21.1287 ± 0.0322	21.2214 ± 0.1073	20.6715 ± 0.2216	///	20.4637 ± 0.4587
507780409	67.850037	-52.458756	23.0356 ± 0.0385	21.3203 ± 0.0121	21.0019 ± 0.0121	20.7608 ± 0.0172	20.6037 ± 0.0508	19.8961 ± 0.2066	20.0266 ± 0.3041	19.5255 ± 0.2173
507785363	67.470004	-52.559327	24.4789 ± 0.13	22.3368 ± 0.027	21.7613 ± 0.0222	21.4934 ± 0.0299	21.2488 ± 0.0884	20.6533 ± 0.3225	20.6363 ± 0.4087	///
507791066	67.361423	-52.654125	22.777 ± 0.0355	20.9881 ± 0.0115	20.5918 ± 0.0103	20.2706 ± 0.0138	20.1095 ± 0.0426	20.2512 ± 0.2678	19.6486 ± 0.2564	18.9594 ± 0.1986
507791331	67.519725	-52.659509	22.5887 ± 0.0331	20.5847 ± 0.0091	20.0805 ± 0.0075	19.7081 ± 0.0098	19.4835 ± 0.028	19.2903 ± 0.1538	18.7168 ± 0.1575	18.3319 ± 0.1223
507791530	67.159439	-52.661824	24.3771 ± 0.1232	22.2965 ± 0.0274	21.7254 ± 0.0219	21.3829 ± 0.0295	21.0487 ± 0.0816	20.8737 ± 0.337	20.3442 ± 0.4227	19.78 ± 0.3309
507803985	67.325717	-52.880165	23.6147 ± 0.0647	21.7564 ± 0.018	21.3175 ± 0.0159	21.0028 ± 0.018	20.8713 ± 0.0692	20.516 ± 0.2842	19.8374 ± 0.2882	20.1467 ± 0.4506
507810919	66.8646	-52.989845	23.2527 ± 0.0481	21.3523 ± 0.0131	20.9483 ± 0.0126	20.631 ± 0.0177	20.4023 ± 0.0505	20.0732 ± 0.2434	19.9002 ± 0.3387	19.4536 ± 0.3144
507820438	67.1093	-53.141275	22.2814 ± 0.0225	20.4405 ± 0.0068	20.0207 ± 0.007	19.6673 ± 0.0072	19.5324 ± 0.0272	19.2047 ± 0.1324	18.9817 ± 0.1372	18.647 ± 0.1656
508217521	69.432208	-58.182331	24.6135 ± 0.1574	22.8099 ± 0.0352	22.486 ± 0.0399	22.1762 ± 0.0578	22.3086 ± 0.2506	21.7479 ± 0.2708	///	21.4014 ± 0.7731
508601732	69.941686	-51.027099	24.8183 ± 0.329	22.1654 ± 0.0476	21.3868 ± 0.0203	20.8769 ± 0.0232	20.6581 ± 0.0926	20.7992 ± 0.3906	19.6832 ± 0.2352	19.9412 ± 0.3366

Table B1 – *continued*

ID	RA	Dec	g	r	i	z	Y	J	H	K_s
618652137	358.88296	-54.30947	22.8707 ± 0.0532	21.0181 ± 0.0112	20.5872 ± 0.0106	20.1606 ± 0.0143	20.085 ± 0.0485	19.9487 ± 0.2035	19.8445 ± 0.3877	18.9431 ± 0.1907
618654757	358.67695	-54.356158	23.549 ± 0.137	21.8112 ± 0.0272	21.4459 ± 0.0274	21.1584 ± 0.0431	21.2514 ± 0.1468	21.0447 ± 0.3029	20.8919 ± 0.477	21.2233 ± 1.0699
618660654	359.14404	-54.461467	22.0072 ± 0.0258	20.3997 ± 0.0077	20.1682 ± 0.009	19.8417 ± 0.0127	19.8875 ± 0.0355	19.6534 ± 0.1604	20.4625 ± 0.7439	19.1208 ± 0.2385
618663972	358.73193	-54.517818	22.8714 ± 0.045	20.9306 ± 0.0113	20.5016 ± 0.0106	20.0363 ± 0.0137	20.0142 ± 0.037	19.4945 ± 0.1769	19.2994 ± 0.1598	18.8724 ± 0.155
618664093	359.04338	-54.519852	23.1158 ± 0.0456	21.2542 ± 0.0124	20.818 ± 0.0123	20.4231 ± 0.0171	20.4425 ± 0.0485	19.9913 ± 0.1884	19.9082 ± 0.4418	19.3846 ± 0.2939
618664306	359.09017	-54.523087	22.9282 ± 0.0433	21.0268 ± 0.0135	20.5623 ± 0.0124	20.2491 ± 0.0187	20.3538 ± 0.0456	19.8083 ± 0.1913	20.1177 ± 0.5618	19.2618 ± 0.2835
618667069	358.8217	-54.567628	23.8333 ± 0.1179	21.8771 ± 0.0233	21.5924 ± 0.0206	21.0456 ± 0.0259	20.9855 ± 0.105	20.6079 ± 0.323	20.1235 ± 0.4174	19.4716 ± 0.2758
618667272	358.80469	-54.571019	23.2565 ± 0.0703	21.2546 ± 0.0138	20.8998 ± 0.0135	20.4648 ± 0.0184	20.735 ± 0.1075	19.8864 ± 0.2031	19.8565 ± 0.2992	19.0797 ± 0.2255